CODEN:LUTEDX/(TEIE-5489)/1-125/(2023)

Industrial Electrical Engineering and Automation

# Wastewater Characterisation for Design and Modelling of Primary Settlers at Municipal Wastewater Treatment Plants



**Louise Westin**

Division of Industrial Electrical Engineering and Automation
Faculty of Engineering, Lund University

# Wastewater Characterisation for Design and Modelling of Primary Settlers at Municipal Wastewater Treatment Plants

by

Louise Westin

Division of Industrial Electrical Engineering and Automation
Department of Biomedical Engineering
Lund University

March 2023

**Supervisor:** Michael Cimbritz (VA-Teknik, LTH)
**Co-supervisors:** Simon Bengtsson (VA SYD/Sweden Water Research), Christoffer Wärff (RISE)
**Examiner:** Ramesh Saagi (IEA, LTH)

# Acknowledgements

This thesis has been carried out on behalf of Sweden Water Research. Lab and office space have been provided by the Department of Chemical Engineering at Lund University and the fractionation and collection of samples has taken place at Källby WWTP and Öresundsverket. It has been a very fun and interesting time diving deeper into this subject and an exciting way to end to my 5-year long Environmental Engineering-studies at LTH.

First of all I would like to extend my deepest gratitude to all of my supervisors **Michael Cimbritz**, **Simon Bengtsson** and **Christoffer Wärff** for all of the help setting up the equipment, trouble-shooting ideas and answering questions throughout this project, in particular from the latter two. Your help and support has been invaluable throughout all of this. While Michael may not have been as actively involved in these parts, I am extremely grateful for all of the help in the more formal matter such as registering and the very valuable input and feedback on the structure of the report.

I would also like to thank the personnel at both Källby WWTP and Öresundsverket for allowing me access and helping me find my way. A special thanks goes to **Naima Forså** at Källby WWTP and **Federico Micolucci** at Öresundsverket for answering questions and providing data and even more so to Federico for all of the help he provided during the measurement campaign at Öresundsverket.

Furthermore I owe many thanks to **Per Falås** at the Department of Chemical Engineering for taking the time to teach me the analysis methods used in the lab.

Finally I would like to thank my friends and family for keeping me sane throughout all of this and a special thanks to my partner **Jonatan Nilsson** for all of your support and willingness to discuss things, despite not always fully understanding the subject.

Louise Westin
Lund, March 2023

**Abstract**

The primary settling tank (PST) is often one of the first treatment steps at a wastewater treatment plant (WWTP) and is the first process in the plant to remove significant amounts of suspended solids. Its role in wastewater treatment however, has oftentimes been neglected and little effort has been made to optimize and model the process. The PSTs have historically been designed based on hydraulic surface loading rates and expected suspended solids removal based on old rules of thumb, without considering the physical properties of the incoming wastewater such as settling properties of the suspended solids and composition of the wastewater in terms of solubles/particulates and biodegradable/inert material.

In this project, the incoming suspended solids, particulate chemical oxygen demand (COD) as well as the inert and biodegradable parts of the particulate COD at two different WWTPs have been characterized based on their settling velocities. A model of the PST using groups with different settling velocities has also been set up to validate the results and it has been used to compare with current design guidelines for the PST. The characterization has been done with a settleometer consisting of five different columns and a calculation procedure for considering the misplacement of particles in the settleometer has been developed. The results indicate that the settling velocity distribution of the particles vary between different WWTPs and that a model based on the particle settling velocity distribution concept yields good results, but some modification of the assigned distribution had to be made. A broader distribution of the settling velocity groups is needed to model the PST outside its normal overflow range.

**Keywords:** Primary Settling Tank, Wastewater Treatment, Settleometer, Particle Settling Velocity Distribution, Modelling.

# List of Abbreviations

5C-settleometer - 5-column settleometer

ASM - Activated sludge model

BOD - Biochemical oxygen demand (biodegradable COD)

BSM - Benchmarking simulation model

COD - Chemical oxygen demand

$COD_p$ - Particulate chemical oxygen demand

$COD_s$ - Soluble chemical oxygen demand

CFD - Computational Fluid Dynamics

CSVD - Cumulative settling velocity distribution

ISS - Inorganic suspended solids

MB - Mass balance

PST - Primary Settling Tank

PSVD - Particle settling velocity distribution

SVG - Settling velocity group

TSS - Total suspended solids = VSS + ISS

VSS - Volatile suspended solids

WWTP - Wastewater treatment plant

$X_B$ - Slowly biodegradable substrate

$X_{OHO}$ - Heterotrophic biomass

$X_P$ - Particulate decay products

$X_U$ - Particulate inert matter

# Contents

# Chapter 1

# Introduction

## 1.1 Background

The primary settling tank (PST) is often one of the first treatment steps at a wastewater treatment plant (WWTP) and is the first process in the plant to remove significant amounts of suspended solids (SS) (Davis, 2010). By reducing the SS load to the biological treatment steps less oxygen will be required to remove the excess carbon, thus reducing the cost associated with the aeration of the biological treatment (one of the most energy-intensive steps at the whole plant (Metcalf & Eddy et al., 2014)). Another benefit of removing more SS in the PST is the improved production of biogas due to the higher biogas potential from the primary sludge in the PST compared to the excess sludge produced in the biological processes (Metcalf & Eddy et al., 2014).

The organic removal can be increased by addition of coagulants and/or flocculants (Metcalf & Eddy et al., 2014). However, different biological steps (activated sludge, granules, biofilm etc.) require different amounts of organic material to remove nitrogen and phosphorus. If too much organic material is removed, inadequate removal of nitrogen and phosphorus is likely to occur. This would in turn require external carbon to be added. In the future, one might even wish to "design" the incoming wastewater composition to optimize the biological treatment step and for this to be done, the PST is of great importance.

PSTs have historically been designed based on hydraulic surface loading rates and expected SS removal based on old rules of thumb, without considering the physical properties of the incoming wastewater such as settling properties of the SS and composition of the water in terms of solubles/particulates and biodegradable/inert material (Metcalf & Eddy et al., 2014). Its role in wastewater treatment has thus oftentimes been neglected and little effort has been made to optimize and model the process (Bachis et al., 2015). Furthermore, the few times the primary settling has been modelled, the models have generally been very robust and simplified (Bachis et al., 2015). A new proposed group of models for the PST is based on the particle settling velocity distribution concept dividing the particles in the wastewater into different settling velocity groups (SVGs) (Bachis et al., 2015) each assigned a specific settling velocity and fraction of the particles. To determine this division of the particles, a settleometer can be used. Here, a settleometer

consisting of 5 columns (later referred to as the 5C-settleometer) and first developed by Poinapen et al. (2009) will be used. The characterization will take place at both Källby WWTP and Öresundsverket for the total, volatile and inorganic suspended solids (TSS, VSS and ISS respectively), the particulate chemical oxygen demand (CODp) as well as the biodegradable and inert parts of the particulate COD. The results from Öresundsverket in particular will be used to set up a model and validate against real data. The model will then be used to compare with the traditional design guidelines in terms of surface area to inflow ratio.

## 1.2 Aim of the thesis

The aim of this project was to characterize the particles in the incoming wastewater at Källby WWTP and Öresundsverket according to their settling velocities. The results have then been used to set up a model of the PST to verify the results. Furthermore, an objective in itself was to evaluate the settleometer as the method is still under development for this purpose. Lastly, the project aimed to compare traditional design guidelines of PSTs with the results given by a model based on a physical and chemical characterization of the wastewater.

## 1.3 Research questions

The following questions will be answered in this thesis:

- How can the 5C-settleometer be used to characterize the settling properties of the wastewater?

- How does the settling velocity distribution differ for the suspended solids, for the biodegradable and inert particulate organics and for different WWTPs?

- How does the result from a model of the PST based on the particle settling velocity distribution compare to the traditional design guidelines in terms of surface area to inflow ratio (i.e. overflow rate)?

# Chapter 2

# Theory

## 2.1 Primary sedimentation

When the wastewater enters the WWTP it normally passes through preliminary treatment steps such as screening and sand traps which remove larger solids such as tissues and heavier particles such as sand and gravel with settling velocities substantially greater than organic matter. Following this the water enters the primary treatment step, where sedimentation is the predominant method, removing the suspended particles by use of gravity. The primary treatment is the first process in the plant to remove significant amounts of suspended solids (SS) (Davis, 2010). The suspended solids consist of the volatile suspended solids (VSS) and the inorganic suspended solids (ISS) and are measured in terms of concentration of the particulates. The sum of these are commonly referred to as the total suspended solids (TSS).

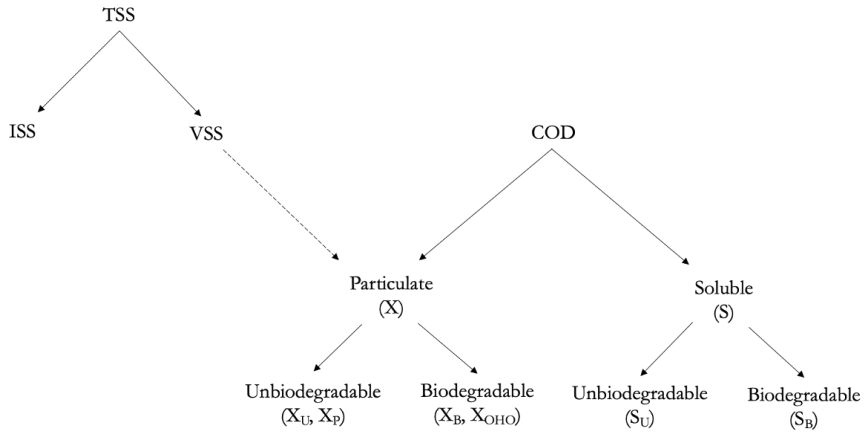


Figure 2.1: An illustration of how the COD and TSS correlate. Particulate substances are commonly denoted with an 'X' and the soluble ones with an 'S'. Due to use of different units the line between the VSS and the particulate COD is dotted.

Another common measurement in wastewater treatment is the chemical or biochemical oxygen demand (COD respectively BOD) and these are measured as the amount of oxygen required to break down the organic matter biologically (under aerobic conditions at a

certain temperature and time) or chemically. The COD and BOD can be measured in total or as only the soluble parts, the difference between the two measurements describe the particulate and colloidal parts of the COD and BOD. Hence, the particulate COD and VSS describe the same particles, but with different measurements and units. An illustration depicting how the different measurements correlate can be seen in Figure 2.1 above. According to Metcalf & Eddy et al. (2014) the primary sedimentation reduces the load to the plant by approximately 50-70% for the SS and 25-40 % for the BOD. Apart from the BOD, inert particulate matter and inorganic suspended solids can also be removed in this step.

The primary sedimentation tank (PST) can have different configurations at different plants, but the two most common ones are circular and rectangular tanks (Davis, 2010; Metcalf & Eddy et al., 2014). An illustration of the two configurations is shown in Figures 2.2a and b below. In the circular PST the wastewater is entering in the middle of the PST and the effluent exits at the outer edges while for the rectangular PST the wastewater passes from one end to the other.

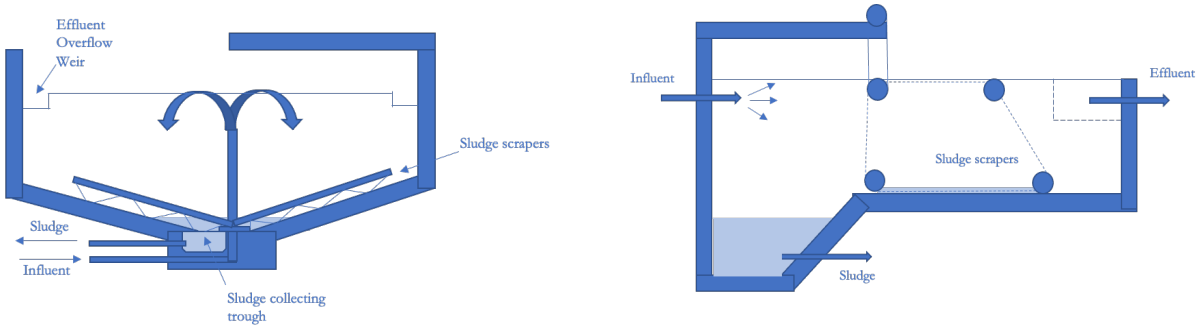


(a) Circular (b) Rectangular

Figure 2.2: Two common configurations of the primary settlers

### 2.1.1 Different types of settling

Depending on the concentration and the interparticle forces between the particles four types of gravitational settling can occur: discrete particle settling, flocculent settling, hindered settling and compression settling (Metcalf & Eddy et al., 2014). When there is no significant interaction between the particles in the water and they settle independently of each other, discrete particle settling occurs. This happens at low concentrations of solids. At slightly higher concentrations flocculation occurs. Due to different velocity gradients, particles of different velocities may collide and aggregate and upon doing so their settling velocities are combined. This mainly happens in the inlet zone where the turbulence is sufficient to create those gradients. Following the formation of the flocculated particles, they then settle as discrete particles. This type(s) of settling is the one(s) mainly encountered in the primary settlers (Amerlinck, 2015). The other types of settling occurs at higher concentrations when interparticular forces work to decrease the settling velocities of the particles (hindered settling) or the particles are in contact with each other in a structured formation and settling only occurs by compression of the structure by the weight of the particles above (Amerlinck, 2015). These two types of settling are more likely to be observed in secondary clarifiers (Amerlinck, 2015).

### 2.1.2 Other processes occurring

Apart from sedimentation and flocculation other processes may also occur in the PST. At too high flows resuspension or scouring may occur where the settled particles become suspended again. Amerlinck (2015) states that there are contradictory observations made regarding the importance of scouring and that this might be explained by the possible differences in operation of the sedimentation tanks (Amerlinck, 2015). Amerlinck (2015) also states that scouring is more likely to be significant when the sludge beds are higher.

Apart from physical processes, chemical and biological processes may also occur in the PST. According to Ribes et al. (2002) the most important biological processes occurring in the primary settlers are hydrolysis (breakdown of slowly biodegradable substrates to more easily biodegradable substrates), ammonification (conversion of soluble organic nitrogen to ammonia/ammonium) and fermentation of primary sludge to produce volatile fatty acids (Ribes et al., 2002). Chemicals may also be added to precipitate and improve the removal of TSS, COD and sometimes phosphorus (Metcalf & Eddy et al., 2014).

## 2.2 Design of the Primary Settling Tanks

The PSTs are generally very simplistic in design and are normally based on the surface loading rate only. In the following subsections some basic theory of how the PST works as well as some current design guidelines are presented.

### 2.2.1 Theory

For discrete particle settling the velocity at which a particle settles in a primary clarifier depends on the gravitational force and the frictional resistance acting on it (Amerlinck, 2015; Metcalf & Eddy et al., 2014). While the gravitational force depends on the weight of both the particle and the displaced fluid, the frictional resistance is correlated to the velocity of the particle. Hence the particle will keep accelerating until the two forces balance each other out. By equating the two forces the terminal settling velocity of the particle could be determined. For laminar flow conditions and spherical particles Stoke's law gives the settling velocity of the particle as follows:

$$v_s = \frac{g \cdot (\rho_p - \rho_f) \cdot {d_p}^2}{18 \cdot \mu} \tag{2.1}$$

where

$v_s$ = the terminal settling velocity of the particle $[m/s]$
$g$ = the acceleration due to gravity $[m/s^2]$
$\rho_p$ = the density of the particle $[kg/m^3]$
$\rho_f$ = the density of the fluid $[kg/m^3]$
$d_p$ = the diameter of the particle $[m]$
$\mu$ = the dynamic viscosity of the fluid $[Ns/m^2]$

The critical settling velocity in a PST is the minimum settling velocity that a PST is designed to remove. This is in other words the lowest settling velocity required for a particle to have and still be able to reach the sludge zone before exiting the basin irrespective of the starting point. This could be determined by the depth ($H$) of the PST and the retention time ($T$) as:

$$v_c = \frac{H}{T} = \frac{H \cdot Q}{V} = \frac{H \cdot Q}{H \cdot A} = \frac{Q}{A} \tag{2.2}$$

where $H$, $T$, $Q$, $V$ and $A$ are the depth and retention time of the PST, the incoming flow and the volume and surface area of the PST respectively. The last expression ($Q/A$) is also known as the overflow rate of the PST. See Figure 2.3 for clarification.

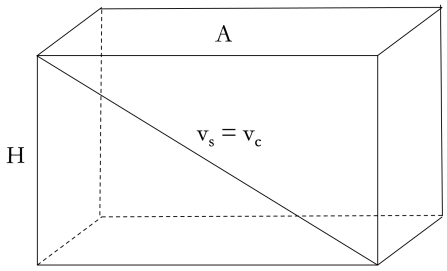


Figure 2.3: Conceptual idea of the critical settling velocity

Assuming instantaneous mixing at the inlet zone where the particles are uniformly distributed over the depth of the basin and that all of the particles will be reaching their maximum settling velocity immediately, all particles in the PST with a settling velocity greater then or equal to the critical settling velocity will be removed. This will happen irrespective of their starting height as they will reach the sludge zone before exiting the basin (Metcalf & Eddy et al., 2014). Moreover, even some of the particles with a settling velocity less then the critical settling velocity may be removed if they start at a low enough height in the basin. Under the same assumptions the fraction of particles with a settling velocity less than the critical velocity to be removed can be described by equation 2.3 (Metcalf & Eddy et al., 2014):

$$X_r = \frac{v_s}{v_c} \tag{2.3}$$

Where $X_r$ is the fraction of the particles with settling velocity $v_s < v_c$ removed.

In real practice though, safety factors need to be added to account for the impact of non-ideally mixed tanks, inlet and outlet turbulence and particle settling velocity distributions of the incoming wastewater (Amerlinck, 2015; Metcalf & Eddy et al., 2014).

### 2.2.2 Design guidelines

Typical values for design and dimensional data for PSTs can be found in Tables 2.1-2.3 below from Metcalf and Eddy (2014) and Norsk Vann (2009) respectively. The PSTs are normally designed based on the surface loading rate (overflow rate) and the choice of

overflow rate together with the total flow rate determines the surface area of the PST. It is important to set the overflow rate low enough that the PST still performs satisfactory at peak flows. Having established the surface area of the PST, the detention time of the PST is determined by the water depth of the tank.

Table 2.1: Typical design information for PSTs followed by secondary treatment. (Adapted from Metcalf & Eddy et al., 2014.)

| **Item** | **Unit** | **Range** | **Typical value** |
|---|---|---|---|
| Detention time | $h$ | 1.5-2.5 | 2.0 |
| Overflow rate: | | | |
| Average flowrate | $m^3/m^2 \cdot d$ | 30-50 | 40 |
| Peak hourly flowrate | $m^3/m^2 \cdot d$ | 80-120 | 100 |
| Weir loading rate | $m^3/m \cdot d$ | 125-500 | 250 |

Table 2.2: Typical dimensional data for rectangular and circular PSTs. (Adapted from Metcalf & Eddy et al., 2014.)

| **Item** | **Unit** | **Range** | **Typical value** |
|---|---|---|---|
| Rectangular: | | | |
| Depth | m | 3-4.9 | 4.3 |
| Length | m | 15-90 | 24-40 |
| Width[1] | m | 3-24 | 4.9-9.8 |
| Flight speed | m/min | 0.6-1.2 | 0.9 |
| Circular | | | |
| Depth | m | 3-4.9 | 4.3 |
| Diameter | m | 3-60 | 12-45 |
| Bottom slope | mm/mm | 1/16-1/6 | 1/12 |
| Fligth speed | rev/min | 0.02-0.05 | 0.03 |

[1] *If width of rectangular mechanically cleaned tanks are greater than 6 m, multiple bays with individual cleaning equipment may be used, thus permitting tank widths up to 24 m or more.*

According to the guidelines by Norsk Vann (2009) a more specific overflow rate is given rather than a range of acceptable values as seen in Table 2.3 below.

Table 2.3: Typical design information for PSTs followed by secondary treatment according to Norsk Vann. (Adapted from Norsk Vann, 2009.)

| **Item** | **Unit** | **Typical value** |
|---|---|---|
| Water depth | $m$ | $\geq 2.5$ |
| Overflow rate: | | |
| Dimensioning flowrate | $m^3/m^2 \cdot d$ | 38.4 |
| Max dimensioning flowrate | $m^3/m^2 \cdot d$ | 60 |

Moreover it is suggested to compensate for the interference in the inlet zone by increasing the total area used when designing by calculating as follows:

$$A_{tot} = AB + B \tag{2.4}$$

where

$A_{tot}$ = Total area for use in design ($m^2$)
$AB$ = Theoretically calculated area ($m^2$)
$B$ = Width of the basin (m)

## 2.3 The Benchmarking Simulation Platform

The Benchmarking Simulation Platform (K. V. Gernaey & Jeppsson, 2014) is a standardized simulation protocol for comparing simulation results with other users and for objectively evaluating different control strategies. The Benchmark Simulation Model No. 2 (BSM2) connects different verified unit process models at the plant and allows for evaluation of control strategies on a plantwide basis using varying influents (K. V. Gernaey & Jeppsson, 2014). The user is however free to modify models describing subunit processes. In BSM2 the model used for the primary clarifier is proposed by Otterpohl & Freund (1992). The model considers the PST to be a single completely mixed tank separating the output empirically into primary effluent and primary sludge streams (K. V. Gernaey & Jeppsson, 2014; Otterpohl & Freund, 1992). This is however a very simple model not taking any consideration to the distribution of settling velocities among the incoming particles. As a base for this project the "Linköping model " developed by Arnell (2013) in MATLAB based on BSM2, modified according to the PSVD concept by Lundin (2014) will be used, later on referred to as "the modified Linköping model".

To model different WWTP processes accurately the wastewater needs to be properly characterized. The Activated Sludge Model (ASM) family provides a common description of concepts, notations and nomenclature for several WWTP processes and is widely accepted internationally (Henze et al., 2000). There are 13 state variables in ASM1. Together with the TSS these make up the state variables calculated on in the primary

Table 2.4: The 14 state variables used in the models

| **Variable** | **Notation** |
|---|---|
| Soluble inert organic matter | $S_U$ |
| Readily biodegradable substrate | $S_B$ |
| Particulate inert organic matter | $X_U$ |
| Slowly biodegradable substrate | $X_B$ |
| Active heterotrophic biomass | $X_{OHO}$ |
| Active autotrophic biomass | $X_{ANO}$ |
| Particulate products arising from biomass decay | $X_P$ |
| Oxygen | $S_O$ |
| Nitrate and Nitrite nitrogen | $S_{NO_x}$ |
| $NH_4^+ + NH_3$ nitrogen | $S_{NH_x}$ |
| Soluble biodegradable organic nitrogen | $S_{B,Org,N}$ |
| Particulate biodegradable organic nitrogen | $X_{B,Org,N}$ |
| Alkalinity | $S_{Alk}$ |
| Total suspended solids | $X_{TSS}$ |

clarifier in BSM2 as well as in the modified Linköping model. These 14 constituents, together with their notations, can be found in Table 2.4. The main symbol $X$ indicates the particulate substrates.

An issue with the characterization used in the ASM in terms of modelling the PST is the fact that it is done based on solubility and biodegradability (as it was initially developed for modelling the activated sludge process) and not on settleability. Hence the particle settling velocity distribution (PSVD) concept involves fractionating the current state variables into subgroups of different settling velocities. The modifications by Lundin (2014) to the Linköping model incorporated the PSVD concept for TSS into the model, something that will be extended here for the different particulate state variables.

## 2.4 Characterisation of settling velocity distribution

As a model for the PST is to be implemented based on the settling velocity distribution of the incoming wastewater, measurements of the water need to be made to determine this distribution. Different settling devices have been proposed and the two main ones in use are described below.

### 2.4.1 The ViCAs settling column

In 2009, Chebbo and Gromaire defined a protocol called ViCAs for the purpose of creating a standard method of measuring the settling velocities of suspended particles. The fractionation device consists of a single sedimentation column with an internal diameter of 70 mm and a height of 64 cm. At the bottom there is a sample trough made of PVC. A guiding tray and a fastening support ensures that the column is positioned upright above the sample trough. At the top of the column a vacuum pump is connected by a hose fitted with a valve to allow filling of the column. A depiction of the setup can be seen in Figure 2.4.

The sample to be analysed is stirred, poured into the trough and drawn up into the column by vacuum pressure in less than 5 seconds. The column is being held under vacuum pressure during the experiment and the settling particles are collected in the aluminium plate placed at the bottom of the column. At gradually longer time periods ($t_i = 1$ min, 2 min, 4 min, 8 min, 16 min, 32 min, 1 h, 2 h, 4 h etc.) the plate is removed and exchanged with a new one. The contents are then filtered to make measurements of the TSS. As the particles do not settle from the same height the cumulative mass of particles collected at each point in time equals the sum of the mass of particles having a settling velocity higher than the height of the column ($H$) divided by the time passed and the mass of particles having a velocity less than that but which settled over a distance less than $H$. The cumulative mass curve $M(t)$ can then be written as (Chebbo & Gromaire, 2009):

$$M(t) = S(t) + t\frac{dM(t)}{dt} \tag{2.5}$$

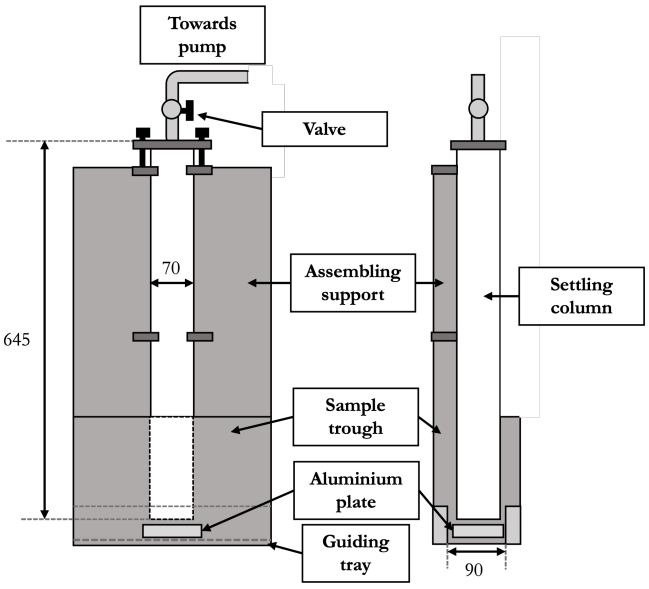


Figure 2.4: A diagram of the ViCAs experimental setup (Adapted from Chebbo and Gromaire, 2009)

where

$M(t)$ = the cumulative mass of particles that have reached the bottom of the settling column between $t = 0$ and $t$

$S(t)$ = the mass of particles having a settling velocity $v_s > \frac{H}{t}$ that have reached the bottom of the settling column between $t = 0$ and $t$

$t\frac{dM(t)}{dt}$ = the mass of particles having a settling velocity $v_s < \frac{H}{t}$ that have reached the bottom of the settling column between $t = 0$ and $t$

The objective of the protocol is to determine the $S(t)$ curve and to transform it into a cumulative settling velocity distribution function $F(v_s)$ which is defined as the fraction of total particle mass with a settling velocity less than $v_s$. To find $F(v_s)$ the differential system in equation 2.5 must be solved and two methods are presented in the protocol for how to do so. From the measurements made of $M(t)$ this is then used to plot $F(v_s)$ against $v_s$.

### 2.4.2 5-Column Settleometer

The 5-column settleometer consists of 5 transparent vertical PVC-columns instead of only a single one like the ViCAs column and the top of one column is connected to the bottom of the next by plastic tubes. Each column has a height of approximately 1 m and in ascending order internal diameters of 45.2, 67.6, 86.4, 105.6 and 134.4 mm. The water to be fractionated is pumped through the smallest column to the largest at a constant flow rate. A schematic design of the set-up used in this project can be seen in Figure 2.5 below.

As the internal diameter of each column increases, the upflow velocity in each column will

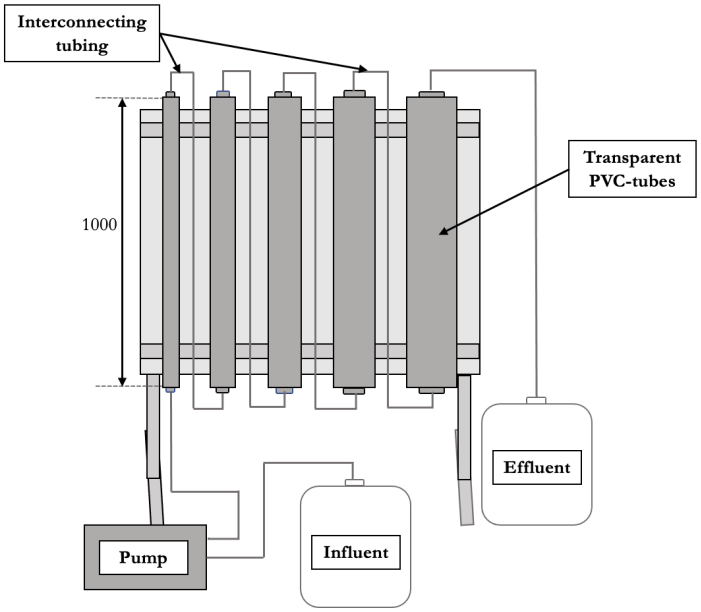


Figure 2.5: A schematic design of the 5C-settleometer

decrease. The upflow velocity of column $i$ can be calculated as follows (Equation 2.6:

$$v_{up,i} = \frac{Q}{A_{in,i}} \tag{2.6}$$

Where $Q$ is the input flow rate and $A_{in,i}$ the internal cross-sectional area of column $i$. Unlike the ViCAs column the principle of the method is to retain particles of different settling velocities in different columns, instead of collecting them at different times. Each column should in theory retain only the particles with a settling velocity ($v_s$) larger than or equal to its upflow velocity ($v_{up}$), causing an accumulation of the fastest settling particles in the first column and a segregation of particle groups of decreasing settling velocities in the subsequent columns accordingly. The organic matter that is not retained in any of the columns will leave the device with the effluent (Matesun et al., 2021; Mazivila, 2022; Poinapen et al., 2009; Polorigni et al., 2021).

The method was first described by Poinapen et al. (2009) using a 4-column settleometer for an Upflow Anaerobic Sludge Bed reactor. The device was later on extended to five columns and used by Matesun et al. (2021), Mazivila (2022) and Polorigni et al. (2021) to characterize incoming wastewater. This is also the settleometer used to characterize the settling velocity distribution in this project.

## 2.5 Existing PST models

Compared to other processes at the WWTP, modelling of the PSTs has been quite neglected over the past decades (Amerlinck, 2015; Bachis et al., 2015). Whether this is because the process in itself is not considered very influential for modelling purposes or if the simple models proposed earlier have been deemed sufficient to describe the behaviour

of the PST is hard to say. However, the primary sedimentation is the first treatment step to remove significant amounts of suspended solids and COD and is important for the overall removal efficiency of the plant (Liu & Garcıa, 2011). A better understanding and modelling of the process will also yield a better characterization of the PST effluent and the primary sludge which will have an impact on subsequent treatment steps (Bachis et al., 2015).

Most models of the PST developed until now are simple empirical data-driven models based on linear regression techniques or more advanced methods. Several phenomenological models have also been implemented in an attempt to include more theoretical knowledge of the settling process. These models can be divided into 4 different groups:

- Models including the particle pathline concept together with a particle settling velocity
- Models addressing the hydraulic behaviour of the settling tank and possible scouring
- 1-D discretized models in vertical direction to account for the dynamic and spatial variation
- Models including the particle settling velocity distribution (PSVD) concept

Finally a more recent type of model which has been developed is the computational fluid dynamics (CFD) model which incorporates numerical analyses of the fluid flow. This however, is much more computationally demanding.

In this section some existing PST models from the different groups are described.

### 2.5.1 Tay, 1982

A simple empirical model of the PST is proposed by Tay (1982). The model depends on the hydraulic retention time ($t_r$) as well as the half-removal time ($T_A$) which is the time at which 50 % of the influent suspended solids is removed. According to the model the fraction removed ($X_r$) can be described according to equation 2.7 (Amerlinck, 2015; Tay, 1982):

$$X_r = \frac{S_0 - S}{S_0} = \frac{t_r}{T_A + t_r} \tag{2.7}$$

By taking the inverse the equation becomes linear with respect to $T_A$

$$\begin{aligned} \frac{S_0}{S_0 - S} &= \frac{S}{S_0 - S} + 1 = \frac{T_A}{t_r} + 1 \\ \frac{S}{S_0 - S} &= \frac{T_A}{t_r} \end{aligned} \tag{2.8}$$

where $S_0$ and $S$ is the influent and effluent SS concentration respectively. By plotting the term $S/(S_0 + S)$ against $1/t_r$, $T_A$ can be determined from the slope of the straight line (Amerlinck, 2015; Tay, 1982).

### 2.5.2 Takács et al., 1991

A well-known phenomenological model for the PST based on a 1-dimensional discretization in the vertical direction is that developed by Takács et al. (1991). While it was mainly developed for the secondary settlers, many models of the PST have been developed from this. In the model the settler is divided into 10 separate layers of constant thickness and a mass balance is performed around each layer considering fluxes of mass due to both gravity and bulk movement of liquid. In the model, as previously stated, only vertical flows are considered and it is assumed that the incoming solids in each clarifier layer are distributed instantaneously and uniformly across the entire cross-sectional area of the layer. A figure depicting the layered settling configuration can be seen in Figure 2.6 below.

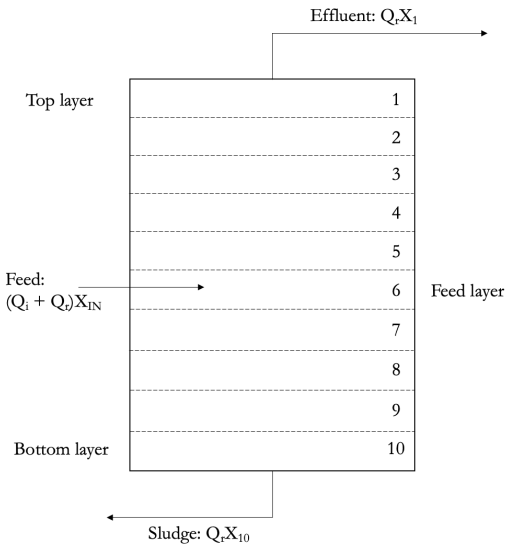


Figure 2.6: The layered settling configuration in the Takács model (Adapted from Takács et al., 1991)

For each layer, the fluxes entering and leaving it are summarized in Table 2.5.

Table 2.5: Input-Output summary for the layers in the model

| | Input | | | Output | |
|---|---|---|---|---|---|
| Layer | Feed | Settling | Bulk liquid flux | Settling | Bulk liquid flux |
| Top layer | - | - | Up | + | Up |
| Layers above feed layer | - | + | Up | + | Up |
| Feed layer | + | + | − | + | Up & Down |
| Layers below feed layer | - | + | Down | + | Down |
| Bottom layer | - | + | Down | - | Down |

Note: "+" = phenomena considered, "-" = phenomena not considered

One of the most commonly accepted settling velocity models is that of Vesilind (Larsen & Vesilind, 1968; Takács et al., 1991):

$$v_s = v_0 e^{-\alpha X} \tag{2.9}$$

where $v_s$ is the settling velocity of the suspension, $v_0$ the maximum settling velocity, $X$ the suspended solids concentration and $\alpha$ a model parameter. The model however, only applies for hindered and flocculent settling. Hence, Takács et al. (1991) used a modified version of the Vesilind equation as seen in equation 2.10 below.

$$v_{s,j} = v_0 e^{-r_h X_j^*} - v_0 e^{-r_p X_j^*} \tag{2.10}$$

where

$v_s$, $v_0$ = The same parameters as before only with $j$ denoting the layer calculated on for $v_s$
$r_h$, $r_p$ = Settling parameters characterizing the hindered settling and settling at low solids respectively
$X_j^*$ = $X_j - X_{min}$, where:
$X_j$ = The suspended solids concentration at layer $j$
$X_{min}$ = $f_{ns} X_{in}$, The minimum attainable suspended solids concentration computed as the product of the SS concentration entering the settler and the fraction of non-settleable solids in the incoming water

In this modified version of the equation the first term reflects the settling velocity of the larger well-flocculating particles while the second term is a correction factor accounting for the smaller, slowly settleable particles. Below a minimum concentration there is hence no gravitational settling (as the water is assumed to only consist of non-settleable solids) and above it the equation above will yield a velocity. The parameters in the expression above are the ones that are calibrated for the model.

With use of the settling velocity the gravity flux (directed downwards) from each layer is calculated as:

$$J_{s,j} = v_{s,j} X_j \tag{2.11}$$

and the bulk movement of the liquid as:

$$J_{bulk} = \begin{cases} J_{up,j} = & \frac{Q_i X_j}{A}, \text{ for } j > \text{feed layer} \\ J_{dn,j} = & \frac{Q_r X_j}{A}, \text{ for } j < \text{feed layer} \end{cases} \tag{2.12}$$

where

$J_{up,j}$ = The bulk liquid flux from layer $j$ directed upwards
$J_{dn,j}$ = The bulk liquid flux from layer $j$ directed downwards
$Q_i$ = The flow of water removed at the top of the PST (overflow)
$Q_r$ = The flow removed at the bottom of the PST (underflow)
$A$ = The surface area of the PST

For each layer except for the feed there is only a single bulk flux going out of the layer, but depending on the placement of the layer relative to the feed it is either directed upwards or downwards. For the feed layer however, the incoming feed with a flow of $Q_i + Q_r$ is split into one downwards flux and one upwards flux according to:

$$\begin{aligned} J_{up,feed} = & \frac{Q_i X_{in}}{A} \\ J_{dn,feed} = & \frac{Q_r X_{in}}{A} \end{aligned} \tag{2.13}$$

where $X_{in}$ is the SS concentration of the incoming feed. The total flux around each layer is the sum of the gravity and bulk liquid flux. The exception to the rule above is if the concentration in a layer is above a certain threshold concentration. In this case the downward flux from the layer above is restricted so that the layer below can handle the incoming flux.

Gerneay et al. (2001) extended the model to also include a detention time for the soluble components, flocculation and ammonification.

### 2.5.3 Ribes et al., 2002

Ribes et al. (2002) developed a model for the primary clarifier including sedimentation, compression processes and biological processes. The model proposed is, like that of Takács et al. (1991) a phenomenological 1-dimensional model where the settler is divided into 10 separate layers and a mass balance is calculated around each layer in accordance with the flux theory. The settling model considers both flocculent settling and hindered settling which are described by the double exponential function in equation 2.10 proposed by Takács et al. (1991). Compression settling is also included and is described by use of the compression factor concept proposed by Härtel and Pöpel (1992):

$$\Omega = \frac{1 - B \cdot h_t^{-(1+2 \cdot F_{SVI})}}{1 - B \cdot [min(h, h_t)]^{-(1+2 \cdot F_{SVI})}} \tag{2.14}$$

where $\Omega$ is the compression factor and h the height in the settler. With $SVI$ denoting the sludge volume index $F_{SVI}$ and $B$ can be computed according to equations 2.15-2.16:

$$F_{SVI} = \frac{SVI}{100 + SVI} \tag{2.15}$$

and

$$B = -\left(\frac{1}{F_{SVI}} + 1\right) \cdot h_c^{1+2 \cdot F_{SVI}} \tag{2.16}$$

Finally $h_c$ and $h_t$ are defined as:

$$h_c = \left(1 - \frac{1}{X_c r_h}\right) \cdot \left(\frac{X_f h_f}{X_c}\right) \tag{2.17}$$

and

$$h_t = min(2 \cdot h_c, h_f) \tag{2.18}$$

where $h_f$ is the height of the feed, $X_f$ is the influent solids concentration, $r_h$ a settling parameter characteristic of the hindered settling zone and $X_c$ is computed as following:

$$X_c = \frac{480}{SVI} \tag{2.19}$$

A biological model which is an extension of ASM2 including fermentation is also incorporated in the model and stationary concentrations are obtained by iterative procedures between the settler model and the biological model. As the two models (the settler model and biological model) use different variables (kg SS/m3 and kg COD/m3 respectively) conversion factors are applied between the two. Finally when the difference in concentration for all components are sufficiently small in two consecutive iterations, the iteration procedure is terminated.

### 2.5.4 Bürger et al, 2013

Another model developed for the secondary settlers is the model by Bürger et al (2013). This model is also one-dimensional dividing the settler into different layers (here, N layers). Around each layer the conservation law is applied by the governing partial differential equations. The partial differential equations describe nonlinear convection-diffusion terms for the solids concentration as a function of depth and time. In the model the outlet concentrations are distinguished from the concentrations in the top and bottom layers of the settler, unlike with the Takács model, and the model allows for use of different constitutive relations within the model to describe processes such as hindered settling, compression settling and dispersion. This allows the user to switch on and off these processes depending on the modelling goal as well as investigate the suitability of different constitutive functions. By turning on and off different processes the settler model could be turned into a primary settler model rather than a secondary one. A possible extension proposed in the article includes distinguishing the particles between different floc sizes (Bürger et al., 2013).

In the article different methods are presented for the secondary settler simulator among which a method-of-lines would enable the model to be used together with ordinary differential equation solvers for the biokinetic model equations describing the biological reactions taking place (Bürger et al., 2013).

### 2.5.5 Models based on particle settling velocity distribution

When trying to describe the settling phenomena based on particle settling velocity, most of the models use only a single settling velocity to describe all of the particles. Particles in the wastewater however, are characterized by a wide range of settling velocities and by characterizing and grouping the particles based on their settling velocities Bachis et al. (2015) hoped to improve the description of the PST. The phenomenological grey-boxed model proposed by Bachis et al. (2015) was originally inspired by the works of Marejouls et al. (2012) that introduced the PSVD approach when modelling retention tanks.

Similar to the model by Takács et al. (1991), they divided the PST into a number of layers and a mass balance was calculated around each layer. For the model, Bachis et al. (2015) divided the particles into five settling velocity groups (SVGs). Originally the use of only three SVGs was tested, but this resulted in a less accurate simulation of the data. In general, adding more SVGs will improve the accuracy, but it comes at the cost of a more computationally demanding model.

To characterize the wastewater into the different SVGs, the team performed several ViCAs experiments. The settling velocity distribution function (% TSS against $v_s$) was calculated in accordance with the ViCAs protocol and when calibrating the model the location of the boundaries of the five settling velocity class were adjusted. When changing the boundaries of the SVGs, the corresponding TSS fraction of the group was adjusted accordingly (Bachis et al., 2015). The calibrated model managed to make good effluent predictions for the TSS. However, while the TSS effluent predictions were good, only the TSS removal was modelled and the TSS was not characterized according to its relevant components. Polorigni et al. (2021) took it a step further attempting to characterize the TSS into it subclasses unbiodegradable particulate inert organic matter ($X_U$), slowly biodegradable matter ($X_B$) and inorganic settleable solids (ISS). When modelling only the TSS concentration, the TSS removed is assumed to settle out at the same fractions as its subcomponents. This however does not need to be the case as observations of removals of $X_U$, $X_B$ and ISS in a PST with a specific wastewater composition have shown removals in ranges of 60-70%, 30-40% and 70-90% respectively (Polorigni et al., 2021) . Not adequately modelling the split of these fractions in the PST will affect the coming processes of biological treatment and anaerobic digestion in a plant-wide model context and for design, not taking this into consideration might yield less than optimal results in subsequent processes.

Hence what Polorigni et al. (2021) did was to, instead of only dividing the TSS into 5 SVGs as Bachis et al. (2015), divide each subclass of TSS into 5 separate SVGs.

### 2.5.6 Computational Fluid Dynamics models

A further step to include the theoretical knowledge of the systems is the use of computational fluid dynamics (CFD) models. As the computational resources are growing, numerical 3D-models are gaining popularity, revealing more details of the settling process (Liu & Garcıa, 2011). In this section 2 different CFD models will be discussed. He et al. (2004) applied a CFD model with the aim of investigating the particle capture rates under various flow conditions in a combined sewer overflow retention treatment basin. In their model they uncoupled the modelling of flow hydrodynamics and that of the particle transport, an approach that was deemed valid for particle concentrations less than 1000 mg/L (He et al., 2004). The simulation of the flow conditions was done by use of a two-phase volume of fluid model with unstructured mesh. The results from this simulation was then used to run the particle transport model. For this part the Euler-Lagrangian approach was used, tracking the movement of individual particles by calculating the balance of forces on them, see equation 2.20:

$$\frac{dv_p}{dt} = C_D(v - v_p) + g\frac{\rho_p - \rho_w}{\rho_p} + F_x \tag{2.20}$$

where

$v$ = The fluid phase velocity
$v_p$ = The particle velocity
$\rho_w$ = The density of the fluid, water
$\rho_p$ = The density of the particle
$C_D$ = The drag coefficient
$F_x$ = The additional forces on the particle

The Euler-Lagrangian approach assumes the particles to be spherical and to not interact with each other. In total two particle sizes were used for the simulations (He et al., 2004).

The second CFD model described in this section is that of Liu and Garcia (2011). The two constructed a CFD model with the aim of improving the design of several large PSTs to be built at the Calumet Water Reclamation Plant, Chicago and the model considers the particulate flow, turbulence, hindered settling and sludge rheology, i.e. an intrinsic property related to the deformation and flow of the sludge (Jiang & Zhou, 2020). To describe the particulate flow a partially mixed two-fluid approach (which assumes the relative velocity between the water and particles to be described by an algebraic function of the water velocity and the particle settling velocity) is used. This approach assumes the particle inertia effect and particle relative acceleration to be negligible in comparison with the fluid phase. A $k - \epsilon$ turbulence model together with a Birmington plastic model is used to describe the turbulence and rheology of the sludge respectively. Finally hindered settling is described by use of the double exponential function proposed by Takács et al. (1991) and the particles are divided into different groups according to their sizes with shear-induced flocculation between the groups being modelled in accordance with Lyn et al. (1992). For a more detailed description of the two models the reader is referred to the articles in question (He et al., 2004; Liu & Garcıa, 2011).

While greatly improving the description of the flow patterns, a process of high importance to the sedimentation performance in the PSTs, the increased complexity of the hydraulic characterization might be accompanied by some incorrect modelling of the settling process. Amerlinck (2015) was critical to the use of the double exponential equation for hindered settling in the model by Liu et Garcia (2011) and the use of only two particle classes for the model by He et al. (2004) as well as the choice of a very high density for the particles. The reason for his critique against the settling velocity model by Takács et al. (1991) was the relation between the settling velocity and the local concentration. While it may describe the hindered settling reasonably well, Amerlinck (2015) was skeptic to how well this would hold for discrete and flocculent settling. This, as in regions of low solids concentrations an average settling velocity could lead to poor estimates of the solids distribution as different sized particles actually settle with different velocities. Furthermore, when dealing with CFD models in general, huge amounts of data would be required for validation of the models and as they are highly computationally demanding the use of the models would be restricted within scenario based optimizations (Amerlinck, 2015).

# Chapter 3

# Methodology

In this project the incoming wastewaters at two different WWTPs were characterized with respect to the settling velocity distribution of the particles in the water. The first WWTP, Källby WWTP, is situated in Lund and treats wastewater from over 100 000 people in Lund and its surrounding areas (VA SYD, 2021). As many other WWTP, Källby WWTP has preliminary treatment physically removing the larger particles, primary treatment (sedimentation), a biological treatment step and a final chemical treatment step. The plant also has treatment of the sludge from the primary, biological and chemical step extracting energy from the organic material. The discharge of the water is made into ponds acting as an extra polishing step before being led out to the river Höje å. The current biological step consists of an activated sludge process with pre-denitrification and internal recirculation (VA SYD, 2021). A process scheme for the plant can be seen in Figure 3.1 below.

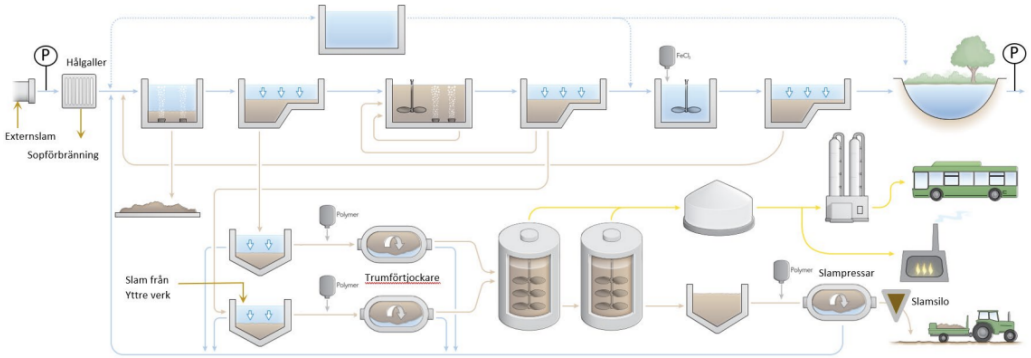


Figure 3.1: Process scheme for Källby WWTP (VA SYD, 2021)

The second WWTP considered in this project is Öresundsverket which is situated in Helsingborg. With about 138 000 people connected and a few smaller and larger industries (NSVA, n.d.-a) the WWTP has a larger load than Källby WWTP. A main characteristic for Öresundsverket is that it is one of the largest WWTPs in Sweden to be run with mainly biological removal of phosphorus. After preliminary treatment with screens and a sand trap, the incoming wastewater is led to the primary settlers. Here the larger particles settle out and some of the primary sludge is hydrolysed and fermented in the sludge pocket

and then resuspended to create an easily biodegradable source of carbon for the following biological treatment step, something that is especially needed when removing phosphorus biologically. The biological treatment at Öresundsverket consists of an activated sludge process and it includes both aerobic, anoxic and anaerobic zones to promote growth of different microorganisms. The sludge from the PSTs and the biological step is thickened and digested and the produced biogas is then upgraded and distributed on the European gas network (NSVA, n.d.-a).

At last after full treatment, the water from Öresundsverket is discharged into Öresund, the strait between Denmark and Sweden (NSVA, n.d.-a). A process scheme for the WWTP can be seen in Figure 3.2 below.

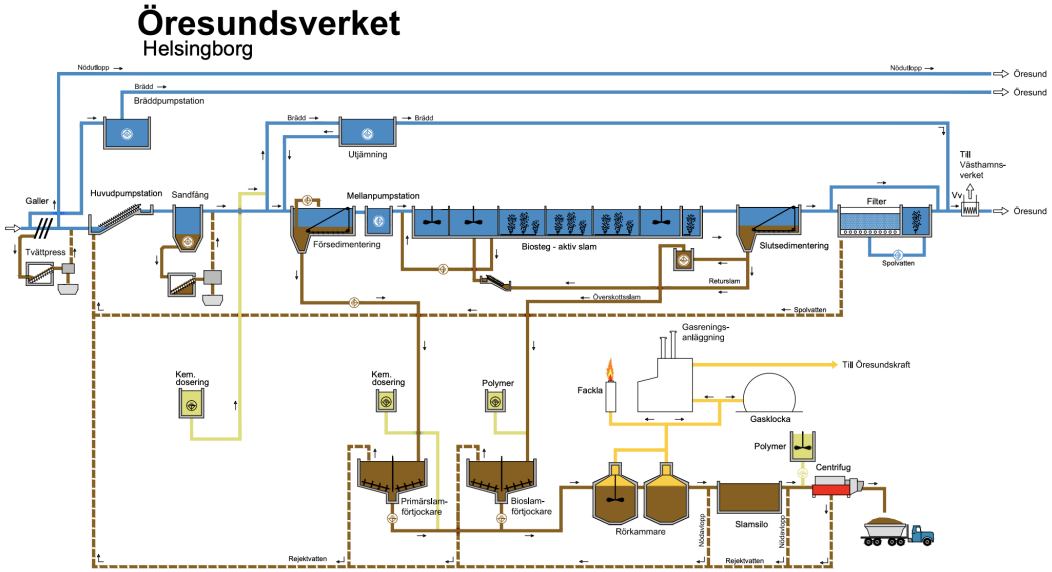


Figure 3.2: Process scheme for Öresundsverket (NSVA, n.d.-b)

## 3.1 Settleometer Set-up and Operation

The 5-column settleometer, previously described in Section 2.4.2, was used for this project. Each column has a height of approximately 1 m and in ascending order internal diameters of 45.2, 67.6, 86.4, 105.6 and 134.4 mm. The water to be fractionated enters through the bottom of the smallest column to the largest at a constant flow rate. A picture of the set-up can be seen in Figure 3.3 below and the corresponding data for the set-up is collected in Table 3.1.

Table 3.1: Data for each column in the 5C-settleometer

| Column | 1 | 2 | 3 | 4 | 5 |
|---|---|---|---|---|---|
| Diameter [m] | 0.0452 | 0.0676 | 0.0864 | 0.1056 | 0.1344 |
| Area [$10^{-3}$ $m^2$] | 1.60 | 3.59 | 5.864 | 8.76 | 14.19 |
| Volume [L] | 1.60 | 3.59 | 5.864 | 8.76 | 14.19 |

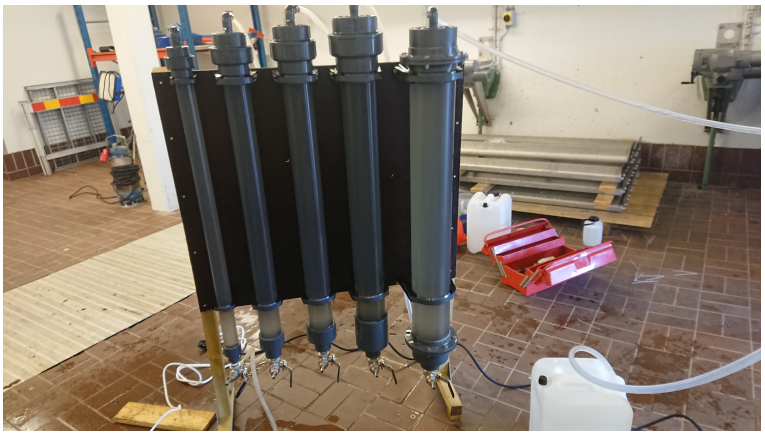

Figure 3.3: The 5C-settleometer, set-up

### 3.1.1 Operation and Collection of Samples

For all of the runs a sample of incoming water was first pumped up and collected in four 20-litre canisters right before the start of the experimentation. The pump used in the experiments was a Shenchen Precision Pump of the M6-series with a capacity of 0.2-1200 mL/min. The water was then poured into a bucket from which it was pumped into the set-up, over time adding more of the collected water into the bucket throughout the duration of the experiment. To ensure that the water in the bucket was thoroughly mixed an aquarium pump was added to stir the water. The water was also sieved (2-3 mm) upon pouring it into the bucket to ensure that nothing in the water will be large enough to clog the pump. This was especially important at Källby WWTP where, at the time, there were some issues with the screens for the pre-treatment. Once the columns had all been filled up, the effluent of the settleometer was collected in another vessel and once the whole experiment was finished the columns were emptied from largest to smallest and samples were collected for each column (and effluent). The influent sample was taken at the beginning by mixing water from the different canisters to get a proportionate sample. Lastly, the settleometer was flushed through by running clean water through it and emptying it again.

Before starting the actual runs the whole set-up was filled up and different pump settings were tested to determine a calibration curve between the flow velocity and the pump frequency. The flow velocity was determined by measuring the effluent volume yielded during a specific time. A good fit of the linear curve was found, however it was later on discovered that the flow velocity could deviate from the curve depending on the amount of air in the system, with a higher flow velocity pushing out more air from the plastic tubes. This mostly resulted in the desired frequency to be slightly lower than estimated from the calibration curve as the use of different (higher) speeds during the calibration had pushed more air out of the tubes before testing the lower frequencies. Hence, the effluent flow velocity during the actual experiments was always measured to verify and determine the actual flow.

In *Evaluation of a data-driven primary sedimentation tank model using settleometer data* Mazivila (2022) had large issues with the pump throughout the experiments as the increasing hydraulic pressure in the columns, among other things, resulted in a progressive

decrease of flow rate in the columns. Something that had to be fixed by altering the pump frequency manually throughout the experiments. Because of this, the time to fill up the individual columns was measured in each experiment here and the flowrates were calculated by use of the column volumes. The time was measured as the time between the overflow of the previous column and the overflow in the current one. The results were varying, but not necessarily decreasing likely due to the different type of pump. As some water was accumulated inside some of the plastic tubes connecting the PVC-columns, the volume filled up during the measured time was in some respect deceiving. It was also noted that with tighter fastenings of the tubes, less water was accumulated and the flow increased. When tightened during the experimentation, this sometimes allowed particles that had previously settled in one column to travel to the next (most notably for column 1 where a large heap of particles could travel to the next). As the tubes occasionally had to be loosened to empty the settleometer, this was a problem that could occur during most of the experiments. To assign a flow velocity to the experiment, the average of the effluent flow velocity measurements was used.

To compensate for the lags in flow velocity when water is accumulated in the tubes and to more accurately predict the flow velocity, some consideration was taken to whether one, before starting the experiment, should fill up the settleometer with clean water. This was, however, not decided as the measurements of the effluent compositions would be less accurate.

### 3.1.2 Choice of flow velocity

For a given flow velocity the upflow velocities in each column can be calculated according to Equation 2.6. Any flow velocity can be used to characterize the water, but for the characterization to be useful the upflow velocities should reflect the characteristics of the PST to be described (and in the case of Öresundsverket, to be modelled). The range of upflow velocities during the trials should therefore include the average overflow rate of the PST. Including a range of higher velocities allows for the prediction of the PST's behaviour at higher flows while including lower velocities better helps describe the removal of particles with a settling velocity less than the overflow rate as well as predicting the behaviour of the PST should its surface area be changed. Maintaining the average overflow rate somewhere in the middle of the upflow velocities is thus desired. However, for the low velocities to be achieved, the time the settleometer has to run needs to be extended causing other issues to arise, such as how feasible it is to run the experiment for a longer time (e.g. managing to start and finish the experiment within a work day as well as delivering the collected samples to a lab where they can be stored in a cold room) not to mention allowing for more degradation to occur. There is thus a trade-off between achieving the lower velocities and the feasibility of the experiment as well as the representativeness of the samples collected.

In the following subsections data for the PSTs at Källby and Öresundsverket will be presented along with choice of flow velocity at each WWTP.

### Källby WWTP

At Källby WWTP there are in total 12 rectangular PSTs with a collective area of 1 600 $m^2$ and a collective volume of around 3 100 $m^3$. The depth of each PST can thus be calculated to around 1.9 meters (VA SYD, 2021). With an average incoming flow to the plant of around 31 000 $m^3/d$, the primary clarifiers have an average retention time of 2.4 h and an average overflow rate of about 0.8 m/h.

At Källby WWTP the chemical sludge is circulated through the PSTs before being collected together with the primary sludge. Also worth mentioning is the fact that the distribution network to Källby WWTP is mainly driven by gravity (VA SYD, 2021), something quite rare which might affect the size of the particles as they have been less processed and broken down by pumps.

For the first two runs at Källby a flow rate of 0.19 L/min was targeted as this would yield the following upflow velocities (Table 3.2), placing the average overflow rate at Källby at the lower limit for the last column.:

Table 3.2: Upflow velocities for $Q = 0.19$ L/min

| | 1 | 2 | 3 | 4 | 5 |
|---|---|---|---|---|---|
| $v_{up,i}$ [m/h] | 7.10 | 3.18 | 1.94 | 1.30 | 0.80 |

While it might be preferably to, as mentioned in the previous section, try to place the average overflow rate somewhere in the middle of the velocity ranges this was not deemed feasible. At a flowrate of 0.19 L/min it would already take close to 3 hours to fill up the 5 columns. If one instead were to place the average overflow rate at Källby as the upflow velocity of column 4, it would take almost 5 hours just to fill up the 5 columns. Upon filling up the 5 columns it is of course then desired to allow the set-up some time to run allowing more particles to exit a column in which they do not belong, making the first choice of flowrate the most feasible one in practice. Thus a flow rate of 0.19 L/min was targeted and a total time for the experiment of slightly more than 4 hours was chosen. Because of the issues of predicting the flow rate based on the pump frequency described in Section 3.1.1, slightly higher flow rates were achieved in practice.

For the third and final run at Källby a much higher flow rate was chosen to verify that the particles were displaced from the smaller columns to the larger ones compared to the previous trials.

### Öresundsverket

At Öresundsverket the water from the pre-treatment is transported through 4 lines, each line containing two primary settlers in parallell with an area of 300 $m^2$ respectively, e.g. 2400 $m^2$ in total (NSVA, n.d.-a). With an average incoming flow of 55 000 $m^3/d$ to the primary sedimentation the average retention time for the PSTs is then about 3.85 h and the average overflow rate 0.95 m/h. Unlike with Källby however, it was here looked into further how the overflow rate changes with time. In Figure 3.4 below the overflow rates during 2021 for the two primary settlers in line 4 at Öresundsverket are plotted. The data

was based on hourly flow measurements and it is clearly seen in the figure that despite the average overflow rate being close to 1 m/h, it is not that uncommon for the overflow rate to drop down to almost half of that. Hence, it might not be sufficient to, as done at Källby, simply place the average overflow rate as the upflow velocity in the final column. 4 runs were in total made at Öresundsverket, the first one done like at Källby placing the

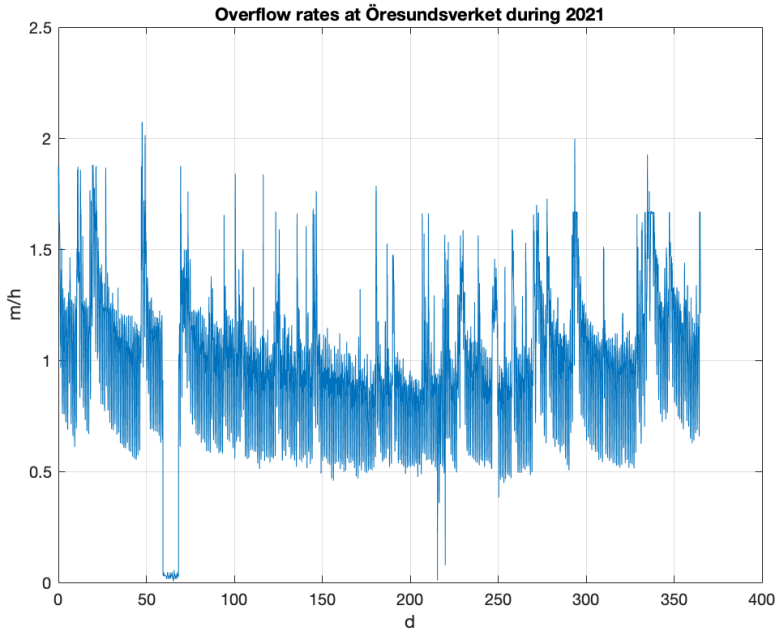


Figure 3.4: Overflow rates at Öresundsverket during 2021. The significant drops in overflow rates are due to measurement errors or emptying and cleaning the settling tank (Wärff, 2022).

average overflow rate as the lowest upflow velocity in the final column. The 3 next runs however were done differently. Simply lowering the flow velocity so that 0.5 m/h would be achieved in the final column would encounter the same issues mentioned previously with the feasibility of the experiment in practice. However, as is seen in Figure 3.4 we are mainly only interested in the particles with settling velocities up to 2 m/h, above that it is no longer as interesting in how the particles are distributed from a modelling perspective. If the flow velocity then were to be lowered to achieve an upflow velocity of around 0.5 m/h in the final column, the upflow velocity in the first column would be much higher than what is relevant for the purpose of this study, see Table 3.3 below for the upflow velocities at this flow rate.

Table 3.3: Upflow velocities for $Q = 0.12$ L/min

| | 1 | 2 | 3 | 4 | 5 |
|---|---|---|---|---|---|
| $v_{up,i}$ [m/h] | 4.49 | 2.01 | 1.23 | 0.82 | 0.51 |

Hence what was done during the last three runs was to disconnect the fifth column from the settleometer and only use the first four, thus decreasing the time it would take to fill the whole set-up compared to before. The time for the experiment was still prolonged to account for the longer time required to fill up the settleometer, but unlike at Källby

WWTP, the flow rate was varied between the three experiments to gain more insight into how the particles are distributed within this settling velocity range.

### 3.1.3 Experiments

#### Källby WWTP

Over the course of the project 3 runs with the settleometer were made at Källby on the 10/10, 18/10 and the 24/10 2022. The flow rates, end times and upflow velocities for the three respective runs can be seen in Table 3.4 below:

Table 3.4: Flow rates, end times and upflow velocities for the three runs at Källby WWTP

| **Date** | **Q** $[L/min]$ | $\mathbf{t_{end}}$ $[h]$ | $\mathbf{v_{up,1}}$ $[m/h]$ | $\mathbf{v_{up,2}}$ $[m/h]$ | $\mathbf{v_{up,3}}$ $[m/h]$ | $\mathbf{v_{up,4}}$ $[m/h]$ | $\mathbf{v_{up,5}}$ $[m/h]$ |
|---|---|---|---|---|---|---|---|
| 10/10 | 0.208 | 4.17 | 7.78 | 3.48 | 2.13 | 1.42 | 0.88 |
| 18/10 | 0.212 | 4.08 | 7.93 | 3.54 | 2.17 | 1.45 | 0.90 |
| 24/10 | 0.539 | 2.08 | 20.14 | 9.01 | 5.51 | 3.69 | 2.28 |

Due to some issues with the anaerobic digesters, where a lot of organic material was coming back with the reject water, the set-up was placed after the screens but before the connection of the reject water and hence also before the sand trap and connection of the chemical sludge. See Figure 3.5 for clarification.

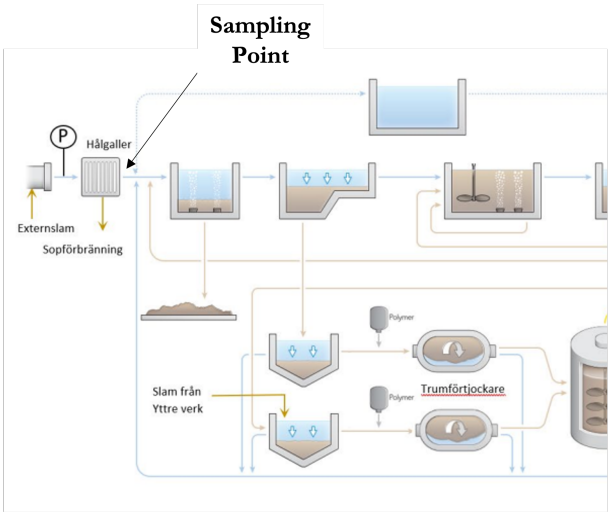


Figure 3.5: Sampling Point at Källby WWTP. (Modified from VA SYD, 2021)

On the times of the three runs, the two first ones had dry-weather flows while wet-weather conditions occurred during the last one due to heavy rains the day before (Forså, 2022).

**Öresundsverket**

At Öresundsverket 4 runs were made in total on the 31/10, 8/11, 15/11 & on the 28/11 2022. The flow rates, end times and upflow velocities for the four runs can be seen in Table 3.5 below:

Table 3.5: Flow rates, end times and upflow velocities for the three runs at Öresundsverket

| **Date** | **Q** $[L/min]$ | $\mathbf{t_{end}}$ $[h]$ | $\mathbf{v_{up,1}}$ $[m/h]$ | $\mathbf{v_{up,2}}$ $[m/h]$ | $\mathbf{v_{up,3}}$ $[m/h]$ | $\mathbf{v_{up,4}}$ $[m/h]$ | $\mathbf{v_{up,5}}$ $[m/h]$ |
|---|---|---|---|---|---|---|---|
| 31/10 | 0.215 | 4.0 | 7.78 | 3.48 | 2.13 | 1.42 | 0.88 |
| 8/11 | 0.090 | 4.75 | 3.37 | 1.50 | 0.92 | 0.62 | - |
| 15/11 | 0.080 | 4.83 | 2.99 | 1.34 | 0.82 | 0.55 | - |
| 28/11 | 0.098 | 4.67 | 3.66 | 1.64 | 1.00 | 0.67 | - |

The water was sampled right before entering the two PSTs in line 4, hence all extra streams were included. In Figure 3.6 the sampling point is indicated in the process diagram of the WWTP.

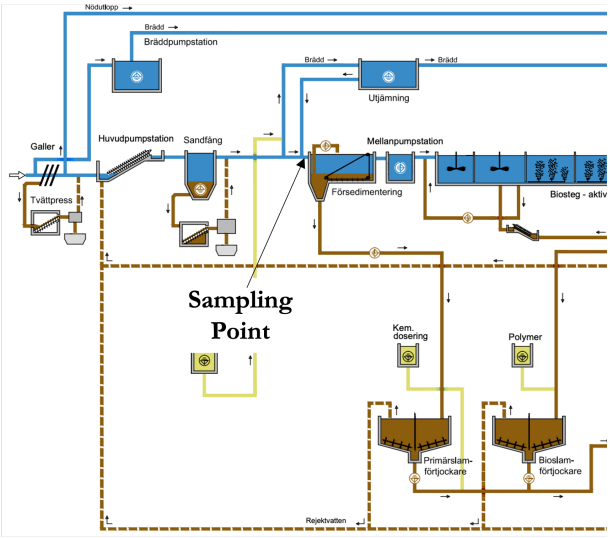


Figure 3.6: Sampling Point at Öresundsverket. (Modified from NSVA, n.d.-b)

All four runs at Öresundsverket had dry-weather conditions (Wärff, 2022) and during the last two runs the samples collected were immediately placed in a cooling box to minimize the biological degradation occurring after the end of the experiment.

## 3.2 Chemical analyses

The samples collected from the settleometer were then to be analyzed. For each sample (i.e. from each of the columns as well as the influent and effluent) the total and soluble COD, the TSS, VSS & ISS as well as the slowly biodegradable and particulate inert substrates are to be determined.

### 3.2.1 COD-analysis

To measure the COD, Hach cuvettes LCK114 (for 150-1000 mg COD/L) and LCK314 (for 15-150 mg COD/L) were used and the corresponding instructions were followed (Hach, n.d.). The first step of the procedure was to invert the cuvettes a few times to bring the sediment into suspension. For each (mixed) sample, 2 ml were added to a clearly labeled cuvette, the cuvette was then closed and inverted to mix the solution before being placed in a heat block for 2 hours at 148 °C. After heating they were again inverted to mix the solution. Before measuring the COD, the cuvettes were placed in a test tube rack to cool down to room temperature. Once cooled down they were placed in the corresponding spectrophotometer unit of the system to read the COD concentration.

If the sample to be analysed was suspected to contain a COD concentration above the range applicable for the cuvettes, the sample was diluted before being added to the cuvettes in the first step. Apart from the total COD, the filtered COD was sometimes analyzed as well. Rather than adding the mixed (and sometimes diluted) sample to the cuvettes, 2 ml of a sample filtered through a 0.1 $\mu$m syringe filter was instead added.

### 3.2.2 TSS, VSS & ISS-analysis

The measurements of TSS, VSS & ISS were made in accordance with the standard methods SS-EN 872:2005 and SS 028112. To measure the TSS of the samples collected, the samples were vacuum filtered through 1.6 $\mu$m glassfibre filters (after thoroughly turning the bottles to mix the samples). The volume of the sample that was filtered was measured (V) and the filters were weighed before ($m_0$) and after drying in an oven at 105 °C for the minimum of one hour ($m_1$). The TSS concentration was then calculated as the difference in weight divided by the volume of the filtered sample:

$$TSS = \frac{m_1 - m_0}{V} \tag{3.1}$$

To measure the VSS-content of the sample the dried filter was then incinerated in an oven at 550 °C for at least 2 hours, measuring the weight of the filter + residue ($m_2$) and calculating the difference compared to before as the volatile substances have combusted.

$$VSS = \frac{m_1 - m_2}{V} \tag{3.2}$$

As some of the weight of the filters will be lost during the procedures the measured masses $m_1$ and $m_2$ were adjusted to account for this. The filter losses for drying and incinerating the filters were measured as the mean loss of drying or incinerating one set of filter papers (i.e. 6-8 filters). This was measured as 0.167 mg for drying and 1.438 mg for incineration.

Finally, the ISS was calculated as the difference between the two:

$$ISS = TSS - VSS \tag{3.3}$$

### 3.2.3 Aerobic degradation

In order to estimate the slowly biodegradable substrate as well as the inert particulate matter in each SVG, a method was used to estimate the inert particulate matter was and by removing it from the initial particulate COD in each group the slowly biodegradable substrate could be determined. This would technically yield both the slowly biodegradable matter and the biomass, however, it is a common assumption to neglect influent heterotrophic biomass as most model calculations always assumes the presence of these organisms anyway (Roeleveld & Van Loosdrecht, 2002). The assumption is based on the theory that the bacterial diversity in the activated sludge is a product of the environment rather than inoculation by the wastewater (Roeleveld & Van Loosdrecht, 2002). Furthermore, for modelling of the PST, the slowly biodegradable substrate and the biomass are here assumed to have the same settling velocity distributions. To determine the inert particulate matter, the proposed method number 2 in Orhon et al. (1994) was used. The theory behind this method is described below.

#### Theory (Orhon et al., 1994)

Two aerated batch reactors, one with unfiltered wastewater and one with filtered, are inoculated with a small amount of biomass previously acclimated to the wastewater and subjected with aerobic conditions long enough to deplete all biodegradable substrates in the water and mineralize all biomass. The initial total ($C_{T0}$) and filtered ($S_{T0}$) COD are measured at the start of the experiment and the final concentrations for the total ($C_T$) and soluble ($S_T$) COD are measured at the end of the experiment.

The total COD in the reactor fed with unfiltered wastewater initially had a composition of input readily biodegradable substrate ($S_{B0}$), slowly biodegradable input substrate ($X_{B0}$), inert soluble substrate in the feed ($S_U$) and inert particulate substrate in the feed ($X_U$).

$$C_{T0} = S_{B0} + X_{B0} + S_U + X_U = C_{B0} + S_U + X_U \tag{3.4}$$

where $C_{B0}$ is the total input biodegradable substrate, i.e. the sum of the input readily biodegradable and slowly biodegradable substrate. Assuming, at the end of the experiment, $S_B$, $X_{OHO}$ (biomass) and $X_B \approx 0$, the final threshold concentrations in reactor 1 will be as follows:

$$C_{T1} = S_{P1} + S_U + X_{P1} + X_U \tag{3.5}$$

and

$$S_{T1} = S_{P1} + S_U \tag{3.6}$$

where $S_P$ and $X_P$ are the soluble and particulate microbial decay products. In ASM the soluble microbial decay products are often deemed negligible and are thereby not included in the model structure (Henze et al., 2000). The particulate final concentrations could then be calculated as:

$$C_{T1} - S_{T1} = X_{P1} + X_U \tag{3.7}$$

and the total amount of COD removed as:

$$\Delta C_{T1} = C_{T0} - C_{T1} = C_{B0} - S_{P1} - X_{P1} \tag{3.8}$$

Assuming the reaction time to be long enough to complete all biological reactions, the sludge age to approach infinity, the hydraulic and particulate dilution rates to approximately equal 0 and the readily biodegradable substrate ($S_B$) to be depleted, the residual particulate and soluble microbial product concentrations ($X_P$ & $S_P$ respectively) can be calculated as follows:

$$X_{P1} = Y_{PX} C_{B0} \tag{3.9}$$

and

$$S_{P1} = Y_{PS} C_{B0} \tag{3.10}$$

where $Y_{PX}$ and $Y_{PS}$ are residual particulate and soluble microbial product coefficients. Hence the total amount of COD removed could be calculated as:

$$\Delta C_{T1} = (1 - Y_{PX} - Y_{PS}) C_{B0} \tag{3.11}$$

Similarly for the second reactor fed with the filtered wastewater the initial COD can be expressed as follows:

$$S_{T0} = S_{B0} + S_U \tag{3.12}$$

and the final threshold concentrations as this:

$$C_{T2} = S_{P2} + S_U + X_{P2} \tag{3.13}$$

$$S_{T2} = S_{P2} + S_U \tag{3.14}$$

Correspondingly the residual particulate microbial products concentration can be directly expressed as:

$$C_{T2} - S_{T2} = X_{P2} \tag{3.15}$$

and the amount of COD removed as:

$$\Delta C_{T2} = S_{T0} - C_{T2} = S_{B0} - S_{P2} - X_{P2} \tag{3.16}$$

Under the same assumptions as the first reactor the residual microbial products concentrations could also be calculated by use of the residual microbial products coefficients.

$$X_{P2} = Y_{PX} S_{B0} \tag{3.17}$$

$$S_{P2} = Y_{PS} S_{B0} \tag{3.18}$$

and the values inserted for $C_{T2}$:

$$\Delta C_{T2} = (1 - Y_{PX} - Y_{PS}) S_{B0} \tag{3.19}$$

Combining equations 3.9 and 3.17 gives:

$$X_{P1} = X_{P2} \frac{C_{B0}}{S_{B0}} \tag{3.20}$$

where $X_{P2}$ is measured directly in the experiments by equation 3.15. Similarly combining equations 3.11 and 3.19 allows the substitution of the removed COD as opposed to the initial biodegradable concentrations.

$$X_{P1} = X_{P2} \frac{\Delta C_{T1}}{\Delta C_{T2}} \tag{3.21}$$

Replacing and subtracting this term into equation 3.7 finally gives the initial inert particulate COD concentration:

$$X_U = C_{T1} - S_{T1} - (C_{T2} - S_{T2})\frac{\Delta C_{T1}}{\Delta C_{T2}} \tag{3.22}$$

In this case 8 reactors were run instead of 2 as 7 unfiltered sample were to be analyzed as opposed to 1. The reactor fed with the filtered wastewater was here assumed to represent the rest as the soluble concentrations in incoming wastewater, the columns and the outgoing water should stay the same throughout the 5C-settleometer. To estimate the amount of time needed for the aerobic degradation experiment a pre-simulation was made.

### Method

Around 700 ml of water collected from the influent, the columns and the effluent were poured into 6-7 different Erlenmeyer flasks (the number depending on the amount of columns used in the previous experiment). Each flask was clearly labeled with its contents and date. For the filtered reactor, roughly 1 litre of influent water (or in the case of the Källby experiment, a mix of the influent, effluent and the three last columns) was prepared. The water was flocculated by use of $ZnSO_4$ (10 ml/L of 100 g/L solution) and by increasing the pH to around 10.5. After letting the particles settle the supernatant was then vacuum filtered through a 1,6 $\mu$m glassfibre filter and collected in an Erlenmeyer flask marked "Filtered Reactor". To each reactor a phosphate buffer ($KH_2PO_4$) was added to a final concentration of 15 mM and the pH adjusted to 7.5. Finally 1-2 ml of active sludge was added to each reactor and the liquid level was marked. Before starting the experiment the total and filtered (0.1 $\mu$m) COD was measured for each sample and a measurement of the total COD for the active sludge was done as well.

Figure 3.7: The aerobic degradation experiment

The reactors were run under intense stirring in a hood for approximately three weeks and COD measurements were done over time to measure the progress. The dissolved oxygen

concentration was verified during the experiments at approximately 8 mg/L. Each time the measurements were made the reactors were first filled up with distilled water to the level marked on each reactor to account for water loss through evaporation. Finally the experiment was ended and full measurements of the total COD and filtered COD were remade and used for calculating the $X_U$. To improve the results the contribution of particulate decay products formed by the activated sludge added was removed from the measured $\mathrm{COD_{Tot,\ end}}$ by use of the same equations as described in the next subsection.

For the aerobic degradation experiment based on the samples collected at Öresundsverket, triplicate measurements of the total and soluble COD were made on each sample to improve the accuracy of the calculated values. The samples collected were also immediately cooled and filtered on-site.

### Calculations

As the measurements for the filtered reactor were too uncertain, resulting in (for some reactors) negative values for the inert particulate fraction, calculations based on ASM1 (Henze et al., 2000) were also made. According to the ASM1 the slowly biodegradable substrate ($X_B$) is converted to readily biodegradable substrate ($S_B$) through hydrolysis. The readily degradable substrate is then removed by growth of heterotrophic bacteria. Not all of the substrate removed forms biomass ($X_{OHO}$) however, some is also oxidized into carbon dioxide. The ratio between the biomass formed and the substrate consumed in g COD/g COD is called the yield ($Y_{OHO}$). The biomass formed later on decays, forming particulate decay products ($X_P$) and slowly degradable substrate at the ratio of $f_P$ and $1 - f_P$ respectively. The slowly degradable substrate then goes through the whole process again until only particulate decay products remain. The whole process is depicted in Figure 3.8 below and is called the death-regeneration concept.

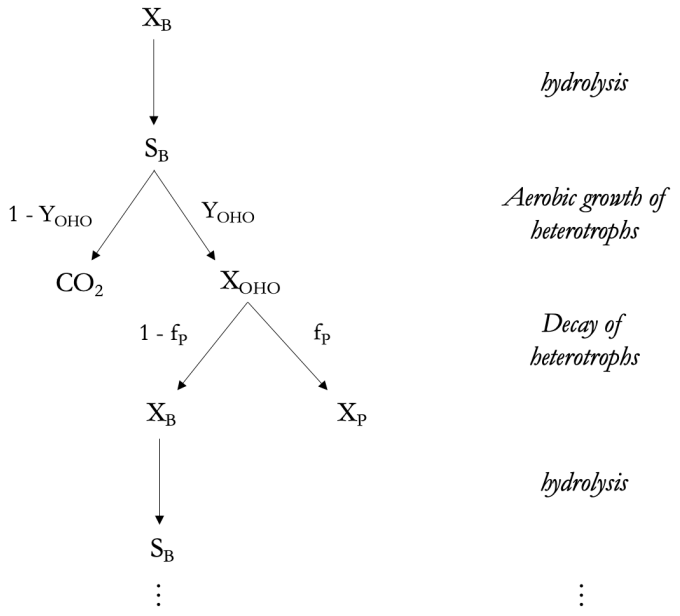


Figure 3.8: The death-regeneration concept of ASM1

1 g of $X_B$ is thus converted to:

$$1 \text{ g } X_B \Rightarrow \sum_{i=0}^{n} X_B \cdot Y_{OHO} \cdot f_P \cdot (Y_{OHO} \cdot (1 - f_P))^i = \frac{X_B \cdot Y_{OHO} \cdot f_P}{1 - Y_{OHO} \cdot (1 - f_P)} \text{ g } X_P \quad (3.23)$$

And the same goes for 1 g of $S_B$. Typical values for $f_P$ and $Y_{OHO}$ are 0.08 and 0.67 respectively (Henze et al., 2000).

With the starting values for the particulate and dissolved COD in each reactor, the particulate decay products produced in each reactor could be calculated assuming a fraction of $X_B$ ($f_{XB}$) from the particulate COD and the amount of inert soluble matter ($S_U$, $S_B$ is calculated as the filtered COD - $S_U$) in each reactor. The concentration of $S_U$ was assumed to be the same in all reactors, but the particulate biodegradable fraction was allowed to differ. The particulate biodegradable fractions as well as the inert soluble concentration was then estimated with the solver in Excel to minimize the sum of squared errors between the calculated particulate COD at the end of the experiment and the measured ones. Boundaries are set for the parameters with the fractions $f_{XB,i} \in [0, 1]$ and the $S_U$ concentration being positive but less or equal than the smallest value for the dissolved COD-concentrations at the end of the experiment. To ensure that the mass balances over the settleometer close, the particulate biodegradable fraction for the last reactor was not estimated, but its concentration calculated from the rest so that the mass balance for $X_B$ became accurate. The inert particulate amount in the final reactor was then finally calculated as the difference between the particulate COD and the slowly biodegradable matter ensuring the mass balance for $X_U$ to close as well.

## 3.3 Mass balances and fractions

When assigning the settling velocities and calculating the settling velocity distributions the fractions of TSS/VSS/ISS/$\text{COD}_\text{p}$/$X_B$/$X_U$ for each SVG were used. However, how these fractions were to be calculated is not entirely obvious. As measurements were made for all streams in the 5C-settleometer, mass balances could be made for each substance according to equations 3.27 and 3.28 by use of the time of the experiment and the measured flow velocity.

**Calculating the volumes and masses of each stream**

$$m_i = V_i \cdot c_i \quad (3.24)$$

$$V_{IN} = t_{end} \cdot Q \quad (3.25)$$

$$V_{OUT} = V_{IN} - \sum_{i=1}^{n} V_i \quad (3.26)$$

**Calculating the mass balance**

$$\text{Mass balance residual} = m_{IN} - \sum_{i=1}^{n} m_i - m_{OUT} \text{ (g)} \quad (3.27)$$

$$\text{Mass balance error} = \frac{\text{Mass balance residual}}{m_{IN}} \cdot 100\ (\%) \tag{3.28}$$

where

$m_i$ = mass of SS/COD/VSS/ISS in stream $i$ (g)
$V_i$ = volume of stream $i$ (L)
$c_i$ = concentration of stream $i$ (g/L)
$t_{end}$ = time of experiment (h)
$Q$ = flowrate (L/h)
$n$ = number of columns in use in the settleometer

The smaller (in absolute value) the mass balance error (MB error), the more reliable the data likely is. Most likely however, this calculated value will not equal zero meaning that the fraction of the incoming wastewater and the fraction of the sum of what is in the columns and what is leaving the system are not equal. In this project it was chosen to alter the measured values to close the mass balances and from this calculate the fractions as:

$$x_i = \frac{m_i^*}{m_{IN}^*} \tag{3.29}$$

where the star indicates that the values are modified. Although all of the modified data yielded from the experiments is presented in the results section, only the data for which the MB error deviated with less than ± 20 % was used in the model.

### 3.3.1 Closing the mass balances

Two methods were used to close the mass balances depending on whether multiple measurements were made or not. In both methods the difference in mass was distributed to the different measurements, equally (if only single measurements were made) or according to how much they varied (if multiple measurements were made). In appendix A.1 examples are shown on how to close the mass balance in the two cases.

Most commonly the original mass balance was positive (i.e. more was going in than out) and the largest variance between the measurements was found in the sample from column 1 (with the heaviest particles).

### 3.3.2 COD

When calculating the settling velocity distribution the particulate COD was of much more interest than the total one as the latter contained soluble COD of similar sizes in all measurements, skewing the proportions. Hence, when closing the mass balance for the particulate COD, the measured particulate COD in each experiment and sample was first calculated before closing the mass balance upon this. In reality the COD, and the soluble one in particular, likely does not close as some degradation may have occurred during the experiments.

For most of the experiments only one measurement was made for the soluble COD (that of the effluent which was believed to be the least affected by degradation) and it was

assumed that the rest would have very similar values. However, for the single experiment (15/11) where the soluble COD was measured for all of the samples it was discovered that the difference was larger than previously assumed. Hence, a similar distribution of the soluble COD in the different samples as found during this run was assumed for the other runs (for the runs with 5 columns in use, the value for the fifth column was taken as the mean of the value for column 4 and the effluent). If no measurement had been made on a run of the soluble COD, a mean was used from the other runs.

### 3.3.3 ISS

For the ISS, the values can be calculated and the mass balances closed as described in Section 3.3.1 above. However, when doing this it is no longer certain that the ISS + VSS concentrations would equal the TSS concentrations. Moreover, as the ISS concentrations are much smaller than the other two, but has the same measurement uncertainty the calculated values would be much more uncertain than for the TSS or VSS and a small change in value could have a much larger relative impact. Rather than doing this, it was for the ISS chosen to calculate the concentration as the difference in the modified TSS and VSS values. However, only the data using the latter method for which the two methods of calculating it had very similar values was chosen.

## 3.4 Assigning settling velocities and fractions to the SVGs

Originally, the purpose of the 5C-settleometer in this project was to simply use the data and fractions derived from the experiments and utilize those for the SVGs in the model. This is also what has been done in previous attempts as the amount of particles misplaced (i.e. particles in a column with a settling velocity less than the upflow velocity of the column) were deemed negligible in comparison with the number of particles in their correct place (Mazivila, 2022). However, after much thought and consideration this was deemed to not be the case here where the flow velocity was significantly decreased compared to previous studies. Hence, like with the ViCAs column, a calculation procedure to fit the data to a cumulative settling velocity distribution function was derived.

### 3.4.1 Background

A particle with a settling velocity $v_s$ travelling through a column indexed $i$ with an upflow velocity $v_{up,i}$, will not travel with same velocity as the water but with a net velocity of:

$$v_{net,i}(v_s) = v_{up,i} - v_s \tag{3.30}$$

This is illustrated in Figure 3.9.

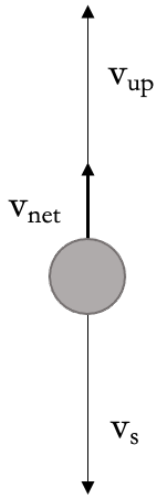


Figure 3.9: Net velocity of the particles in the settleometer

If $v_{up,i} > v_s$ then the particle will travel upwards in the column, while if the opposite holds true, the particle will be retained in the column. In the calculations that follow only the former will be considered as the particles otherwise will stay there. As each column has a height of 1 m, the time it will take for a particle of settling velocity $v_s$ to pass through the column can then be calculated as follows:

$$t_i(v_s) = \frac{1}{v_{net,i}(v_s)} \tag{3.31}$$

The smaller the net velocity is, the longer time it will take for the particle to exit the column. Examples can be seen in Table 3.6 where a net velocity of 0.5 m/h results in 2 hours to exit a column (approximately half of the experiment time for most of the runs) and a net velocity of 0.2 m/h results in a longer time to exit the column than what any of the experiments is actually run.

Table 3.6: Time to exit the column vs difference in velocity

| **Net velocity** (m/h) | 0.1 | 0.2 | 0.3 | 0.4 | 0.5 | 1 | 1.5 | 2 | 5 | 10 |
|---|---|---|---|---|---|---|---|---|---|---|
| **Time to exit column** (h) | 10 | 5 | 3.33 | 2.5 | 2 | 1 | 0.67 | 0.5 | 0.2 | 0.1 |

In theory column $i$ should retain all particles in the settling velocity range $[v_{up,i},\ v_{up,i-1}]$ and hence $v_{up,i}$ should be the smallest settling velocity of the particles retained within the column (with the exception of the particles just passing through that, with time, should become negligible in comparison). However, in practice due to the slow rate by which a particle pass through a column as their settling velocity approaches the upflow velocity together with the limited time the experiment is run, some particles of lower settling velocities than $v_{up,i}$ will not even exit the column during the time of the experiment. The smallest velocity for which this holds true in column $i$ is here denoted as $v^*_{up,i}$. For this velocity the time it requires to pass all previous columns as well as the current one equals the total time the experiment is run. $v^*_{up,i}$ can hence be determined as the minimum

velocity to solve equation 3.32 below. The other solutions to the equation correspond to the $v^*_{up,j}$ for the previous columns.

$$\sum_{j=1}^{i} t_j(v_s) = t_{end} \tag{3.32}$$

Assuming the influent concentration and particle settling velocity distribution to be constant the mass of particles of a certain settling velocity in a column is either 0, increasing with time or at a steady-state value. The first case occurs for particles with higher settling velocities that have not reached the column (either due to being retained in previous columns or because they have not yet reached the column, i.e. $v_s \geq v^*_{up,i-1}$). The second case occurs for particles with a settling velocity within the theoretical velocity range for the column or for particles that have not yet exited the column. Lastly for particles with a settling velocity less then $v^*_{up,i}$ (i.e. they have entered and exited the column during the experiment), the concentration of these particles is originally 0 then increasing until a steady-state concentration is reached. The mass of the particles for a certain settling velocity in the latter case can be computed, according to equation 3.33 as the product of the concentration of the particles in the incoming wastewater and the time during which particles of that settling velocity accumulate within the column.

$$m_i(v_s) = Q \cdot t_i(v_s) \cdot \frac{S(v_s)}{V_{in}} = \frac{Q}{V_{in}} \cdot t_i(v_s) \cdot S(v_s) \tag{3.33}$$

where

$S(v_s)$ = A function describing the total mass of SS/COD of the particles in the incoming wastewater with a settling velocity $v_s$

$Q$ = The flow velocity

$t_i(v_s)$ = A function describing the time during which particles of settling velocity $v_s$ accumulate within the column

$c(v_s)$ = $\frac{S(v_s)}{V_{in}}$, A function describing the concentration of particles with settling velocity $v_s$ in the incoming wastewater

Hence, the concentration of the particles in the columns at steady state will be higher than the concentration in the incoming wastewater, due to their slower upflow velocity relative the water. Once steady state has been reached however and the particles have started leaving the column, the effluent concentration of the particles with the specific settling velocity will be the same as that of the incoming wastewater.

### 3.4.2 Derivation of Calculation Procedure

To establish a calculation procedure, one must first be able to describe the data acquired, i.e. what is collected from each column. If the mass of the particles in column $i$ is denoted $m_i$, none of these particles will have a settling velocity higher than the upflow velocity of the previous column (if $i \neq 1$, else the settling velocity can reach as high as infinity). Some of the particles in the column however will have a settling velocity lower than its upflow velocity. The particles in the column at the end of the experiment can thus be

divided into two groups according to equation 3.34 depending on their settling velocities.

$$m_i = S_i + h_i \tag{3.34}$$

where

$S_i$ = the mass of particles in column $i$ with a settling velocity within the theoretical velocity range, i.e. $v_s \in [v_{up,i}, v_{up,i-1}]$ for $i \neq 1$ or $v_s \in [v_{up,1}, \infty]$ if $i = 1$.
$h_i$ = the mass of particles in column $i$ with a settling velocity less than the upflow velocity of the column, i.e. $v_s < v_{up,i}$.

The two terms in equation 3.34 can then be described in more detailed. The first term $S_i$ can be described as the total amount of particles in the incoming wastewater with a settling velocity within the given range entering the set-up subtracted with the amount of particles within this settling velocity range still stuck in previous columns. The amount of particles still stuck in previous columns can furthermore be divided into particles with a settling velocity low enough to reach column $i$ and the ones which are close enough in size to the previous upflow velocity as to not even exit the previous column and reach its correct destination. The former of the two can be described using equation 3.33 while the latter can be described the same way as the amount of particles entering the set-up. The second term $h_i$ can, like the particles stuck in previous columns, be divided into two subterms depending on the settling velocity of the particles (i.e. whether particles of that settling velocity exit the column or not during the experiment). The mass of particles exiting the column can be calculated using equation 3.33 while the mass of the ones not exiting is calculated like $S_i$, i.e. the sum of what enters the set-up subtracted with what is found in previous columns. The equations for the two terms are found below in equations 3.35 and 3.36 for $S_i$ and $h_i$ respectively.

$$S_i = \frac{Q}{V_{in}} \left( \underbrace{t_{end} \int_{v_{up,i}}^{v_{up,i-1}} S(v_s) dv_s}_{\text{Total Incoming}} - \underbrace{\overbrace{\sum_{j=1}^{i-1} \int_{v_{up,i}}^{v^*_{up,i-1}} t_j(v_s) \cdot S(v_s) dv_s}^{v_s \text{ reaching column i}} - \overbrace{t_{end} \int_{v^*_{up,i-1}}^{v_{up,i-1}} S(v_s) dv_s}^{v_s \text{ not reaching column i}}}_{\text{Particles in previous columns}} \right) \tag{3.35}$$

and

$$h_i = \frac{Q}{V_{in}} \left( \underbrace{\int_{-\infty}^{v^*_{up,i}} t_i \cdot S(v_s) dv_s}_{v_s \text{ exiting column i}} + \underbrace{\int_{v^*_{up,i}}^{v_{up,i}} \left( t_{end} - \sum_{j=1}^{i-1} t_j(v_s) \right) \cdot S(v_s) dv_s}_{v_s \text{ not exiting column i}} \right) \tag{3.36}$$

where

$Q$ = flow velocity during the experiment $[m^3/h]$
$V_{in}$ = total volume entering the set-up during experiment $[m^3]$
$t_{end}$ = total time the experiment was running $[h]$
$S(v_s)$ = function describing the total mass (SS/COD) of all particles in the incoming water of settling velocity $v_s$
$v_{up,i}$ = upflow velocity in column $i$ $[m/h]$
$v^*_{up,i}$ = minimum velocity not exiting column $i$ during experiment $[m/h]$

$t_j(v_s)$ = function describing the time it takes for a particle of settling velocity $v_s$ to exit column $j$

To clarify, a negative settling velocity simply means that the particle floats rather than sinks. If $i = 1$, no particles within the given velocity range will be stuck in previous columns. The upper limit of the velocity range will also be infinity compared to the previous value of the upflow velocity in the column before. The expression for $S_i$ will thereby be reduced to:

$$S_1 = \frac{Q}{V_{in}} \left( t_{end} \int_{v_{up,1}}^{\infty} S(v_s) dv_s \right) \tag{3.37}$$

and the expression for $h_i$ reduced to:

$$h_1 = \frac{Q}{V_{in}} \left( \int_{-\infty}^{v^*_{up,1}} t_i \cdot S(v_s) dv_s + \int_{v^*_{up,1}}^{v_{up,1}} t_{end} \cdot S(v_s) dv_s \right) \tag{3.38}$$

Adding equations 3.35 and 3.36 finally yields the expression for $m_i$ as:

$$\begin{aligned} m_i = \frac{Q}{V_{in}} \Bigg( & t_{end} \int_{v_{up,i}}^{v_{up,i-1}} S(v_s) dv_s - \sum_{j=1}^{i-1} \int_{v_{up,i}}^{v^*_{up,i-1}} t_j(v_s) \cdot S(v_s) dv_s - t_{end} \int_{v^*_{up,i-1}}^{v_{up,i-1}} S(v_s) dv_s \\ & + \int_{-\infty}^{v^*_{up,i}} t_i \cdot S(v_s) dv_s + \int_{v^*_{up,i}}^{v_{up,i}} \left( t_{end} - \sum_{j=1}^{i-1} t_j(v_s) \right) \cdot S(v_s) dv_s \Bigg) \end{aligned} \tag{3.39}$$

or, if $i = 1$:

$$m_1 = \frac{Q}{V_{in}} \left( t_{end} \int_{v_{up,1}}^{\infty} S(v_s) dv_s + \int_{-\infty}^{v^*_{up,1}} t_i \cdot S(v_s) dv_s + \int_{v^*_{up,1}}^{v_{up,1}} t_{end} \cdot S(v_s) dv_s \right) \tag{3.40}$$

Dividing both sides with the total mass of SS/COD in the incoming water, the equation rather than dealing with mass instead concerns fractions of the total mass. Hence the equation becomes:

$$\begin{aligned} x_i = \frac{Q}{V_{in}} \Bigg( & t_{end} \int_{v_{up,i}}^{v_{up,i-1}} f(v_s) dv_s - \sum_{j=1}^{i-1} \int_{v_{up,i}}^{v^*_{up,i-1}} t_j(v_s) \cdot f(v_s) dv_s - t_{end} \int_{v^*_{up,i-1}}^{v_{up,i-1}} f(v_s) dv_s \\ & + \int_{-\infty}^{v^*_{up,i}} t_i \cdot f(v_s) dv_s + \int_{v^*_{up,i}}^{v_{up,i}} \left( t_{end} - \sum_{j=1}^{i-1} t_j(v_s) \right) \cdot f(v_s) dv_s \Bigg) \end{aligned} \tag{3.41}$$

or, if $i = 1$:

$$x_1 = \frac{Q}{V_{in}} \left( t_{end} \int_{v_{up,1}}^{\infty} f(v_s) dv_s + \int_{-\infty}^{v^*_{up,1}} t_i \cdot f(v_s) dv_s + \int_{v^*_{up,1}}^{v_{up,1}} t_{end} \cdot f(v_s) dv_s \right) \tag{3.42}$$

where

$x_i$ = fraction of total mass (SS/COD) in column $i$

$f(v_s)$ = function describing the fraction of the total mass (SS/COD) all particles with settling velocity $v_s$ corresponds to

The fraction of SS/COD in the outgoing sample is then simply calculated as:

$$x_{OUT} = 100 - \sum_{i=1}^{n} x_i \tag{3.43}$$

where $n$ is the number of columns.

The final step in the calculation procedure is to determine the function $f(v_s)$ as this is currently unknown. However, as we are mainly doing this to find the cumulative settling velocity distribution curve $F(v_s)$, a function describing this curve is rather proposed and $f(v_s)$ can be found by differentiating the proposed function $F(v_s)$. According to Tyack et al. (1996) the natural cumulative settling velocity distribution of a sewage is in the shape of an S, asymptotic to the minimum and maximum percentage of mass, i.e. 0 and 100 %, as $v_s$ approaches -$\infty$ and $\infty$ respectively. However, as we for the model are only interested in the positive values (i.e. the particles that sink) only the positive settling velocities are considered by the function.

Two different functions are proposed and tested to described $F(v_s)$, see equation 3.44. The first of the two has taken inspiration from Tyack et al. (1996) while the second has a similar shape.

$$F(v_s) = \int f(v_s)dv_s = \begin{cases} (100-c)\cdot\left(1-\frac{a}{a+v_s^b}\right)+c, & (1) \\ \\ (100-c)\cdot\left(1-e^{-a\cdot v_s^b}\right)+c, & (2) \end{cases} \tag{3.44}$$

where $a$, $b$ and $c$ are parameters. Differentiating the two proposed functions thus give the proposed functions for $f(v_s)$ which can be seen in equation 3.45.

$$f(v_s) = \begin{cases} (100-c)ab\cdot\frac{v_s^{b-1}}{a+v_s^b}, & (1) \\ \\ (100-c)ab\cdot v_s^{b-1}\cdot e^{-a\cdot v_s^b}, & (2) \end{cases} \tag{3.45}$$

The parameters to the functions are then numerically adjusted to minimize the sum of squared errors between the collected data and the calculated values by use of equations 3.41 and 3.42.

As the suggested functions are applicable only for the positive values a slight modification had to be made to equations 3.41 and 3.42 to account for the first term of $h_i$ where $t_i(v_s)\cdot f(v_s)$ was integrated from $-\infty$ to $v^*_{up,i}$. The integral was split into two, one from $-\infty$ to 0 and one from 0 to $v^*_{up,i}$:

$$\int_{-\infty}^{v^*_{up,1}} t_i\cdot f(v_s)dv_s = \int_{-\infty}^{0} t_i\cdot f(v_s)dv_s + \int_{0}^{v^*_{up,1}} t_i\cdot f(v_s)dv_s \tag{3.46}$$

where the first of the two integrals was estimated based on the total fraction of the particles with a negative settling velocity. As those particles will travel faster than the water, the concentration of those particles in the column will be less than their concentration in the incoming water. Hence the expression can be rewritten as follows:

$$\frac{Q}{V_{in}} \int_{-\infty}^{0} t_i \cdot f(v_s) dv_s = \frac{V_i}{V_{in}} \int_{-\infty}^{0} f(v_s) dv_s \cdot d = \frac{V_i}{V_{in}} F(0) \cdot d \tag{3.47}$$

where $d \in [0,\ 1]$ is a real number to be estimated. Finally, instead of using $\infty$ as the upper boundary in equations 3.40 and 3.42 for the first column, a velocity of 10 000 m/h was deemed sufficiently large.

The MATLAB script for the calculation procedure can be found in Appendix A.2.

### 3.4.3 Assigning the settling velocities

For each of the SVGs and substances a settling velocity should be assigned as well as a fraction. In Figure 3.10 below the hourly overflow rates for line 4 at Öresundsverket during 2021 are plotted. From this, one can clearly see that the overflow rate rarely reaches above 2 m/h or below 0.5 m/h. The SVGs are thereby partitioned so that one includes the particles that practically always settle (SVG 5) and one includes the particles that almost never do (SVG 1). The rest of the groups are selected in the middle range of what is left.

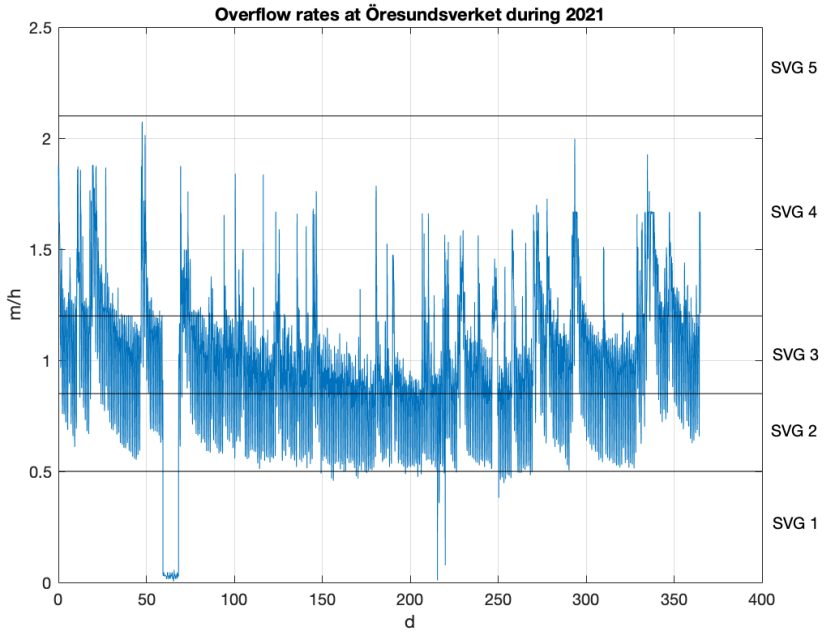


Figure 3.10: Choice of SVGs

In Table 3.7 the boundaries and assigned settling velocity for each group is presented. The assigned velocity is calculated as described by Bachis et al. (2015) as the geometrical mean of the boundaries. For the first group the lower boundary is taken as the same as

a low enough settling velocity, taking inspiration from Bachis et al. Finally the upper boundary for SVG 5 is set to 40 m/h choosing a high enough value, despite several of the combined cumulative settling velocity distribution curves (CSVD-curves) not reaching 100 % at this velocity.

Table 3.7: Boundaries and assigned settling velocity for the 5 SVGs

| | **Lower limit [$v_s$]** | **Upper limit [$v_s$]** | **Mean velocity [m/h]** |
|---|---|---|---|
| **SVG 1** | 0.01 | 0.5 | 0.071 |
| **SVG 2** | 0.5 | 0.85 | 0.652 |
| **SVG 3** | 0.85 | 1.2 | 1.010 |
| **SVG 4** | 1.2 | 2.1 | 1.732 |
| **SVG 5** | 2.1 | 40 | 9.165 |

### 3.4.4 Assigning the fractions

Once the parameters $a$, $b$ and $c$ (and $d$) are estimated the cumulative settling velocity distribution curve (CSVD curve) can be found by plotting $F(v_s)$. The curves can be determined for the individual runs as well as for the total when including all of the results. The fraction of the SVG is determined as the difference in % between the cumulative fractions at the boundaries of each group.

## 3.5 PST Model

As previously mentioned, the "Linköping model" developed by Arnell (2013) in MATLAB based on BSM2, modified according to the PSVD concept by Lundin (2014) and here referred to as "the modified Linköping model", acted as a base for this project.

The modified Linköping model uses the Takács model described in Section 2.5.2, but has modified it to include the PSVD concept. Hence, instead of calculating the settling velocity using the modified Vesilind equation (equation 2.10), the settling velocity was given to the model as an actual number for each SVG and was the same in each layer. The incoming TSS in the model was also divided into the five different SVGs according to an equation based on the flow and chemical dosing. In this project however, as no chemical addition was included, the fractionation of the TSS into the SVGs was constant based on the results from the experiments. The same procedure was also extended to the incoming slowly biodegradable substrate ($X_B$), the heterotrophic biomass ($X_{OHO}$), the inert particulate substrate ($X_U$), the decay products ($X_P$) and the ISS. The slowly biodegradable substrate and the biomass as well as the inert particulate substrate and the decay products were grouped together separately, assuming the same settling velocity distribution for the two groups.

As the PSTs at Källby WWTP were currently accumulating sludge and operating with a clear phase of about 2 dm (Forså, 2022) (i.e. quite far from optimal), the focus of the modelling part of this project was on Öresundsverket.

To better describe the PSTs at Öresundsverket a hydrolysis term was included based on ASM2d (Henze et al., 2000) converting the slowly biodegradable biomass to readily biodegradable biomass. Only the anaerobic hydrolysis was considered and the rate can be seen in equation 3.48 below:

$$\text{Hydrolysis rate} = k_h \cdot \eta_{fe} \cdot \left(\frac{X_B/X_{OHO}}{K_X + X_B/X_{OHO}}\right) \cdot \left(\frac{K_{O_2}}{K_{O_2} + S_{O_2}}\right) \cdot \left(\frac{S_{NOx}}{K_{NOx} + S_{NOx}}\right) \cdot X_{OHO} \tag{3.48}$$

A decay reaction of the heterotrophic biomass was also considered as follows:

$$\text{Decay rate} = b_{OHO} \cdot \eta_{red} \cdot X_{OHO} \tag{3.49}$$

where

$k_h$ = Hydrolysis rate constant (temperature dependent)
$K_X$ = Half-saturation coefficient for hydrolysis of slowly biodegradable substrate
$K_{O_2}$ = Oxygen half-saturation coefficient for heterotrophic biomass
$\eta_{k_h}$ = Correction factor for hydrolysis under anaerobic conditions
$K_{NO}$ = Nitrite/Nitrate half-saturation coefficient for denitrifying heterotrophic biomass
$b_{OHO}$ = Heterotrophic decay rate constant (temperature dependent)
$\eta_{b_{OHO}}$ = Correction factor for decay under anaerobic conditions

$X_B$, $X_{OHO}$, $S_{O_2}$ and $S_{NOx}$ are all state variables described in Table 2.4 in Section 2.3.

The temperature dependency of the reactions constants will be calculated based on the following equation (Henze et al., 2000):

$$k(T) = k(20\ ^\circ\text{C}) \cdot \theta_k^{(T-20\ ^\circ\text{C})} \tag{3.50}$$

where $\theta_k$ is a temperature correction factor for parameter $k$. The starting values for the kinetic parameters were taken as the standard values from ASM2d and only the hydrolysis rate constant, the correction factor for hydrolysis under anaerobic conditions and the temperature correction factor for the hydrolysis are modified.

To verify the model, the mass balance of the total COD and the inert and decay particulate substrate was checked at a constant input. For the calibration and validation of the model a recirculation pump is also added in accordance with BSM1 (K. V. Gernaey & Jeppsson, 2014) to describe the resuspension of the hydrolyzed primary sludge at Öresundsverket. Values for the sludge outtake and recirculation flows are set according to the plant specifications.

### 3.5.1 Model calibration and validation

To validate and calibrate the model a measuring campaign was held at Öresundsverket on the $10^{th}$ of January 2023 collecting data of the incoming and outgoing streams of the two PSTs in line 4 (the line from which water was collected for the experiments) flow-proportional with a time frequency of two hours. On each sample, measurements were made regarding TSS, VSS & ISS, total COD and soluble COD. The soluble COD was

here measured filtered through 0.45 $\mu$m syringe filters and ammonium nitrogen was also measured. The model was then simulated based on the incoming data and the simulated outflows compared with the measured ones. Calibration took place by altering the rate of the hydrolysis as well as modifying the assigned settling velocity distribution.

Due to uncertainties with the measured values (as there were a lot of issues surrounding the sampling equipment) the calibrated model was also validated for hourly incoming data during a full year (2020). The incoming data was derived based on measured incoming data for the total COD during 2020 fractionated according to the results from a previous characterization project with added loads from simulated recirculation streams during the year (Wärff, 2022). The simulated effluent from the model were validated against the measured TSS and total COD taken at the plant throughout the year as flow-weighted daily means. The filtered COD had also been measured at Öresundsverket by use of 6-10 $\mu$m filters. Previous work (Tebini, 2020) has shown that the COD values measured after filtration with pore size in this range is considerably higher (70-190 mg/L) than the soluble COD (i.e. as measured with 0.1 $\mu$m filters). The measured values for the filtered COD at Öresundsverket have here thus been reduced by 70 mg/L to assume a reasonable estimate of the dissolved COD from the measured values for comparison with the model predictions. For this data set only the temperature dependency of the hydrolysis rate constant was altered to better fit the measured values.

### 3.5.2 Comparing with the design guidelines

Once the model had been validated it was used to compare with the recommendations in design guidelines with respect to the overflow rate. This was done for a hypothetical PST with the same conditions as at Öresundsverket, but without the recirculation streams.

# Chapter 4

# Results and Discussion

## 4.1 Chemical analyses

In the two next subsections the results at Källby WWTP and Öresundsverket are presented respectively. The measured values and a more thorough description of the results can be found in Appendices B.1 and B.2.

### 4.1.1 Källby WWTP

Three runs were made at Källby. For these runs the TSS, the VSS and ISS (for the second and third run) as well as the total and particulate COD were measured. For the second run an aerobic degradation experiment was also conducted.

In Table 4.1 the mass balance errors before closing the mass balances for each set of measurements are shown as well as the method for closing it. As can be seen there is a learning

Table 4.1: Mass balances before closing, Källby WWTP

| | Date | Mass balance error (%) | Method for closing MB |
|---|---|---|---|
| TSS | 10/10 | 28.8[a] | Single measurement |
| | 18/10 | 32.8[a] | Multiple measurements |
| | 24/10 | 6.5 | Single measurement |
| VSS | 18/10 | 33.4[a] | Multiple measurements |
| | 24/10 | 4.3 | Single measurement |
| $COD_{tot}$ | 10/10 | 3.2 | Single measurement |
| | 18/10 | 22.5[a] | Single measurement |
| | 24/10 | -10.9 | Single measurement |
| $COD_p$ | 10/10 | 3.2[b] | Single measurement |
| | 18/10 | 25.3[a] | Single measurement |
| | 24/10 | -12.4 | Single measurement |

[a] MB error out of range (>20 %)

[b] Mean value from the other runs used for estimating $COD_s$

curve for collecting and taking the measurements, where much better mass balances are found for the last run at Källby WWTP and the following runs at Öresundsverket. Due to the large inaccuracies only the last run at Källby WWTP fell within the accepted range for the mass balance error (i.e. $< 20$ %), the exception being the COD (total and particulate) during the first run.

The figures shown in the rest of this section all depict the measurements after closing the mass balances. If one is interested in the values before doing this, the reader is referred to Appendix B.1.1 where the absolute values before and after closing of the mass balances can be found.

### TSS, VSS & ISS

The distribution of TSS in the columns for run 1-3 at Källby WWTP can be found in Figure 4.1 below. The third run was made at a flow velocity about 2-3 times higher than the others, explaining the different shape of the distribution curve for this run compared to the other two. Something interesting to note is the displacement of the maximum amount of particles from the first to the second column during this last run indicating that most of the particles in the first samples during the first two runs belong to the settling velocity range for the second column during the last run.

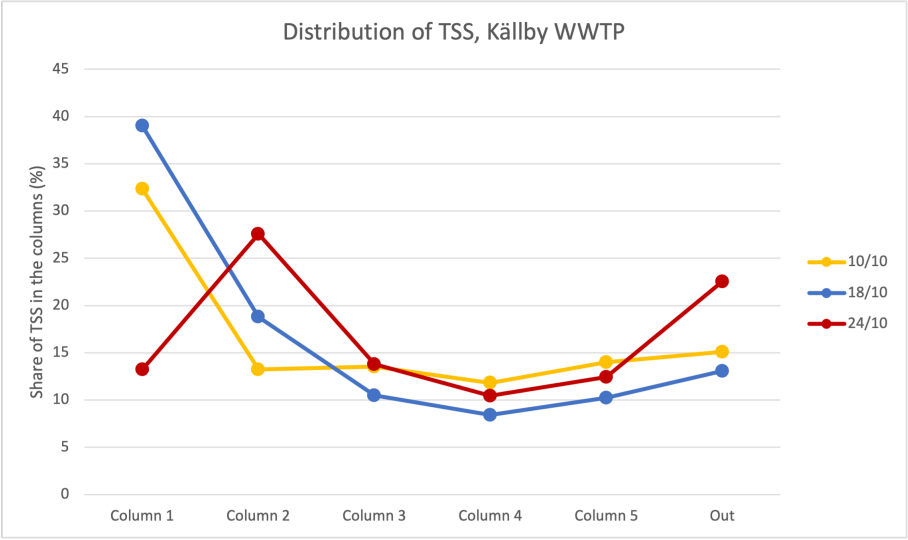


Figure 4.1: Distribution of TSS in the settleometer

As the TSS is comprised of the VSS and the ISS, only the ratios of the VSS and ISS to TSS are shown. The VSS and ISS was measured only at the last two runs and among these only the very last run fulfilled the requirement as stipulated in Section 3.3.3 for the ISS. Interestingly enough the values for the ISS for this run were completely identical when using the two methods.

As is seen in Figure 4.2, the VSS make up the most of the TSS, although the fraction of the TSS seems to be more even throughout the columns in the last run at a higher velocity.

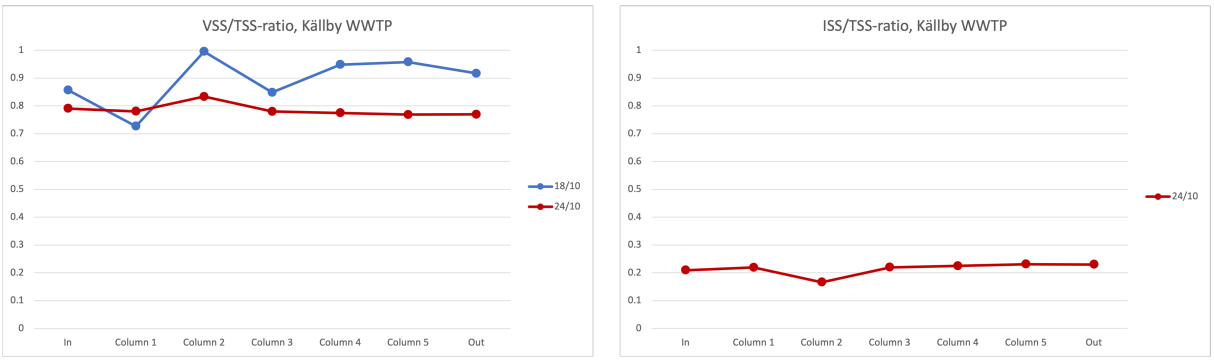


(a) VSS/TSS-ratios

(b) ISS/TSS-ratios

Figure 4.2: Measured VSS/TSS and ISS/TSS-ratios, Källby WWTP

### COD

For the COD, the distribution of the particulate COD is shown in Figure 4.3. Compared to the TSS, these curves start lower, but ends at approximately the same level. Hence, there is a much clearer "minimum" in the middle columns. The effect is even more pronounced for the total COD where the soluble COD has more of an impact, for the distribution of the total COD the reader is referred to the Appendix.

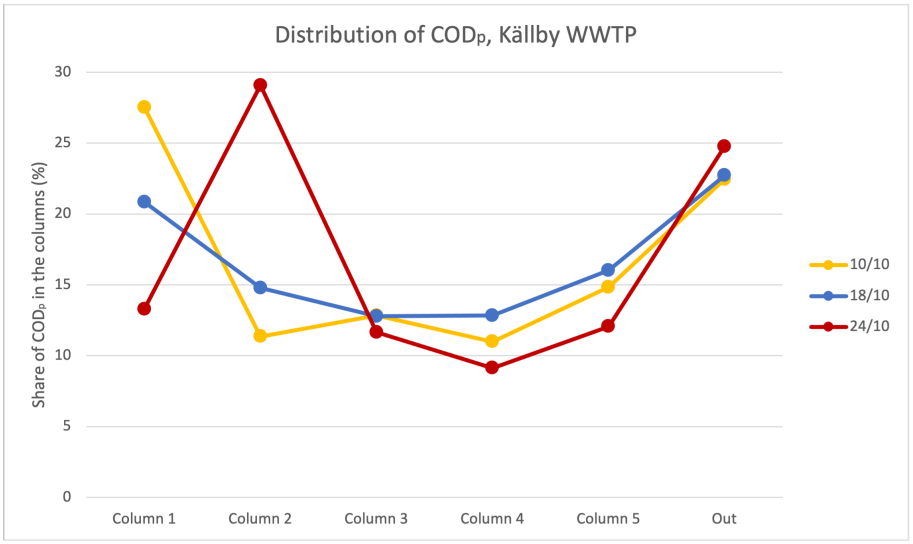


Figure 4.3: Distribution of $COD_p$ in the settleometer

On the samples from the second run an aerobic degradation experiment was performed as well. Unfortunately this was the only one of the three runs with unsatisfactory measurements of the COD, however the results from the experiment were still used to calculate the CSVD curves for lack of better options. As described in Section 3.2.3, two methods were used to try and calculate the inert particulate and the initial slowly biodegradable substrate. The results from the two methods can be seen in Table 4.2 below. As is clearly seen the calculated values for the inert particulate substrate by use of the first method were negative, hence the use of the second method.

Table 4.2: Calculated distribution of $X_B$ and $X_U$ at Källby WWTP

| **Method by Orhon:** | **In** | **1** | **2** | **3** | **4** | **5** | **Out** |
|---|---|---|---|---|---|---|---|
| $X_U$ (mg/L) | -239 | -1085 | -290 | -181 | -146 | -120 | -170 |
| $X_{B,0}$ (mg/L) | 597 | 3003 | 833 | 449 | 325 | 272 | 361 |
| Distribution of $X_{B,0}$ (%) | - | 20.4 | 12.7 | 11.2 | 12.0 | 16.4 | 27.4 |
| **ASM calculations:** | **In** | **1** | **2** | **3** | **4** | **5** | **Out** |
| $X_U$ (mg/L) | 27.7 | 246.1 | 78.9 | 24.4 | 9.77 | 19.2 | 14.6 |
| $X_{B,0}$ (mg/L) | 320 | 2101 | 665 | 369 | 255 | 185 | 214 |
| Distribution of $X_{B,0}$ (%) | - | 20.3 | 14.4 | 13.0 | 13.4 | 15.8 | 23.1 |
| Distribution of $X_U$ (%) | - | 27.4 | 19.7 | 9.9 | 5.9 | 18.9 | 18.2 |
| $X_{B,0}/COD_p$-ratio (%) | 92.0 | 89.5 | 89.4 | 93.8 | 96.3 | 90.6 | 93.6 |
| $X_U/COD_p$-ratio (%) | 7.98 | 10.5 | 10.6 | 6.20 | 3.69 | 9.39 | 6.38 |
| **Distribution of $COD_p$:** | **In** | **1** | **2** | **3** | **4** | **5** | **Out** |
| Distribution of $COD_p$ (%) | - | 20.8 | 14.8 | 12.8 | 12.8 | 16.0 | 22.7 |

Interestingly enough the calculated distribution of the initial slowly biodegradable substrate from the first method (when dividing by the sum of what is found in the samples from the columns and the outgoing sample) is still quite similar to the calculated distribution by use of the second method, as well as the distribution of the initial particulate COD. However, the mass balance error for the calculated concentrations is as much as 22 %. To further illustrate this the different distributions are also visualized in Figure 4.4 below. Part of the similarity between the two methods is probably due to the solver in Excel in the latter method putting most of the errors between the calculated and measured concentrations at the end on the incoming sample. A possible reason as for why the distribution of $X_U$ differs compared to the others is likely the fact that the $COD_p$ and $X_B$ levels are much higher. Hence, a small difference in mass between these substances will only give a very small impact on the relative distribution between the two, while for the $X_U$ the relative impact would be much larger.

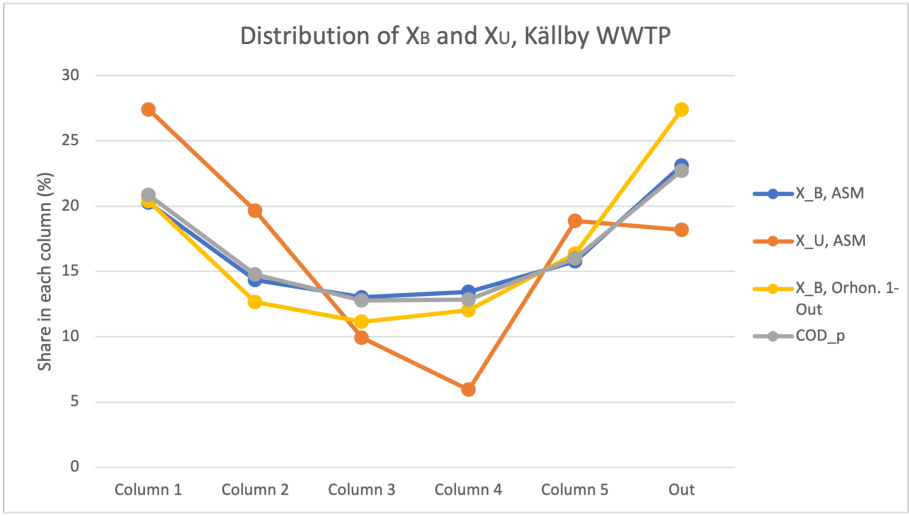


Figure 4.4: Distribution of $X_B$ and $X_U$ in the settleometer

Finally the $X_B/COD_p$ and $X_U/COD_p$-ratios within the samples collected from the set-

tleometer are shown in Figure 4.5 below. Around 90 % of the particulate COD belongs to the former class. The $X_B/COD_p$ fraction reaches its maximum in the sample from the fourth column where as much as 96 % of the particulate COD belongs to this fraction.

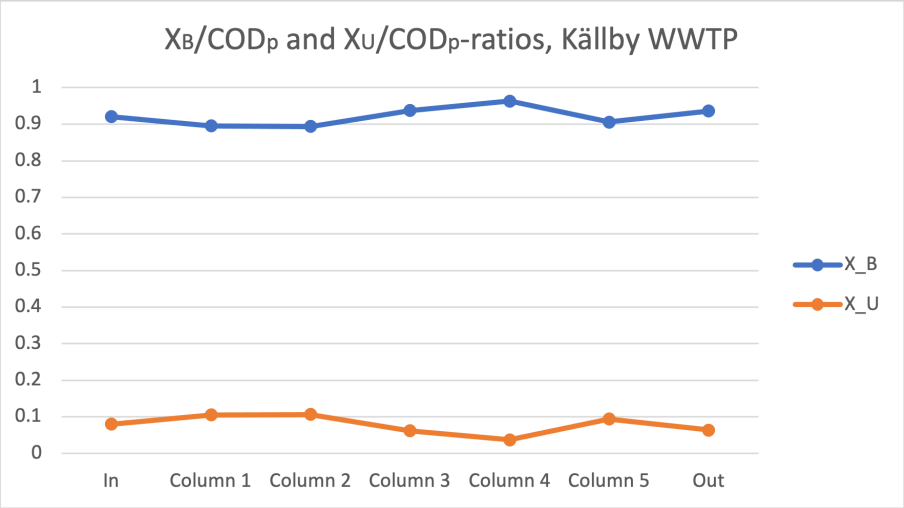


Figure 4.5: $X_B/COD_p$ and $X_U/COD_p$-ratios, Källby WWTP

### 4.1.2 Öresundsverket

At Öresundsverket four runs were made in total. Like at Källby, the TSS, VSS, total and particulate COD and ISS was measured for each run. Finally an aerobic degradation experiment was conducted with the samples from run number three. In Table 4.3 the

Table 4.3: Mass balances before closing, Öresundsverket

| | Date | Mass balance error (%) | Method for closing MB |
|---|---|---|---|
| TSS | 31/10 | -2.7 | Single measurement |
| | 8/11 | 11.0 | Multiple measurements |
| | 15/11 | 12.3 | Multiple measurements |
| | 28/11 | 7.7 | Multiple measurements |
| VSS | 31/10 | -1.9 | Single Measurement |
| | 8/11 | 11.0 | Single Measurement |
| | 15/11 | 10.4 | Multiple Measurements |
| | 28/11 | 7.6 | Multiple Measurements |
| $COD_{tot}$ | 31/10 | -9.2 | Single measurement |
| | 8/11 | 25.9[a] | Single measurement |
| | 15/11 | 0.5 | Multiple measurements |
| | 28/11 | 7.1 | Multiple measurements |
| $COD_p$ | 31/10 | -11.8[b] | Single measurement |
| | 8/11 | 28.7[a] | Single measurement |
| | 15/11 | -5.0 | Multiple measurements |
| | 28/11 | 5.0 | Multiple measurements |

[a] MB error out of range (>20 %)
[b] Mean value from the other runs used for estimating $COD_s$

mass balance errors before closing the mass balances for each set of measurements at Öresundsverket are shown.

### TSS, VSS & ISS

In Figure 4.6 below the distribution of TSS can be seen within the columns for the four runs. For the three latter runs one less column is used to yield lower upflow velocities in a feasible amount of time. For all of the experiments the first column seems to hold most of the suspended particles while there is a dip in the middle columns. A clear difference when decreasing the velocity is the smaller fraction of particles found in the outgoing sample, potentially because of the smaller volume of this sample.

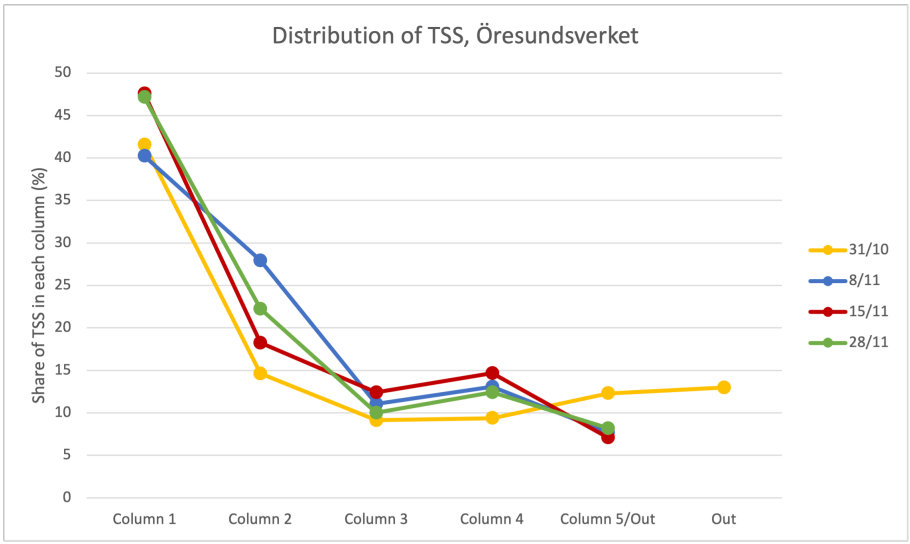


Figure 4.6: Distribution of TSS in the settleometer

As the TSS is comprised of the VSS and the ISS, again only the ratios of the VSS and ISS to TSS are shown. The VSS and ISS were measured during all of the runs, but among these only the first and last run fulfilled the requirement as stipulated in Section 3.3.3 for the ISS. Once more, interestingly enough the values for the ISS for these runs were near-identical when calculating it using the two methods, the largest difference of 6 mg/L (out of 200) occurring for the samples in the first column from the last run.

As is seen in Figure 4.7, the VSS here as well make up the most of the TSS, with the ratios from the second and third run varying a lot more even going above 1 for the former for the adjusted values. In the right subfigure the ISS/TSS-ratio is shown and a clear trend for the two curves is the ratio increasing towards the end.

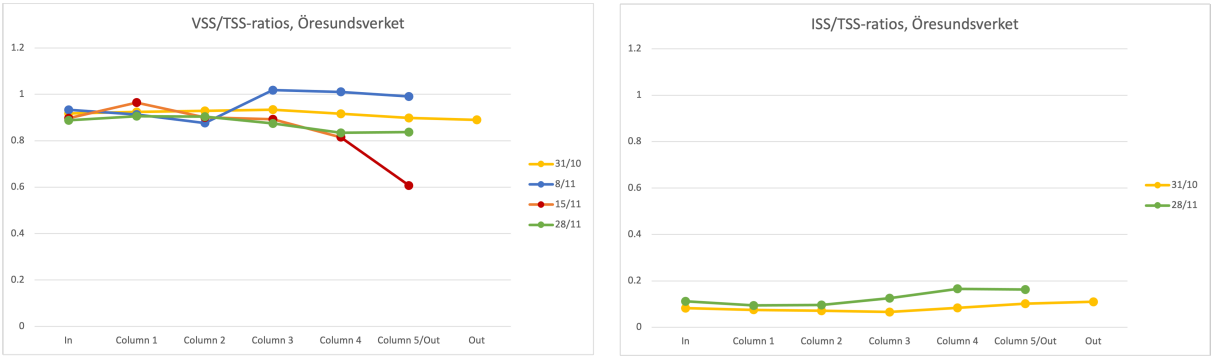


(a) VSS/TSS-ratios

(b) ISS/TSS-ratios

Figure 4.7: Measured VSS/TSS and ISS/TSS-ratios, Öresundsverket

### COD

For the COD, the distribution of the particulate COD is shown in Figure 4.8. If interested, the distribution for the total COD can be found in Appendix B.2. For the results from Öresundsverket the curves have, like at Källby WWTP, a more pronounced "minimum" in the middle columns compared to the TSS. The effect is more pronounced for the total COD where the soluble COD has more of an impact.

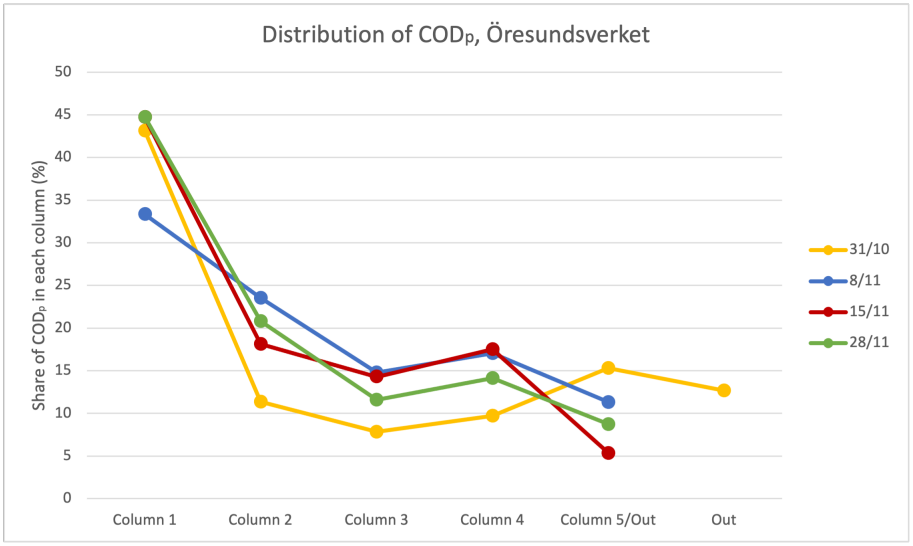


Figure 4.8: Distribution of $COD_p$ in the settleometer

On the samples from the third run an aerobic degradation experiment was performed as well, this time using triplicate measures of the COD from the different samples. For the two methods used the former once again resulted in negative calculated concentrations for the inert particulate substrate, however this time only for the outgoing reactor. The results from the two methods can be seen in Table 4.4 below.

Table 4.4: Calculated distributions of $X_B$ and $X_U$ at Öresundsverket

| **Method by Orhon:** | **In** | **1** | **2** | **3** | **4** | **Out** |
|---|---|---|---|---|---|---|
| $X_U$ (mg/L) | 34.9 | 147.4 | 7.24 | 15.4 | 8.86 | -0.66 |
| $X_{B,0}$ (mg/L) | 250 | 1855 | 330 | 153 | 124 | 102 |
| Distribution of $X_{B,0}$ (%) | - | 45.9 | 18.2 | 13.8 | 16.7 | 5.3 |
| **ASM calculations:** | **In** | **1** | **2** | **3** | **4** | **Out** |
| $X_U$ (mg/L) | 57.9 | 375.5 | 48.1 | 40.7 | 30.3 | 19.0 |
| $X_{B,0}$ (mg/L) | 227 | 1469 | 286 | 121 | 102 | 86 |
| Distribution of $X_{B,0}$ (%) | - | 44.3 | 19.3 | 13.3 | 16.8 | 5.4 |
| Distribution of $X_U$ (%) | - | 44.8 | 12.9 | 17.8 | 19.8 | 4.8 |
| $X_{B,0}/COD_p$-ratio (%) | 79.7 | 79.6 | 85.6 | 74.8 | 77.1 | 81.8 |
| $X_U/COD_p$-ratio (%) | 20.3 | 20.4 | 14.4 | 25.2 | 22.9 | 18.2 |
| **Distribution of $COD_p$:** | **In** | **1** | **2** | **3** | **4** | **Out** |
| Distribution of $COD_p$ (%) | - | 44.7 | 18.1 | 14.3 | 17.5 | 5.3 |

Again, interestingly enough the calculated distribution of the initial slowly biodegradable substrate from the first method (when dividing by the sum of what is found in the samples from the columns and the outgoing sample) is very similar to the calculated distribution by use of the second method, as well as the distribution of the initial particulate COD, this time even more so than the last as visualized in Figure 4.9 by three practically overlapping lines. Part of the similarity between the two methods is probably again due to the solver in Excel in the latter method putting most of the errors on the incoming sample.

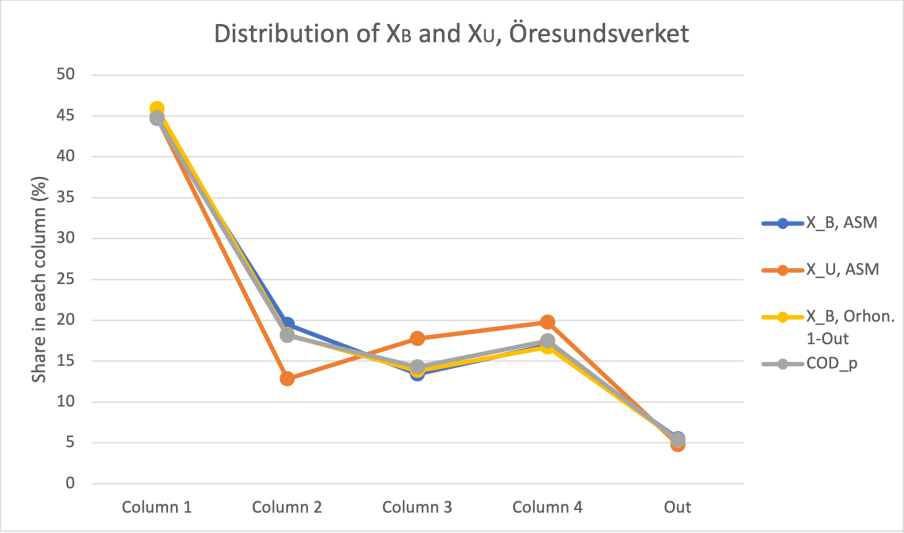


Figure 4.9: Distribution of $X_U$ and $X_B$ in the settleometer

Finally the $X_B/COD_p$ and $X_U/COD_p$-ratios within the samples collected from the settleometer are shown in Figure 4.10 below. Here the $X_B$ fraction only amounts to about 80 % of the particulate COD with the largest variation between the samples from the second and third column.

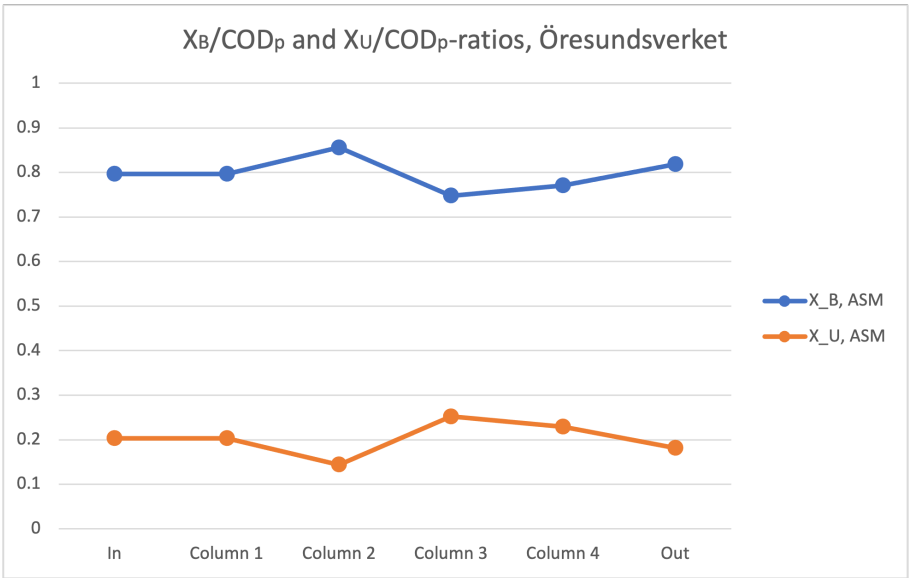


Figure 4.10: $X_B/COD_p$ and $X_U/COD_p$-ratios, Öresundsverket

## 4.2 Cumulative Settling Velocity Distribution Curves

The MATLAB script for estimating the CSVD curves was run for the individual data sets as well as for all of the valid ones combined. The combined CSVD curve was later on used for assigning fractions to the SVGs when modelling the PST at Öresundsverket. Two functions were tested, see equation 3.44, and the one yielding the best fit is shown for each data set. The estimated parameters for all data sets and substances can be found in Appendices B.1.5 and B.2.5 for Källby WWTP and Öresundsverket respectively.

### 4.2.1 Källby WWTP

At Källby WWTP most of the measured data did not fulfill the requirement of a maximum mass balance error of 20 %. In fact, with the exception of the $COD_p$, only the third run fulfilled this requirement. Despite this, all were calculated on at Källby to see the difference when including more data.

#### TSS, VSS & ISS

In Figure 4.11 below the CSVD curves for the combined TSS data sets 1-3 as well as the individual data sets are shown. As is clearly seen in the figure, the combined CSVD-curve follows that of the third run quite well and stays between the other two in the range of upflow velocities used during the experiments. No particular difference could be seen for run number three where wet-weather flow conditions occurred.

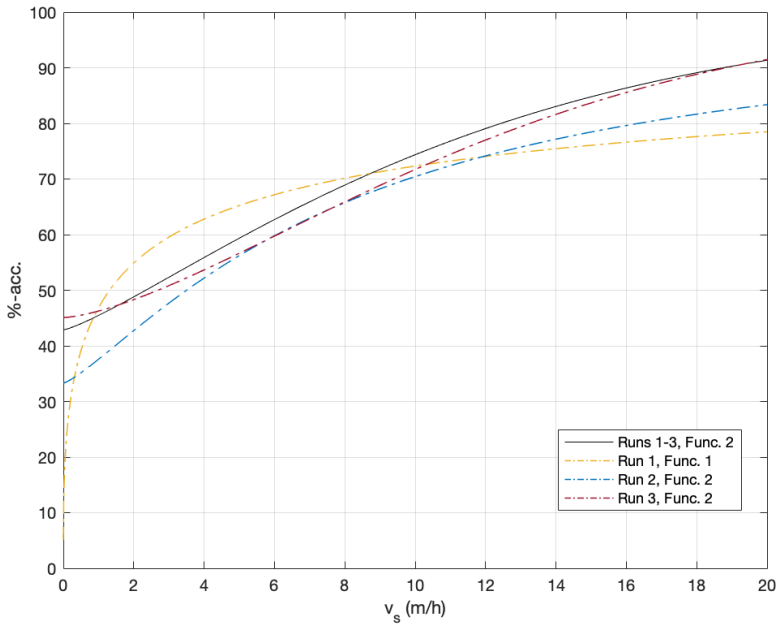


Figure 4.11: Fitted CSVD-curves to runs 1-3, TSS, Källby WWTP

The individual runs had a better fit when calculating the fractions of TSS found in each column, most likely as there were less values to consider. The curve for the first run had a much smaller non-settleable fraction than the other two, something that holds true for the CSVD-curves for the other substances at Källby as well. Likewise the $d$-parameter, i.e. the parameter describing the contribution of the non-settleable fraction in each column, was zero or close to it in all these cases, for the rest it commonly had a value of 1. Potentially, being the first time using the equipment, this anomaly can be explained by some issues in the operation or measurements made during the experiment.

The two functions used for estimating the CSVD-curves yielded very similar results within the upflow velocity range used in the experiments. Generally Function 2 had a lower non-settleable fraction than Function 1 as well as a (slightly) steeper incline. In Figure 4.12 below, the measured (with the settleometer) and calculated (from the MATLAB script) fractions in each column (all using closed mass balances and considering the misplacement of particles) are presented for the combined CSVD-curve. The calculated values are shown in a lighter colour in the figures compared to the measured ones. As seen in the figures, the two functions yielded very similar results and thus for the remaining substances only the result from the best fitting function will be presented.

**Results TSS Källby WWTP, measured vs calculated data**

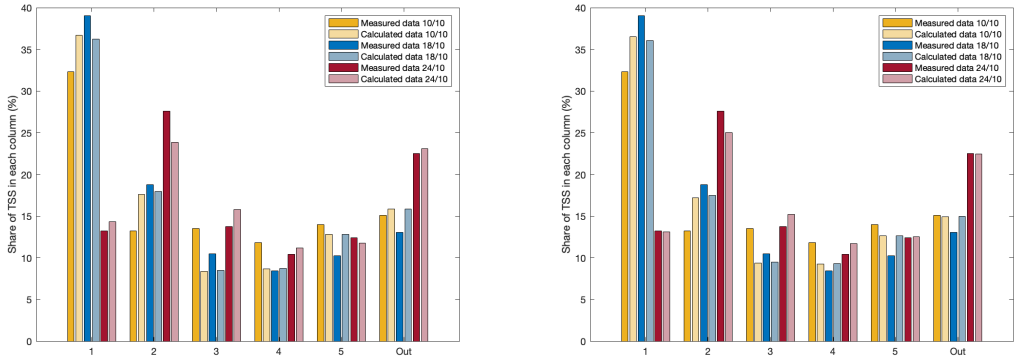


(a) Function 1 (b) Function 2

Figure 4.12: Estimated values using fitted CSVD-curve to runs 1-3, TSS

In Figure 4.13 the CSVD-curves for the VSS and the ISS are shown, both individual and combined. For the ISS though there was only one set of measurements available. The CSVD-curves for the VSS are somewhat similar to those for the TSS, while the CSVD-curves for the ISS differ more. The $R^2$-value for the combined data set for the VSS is also slightly better than that for the TSS.

**Cumulative Settling Velocity Distribution Curves, VSS & ISS, Källby WWTP**

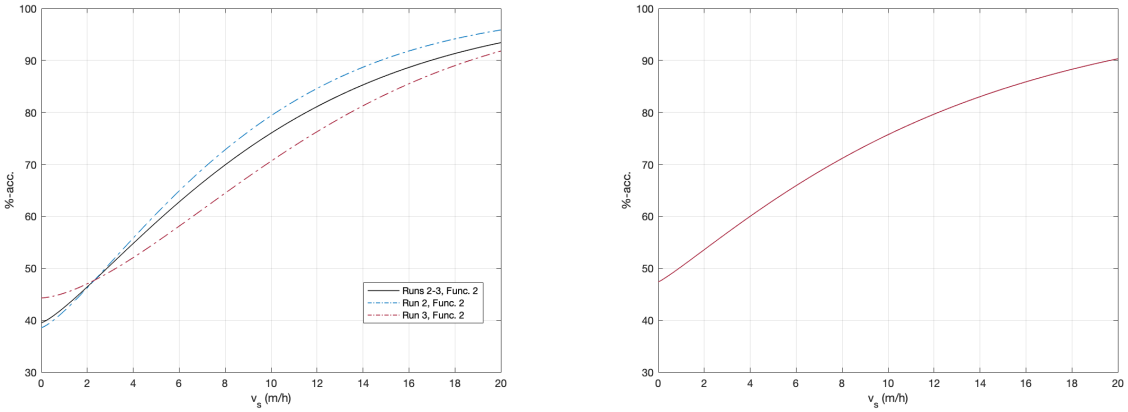


(a) VSS (b) ISS

Figure 4.13: Fitted CSVD-curves for the VSS & ISS, Källby WWTP

Finally the calculated proportions of the VSS and ISS fractions in each column using the parameters from the combined parameter estimations can be compared to the measured data in Figure 4.14 below.

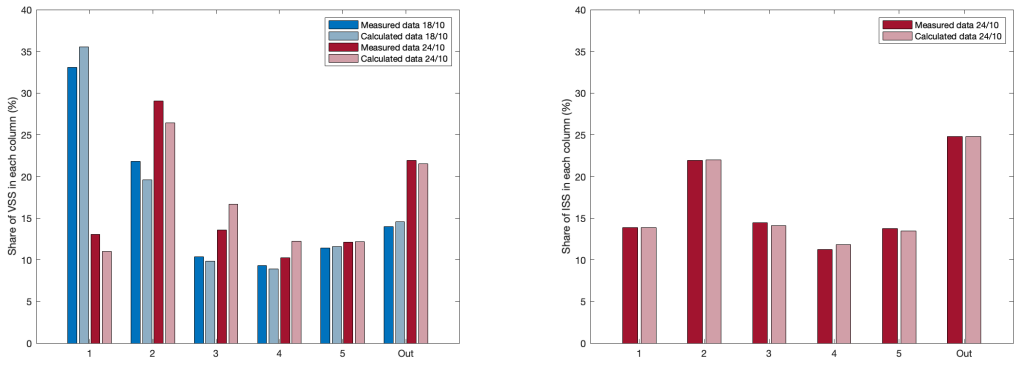


(a) VSS (b) ISS

Figure 4.14: Estimated values using fitted CSVD-curve to the experiments, VSS & ISS

## COD

In Figure 4.15 the CSVD curves for the combined $COD_p$ data sets 1 & 3 as well as the individual data sets are shown. As there actually were two data sets fulfilling the requirement for the mass balance, unlike the other substances at Källby WWTP, these two were used rather than utilizing all of the measured data. However, the CSVD-curve for run number 1 is still, like with the other substances, showing a very small non-settleable fraction. In contrast the other two (number three and the combined) indicate a very high non-settleable fraction at above 50 % which sounds almost unreasonably high and would mean that not much of the COD settle at all, especially when including the soluble matter.

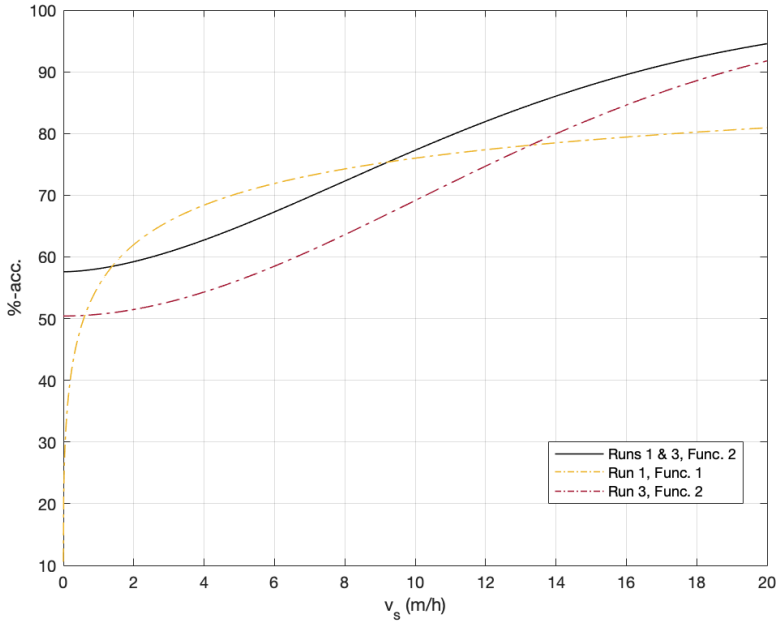


Figure 4.15: Fitted curve to experiments 1-4, CODp

The calculated proportions of the $COD_p$ fractions in each column considering the misplacement of particles can be compared to the measured data in Figure 4.16 below.

**Results $COD_p$ Källby WWTP, measured vs calculated data**

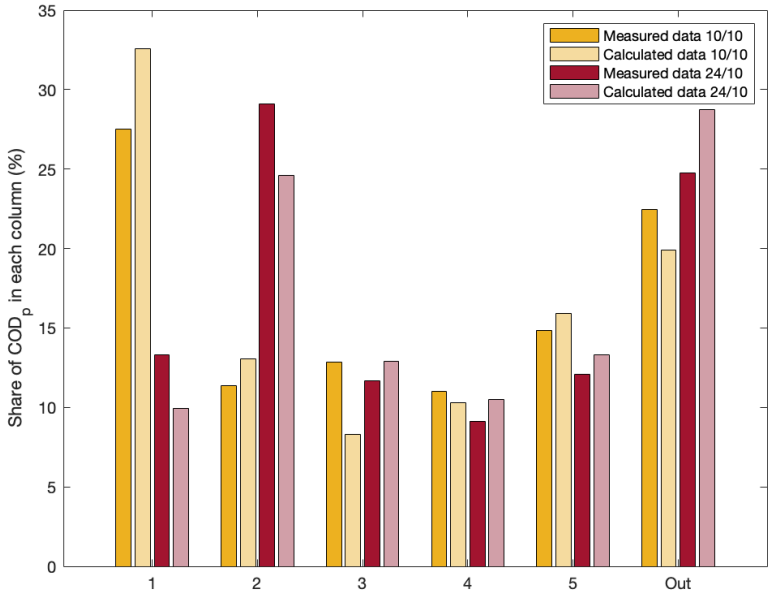


Figure 4.16: Estimated values using fitted CSVD-curve to runs 1 & 3, $COD_p$

Finally in Figure 4.17 below the CSVD-curves fitted to the $X_B$ & $X_U$ are shown, here for both functions. The best fitting function is shown with a solid line for each substance. As is seen the two functions are very similar in the range 1-8 m/h, i.e. the upflow velocity range for the second run at Källby WWTP.

**Cumulative Settling Velocity Distribution Curves, $X_B$ & $X_U$, Källby WWTP**

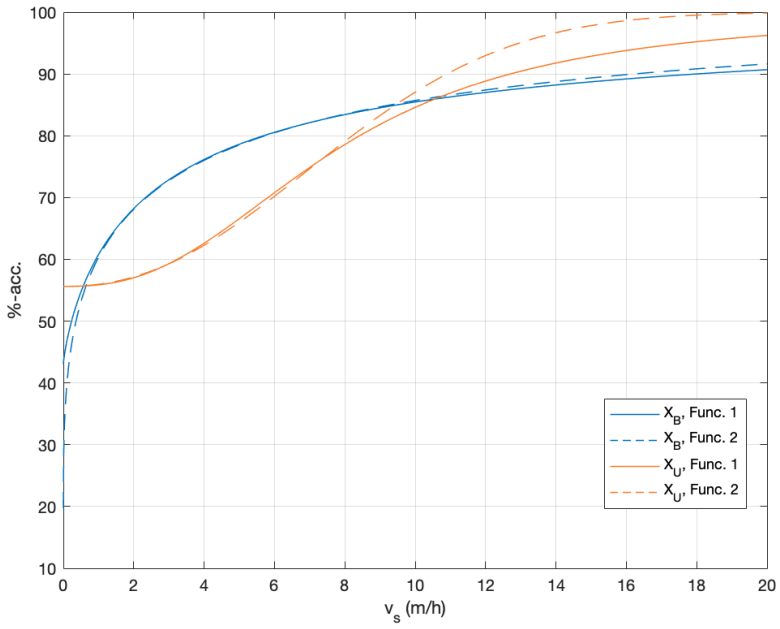


Figure 4.17: Fitted CSVD-curve for the $X_B$ and $X_U$

The measured fractions of $X_B$ & $X_U$ in each column are compared to the calculated ones using the CSVD-curve in Figure 4.18 below. As is seen the calculated fractions describe the measured ones for the most part quite accurately.

**Results $X_B$ & $X_U$ Källby WWTP, measured vs calculated data**

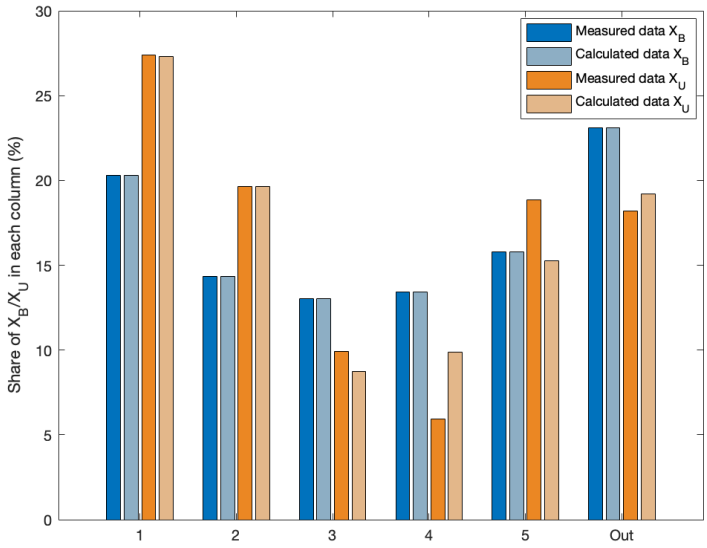


Figure 4.18: Estimated values using fitted CSVD-curve to the $X_B$ and $X_U$

### All distributions

To see how the different distributions compare with each other, all of them are shown in Figure 4.19 below. The TSS and VSS-distributions are quite similar, and follow a similar curve as the distribution of the ISS and the particulate COD after $v_s = 8$ m/h. Before that, however, they differ quite a lot. The steepest incline among the CSVD-curves is found for the $X_B$.

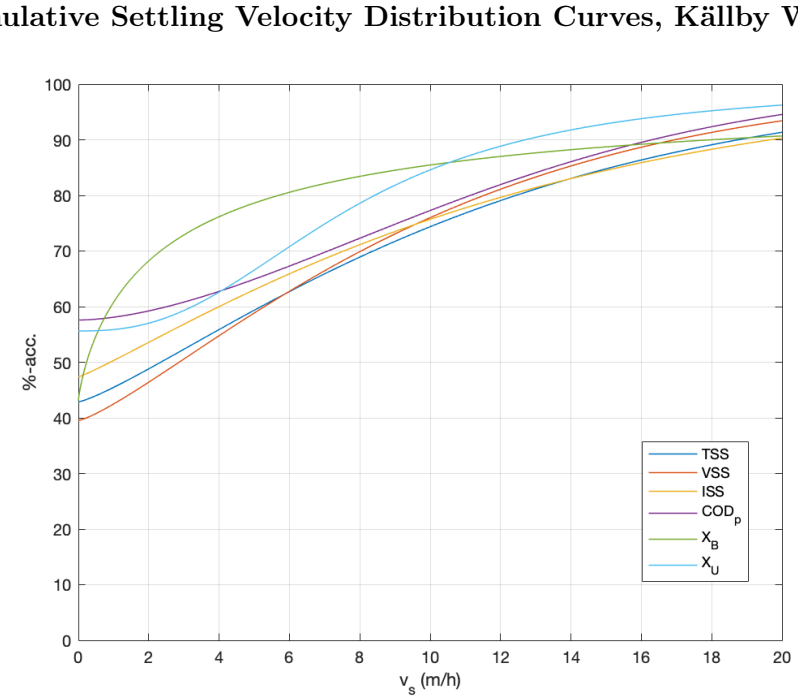


Figure 4.19: Combined CSVD-curves for the different substances at Källby WWTP

## 4.2.2 Öresundsverket

At Öresundsverket much more of the measured data fulfilled the requirement on the mass balance, hence more consideration was taken when choosing which data sets to include in the combined parameter estimations.

### TSS, VSS & ISS

In Figure 4.20 below the CSVD curves for the combined TSS data sets 1-4 as well as the individual data sets are shown. As is clearly seen the CSVD-curve corresponding to the first run is much more flat than the others, something that holds true for the other substances as well. Why this is the case can only be speculated on, but it may potentially be due to the higher flow velocity used during this experiment. Regardless of why, it clearly has an effect on the shape of the combined CSVD-curve.

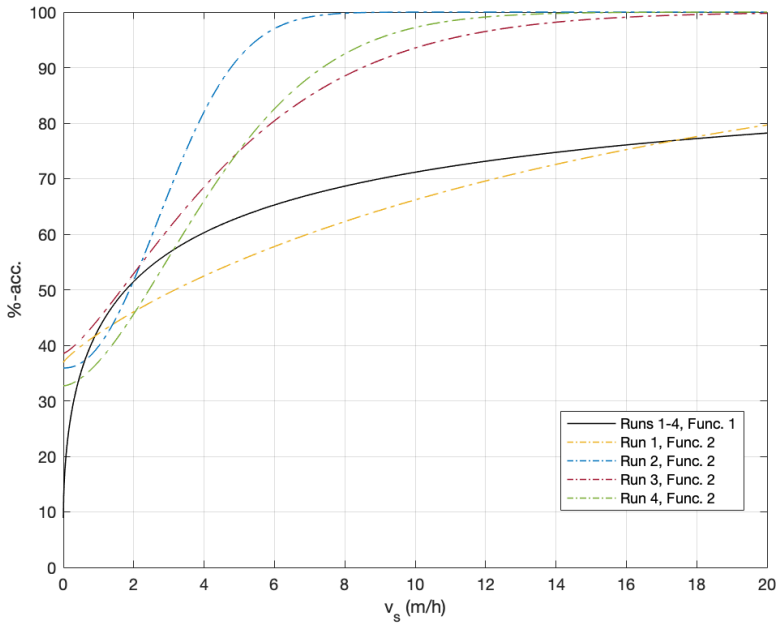


Figure 4.20: Fitted CSVD-curves to runs 1-4, TSS, Öresundsverket

A clear difference compared to at Källby WWTP is the much larger variation in the shapes of the curves at higher settling velocities. This is likely due to the fact the focus for the measurements at Öresundsverket has been on the lower upflow velocity range, i.e. below 3-4 m/h, unlike at Källby.

Once again the individual runs had a better fit when calculating the fractions of TSS found in each column, most likely as there are less values to consider. Moreover, the non-settleable fraction is much higher for the individual curves compared to the combined one, something also seen in Figure 4.20 above. The lower value for the non-settleable fraction found in the combined data sets were often also combined with a lower value for the $d$-parameter, i.e. the parameter describing the contribution of the non-settleable fraction in each column.

The two functions used for estimating the CSVD-curves yielded very similar results, differentiating only at settling velocities above 3-4 m/h. The largest difference was found with the combined data sets and generally Function 2 had a lower non-settleable fraction than Function 1 as well as a steeper incline, something more pronounced here than at Källby.

In Figure 4.21 below, the measured and calculated fractions in each column using closed mass balances and considering the misplacement of particles (i.e. the values fitted against each other in the calculation procedure) are presented for the combined CSVD-curve. As seen in the figure, the two functions yielded very similar results, and for the remaining substances only the result from the best fitting function will be presented.

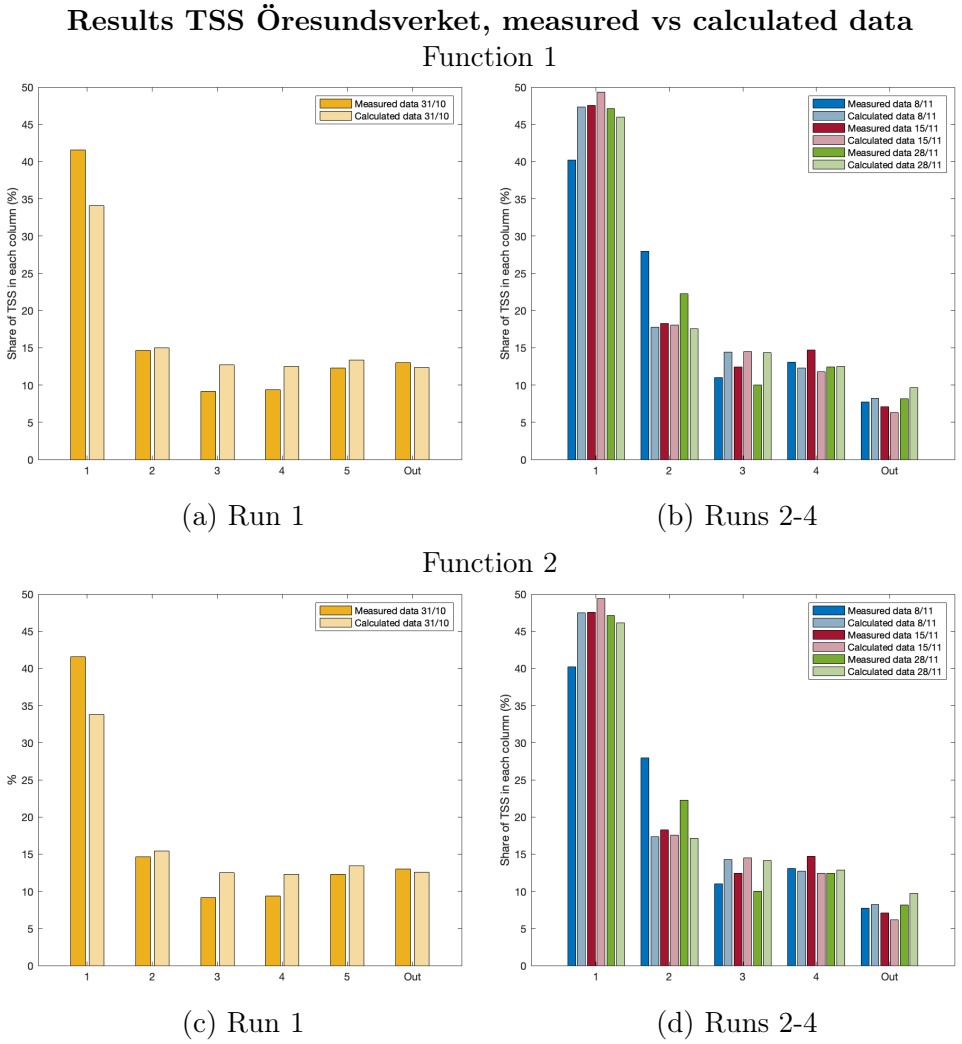


(a) Run 1 (b) Runs 2-4

(c) Run 1 (d) Runs 2-4

Figure 4.21: Estimated values using fitted CSVD-curve to experiments 1-4, TSS

In Figure 4.22 the CSVD-curves for the VSS and the ISS are shown, both individual and combined. The CSVD-curves for the VSS are very similar to those for the TSS, while the CSVD-curves for the ISS differ much more. The $R^2$-value for the combined data set for the VSS is also slightly larger than that for the TSS and even better is the ISS although this might be due to fewer measurements. Quite notably, the combined function for the ISS is not in between the two individual functions as expected, why this is the case is uncertain and it has been recalculated to ascertain that it is correct.

At last, the calculated proportions of the VSS and ISS fractions in each column using the parameters from the combined estimation and considering the misplacement of particles can be compared to the measured data in Figure 4.23.

**Cumulative Settling Velocity Distribution Curves, VSS & ISS, Öresundsverket**

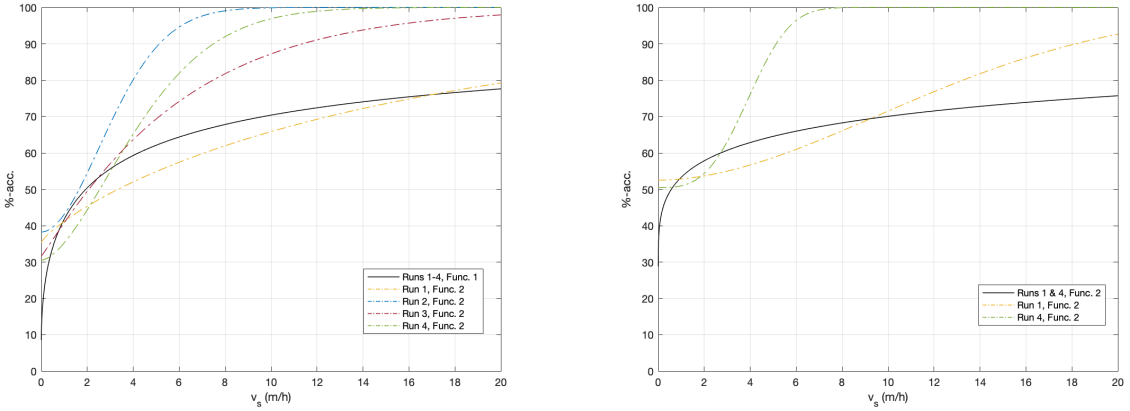


(a) VSS (b) ISS

Figure 4.22: Fitted CSVD-curves for the VSS & ISS, Öresundsverket

**Results VSS & ISS Öresundsverket, measured vs calculated data**

VSS, Function 1

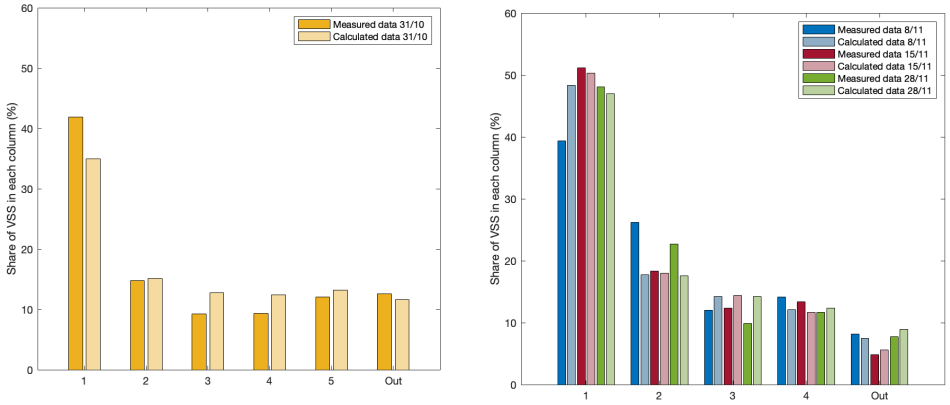


(a) Run 1, VSS (b) Runs 2-4, VSS

ISS, Function 2

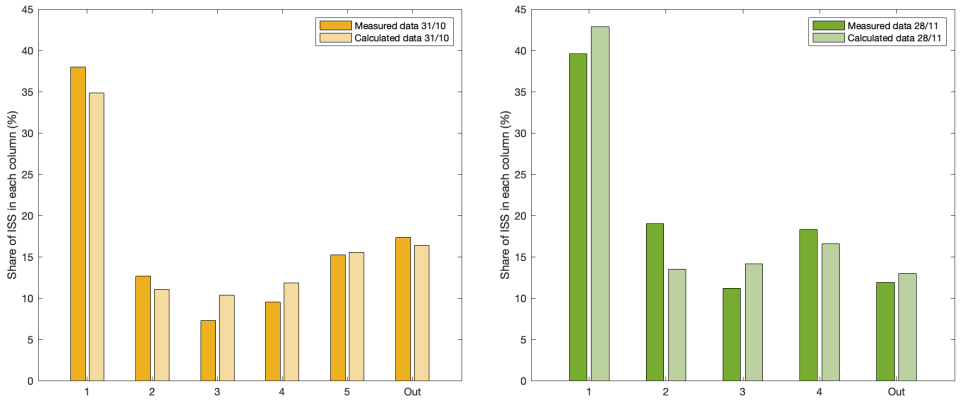


(c) Run 1, ISS (d) Run 4, ISS

Figure 4.23: Estimated values using fitted CSVD-curves to the experiments, VSS & ISS

## COD

In Figure 4.24 the CSVD curves for the combined $COD_p$ data sets as well as the individual data sets are shown. Note that the combined CSVD curve was only made for runs 1, 3 and 4 as the second run was excluded due to a poor mass balance. In the figure the CSVD-curve for the last two runs combined was included as well as they were the only ones cooled and analyzed with multiple measurements. The $R^2$-value for this fit was also relatively high and the function follows, as seen in Figure 4.24, the two others of a different shape than the CSVD-curve for the first run. For the model, however, the option of including all available data (data set 2 excluded) is chosen as this would give a better average estimation of the fractions.

**Cumulative Settling Velocity Distribution Curve, $COD_p$, Öresundsverket**

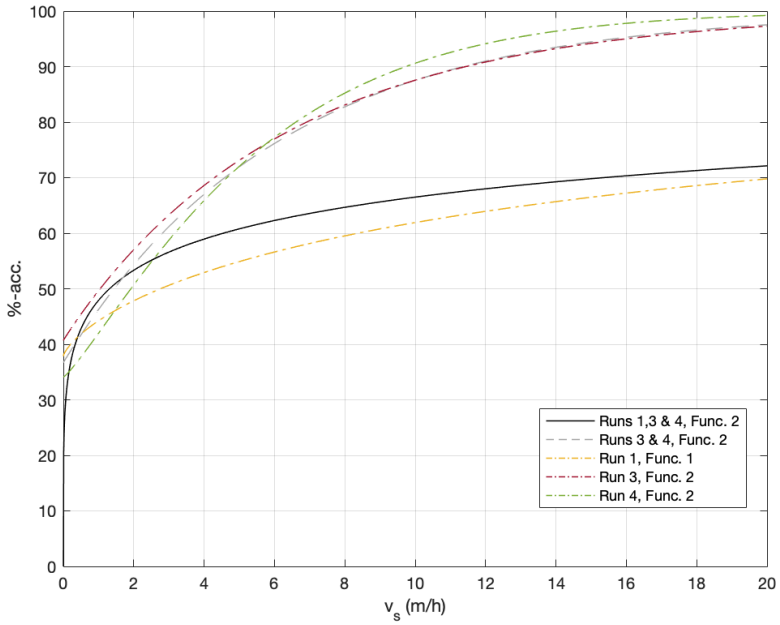


Figure 4.24: Fitted CSVD-curves to runs 1-4, $COD_p$, Öresundsverket

In Figure 4.25 below the measured and calculated fractions in each column (using closed mass balances and considering the misplacement of particles) are presented for the combined CSVD-curve (runs 1, 3 & 4).

**Results $COD_p$ Öresundsverket, measured vs calculated data**

Function 2

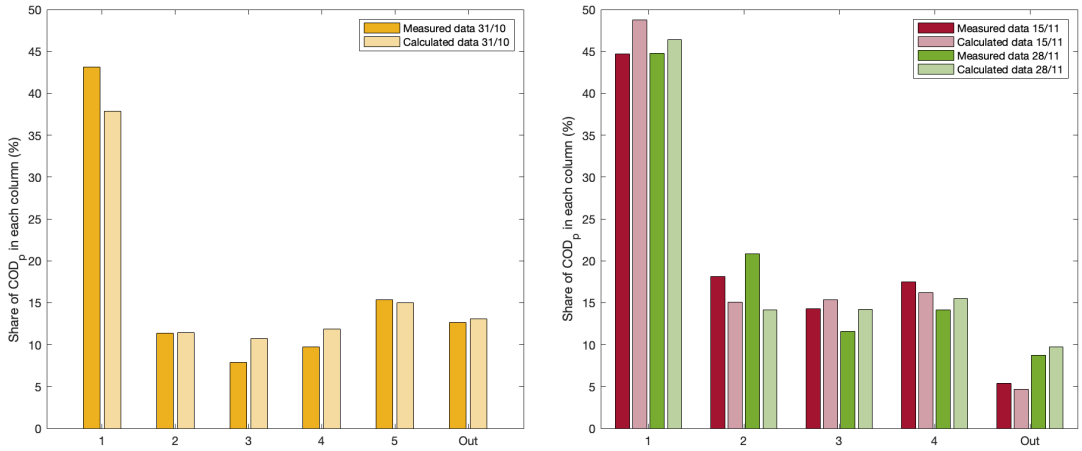


(a) Experiment 1 (b) Experiments 3-4

Figure 4.25: Estimated values using fitted CSVD-curve to runs 1, 3 & 4, $COD_p$

For the $X_B$ and $X_U$ only one set of data was available. In Figure 4.26 below, the CSVD-curves using both functions are shown, the ones with the best fit are shown using solid lines. Here it is clearly demonstrated what was mentioned above with the TSS at Öresundsverket, that the two functions yield very similar results for lower settling velocities but differentiate more as the settling velocity increases. Comparing the two, the $X_B$ has a much steeper incline than the $X_U$.

**Cumulative Settling Velocity Distribution Curve, $X_B$ & $X_U$, Öresundsverket**

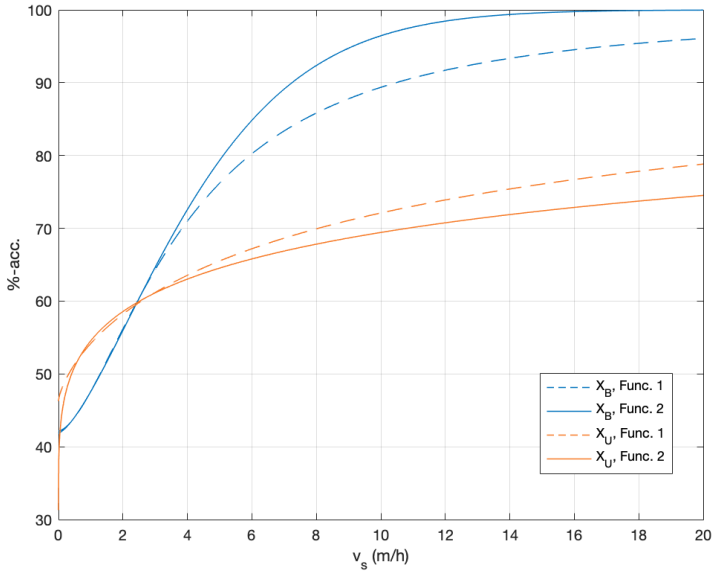


Figure 4.26: Fitted CSVD-curve for the $X_B$ and $X_U$

Finally in Figure 4.27 the measured and calculated fractions in each column (using closed mass balances and considering the misplacement of particles) are presented for the CSVD-curves for the $X_B$ and $X_U$ respectively.

**Results $X_B$ & $X_U$ Öresundsverket, measured vs calculated data**

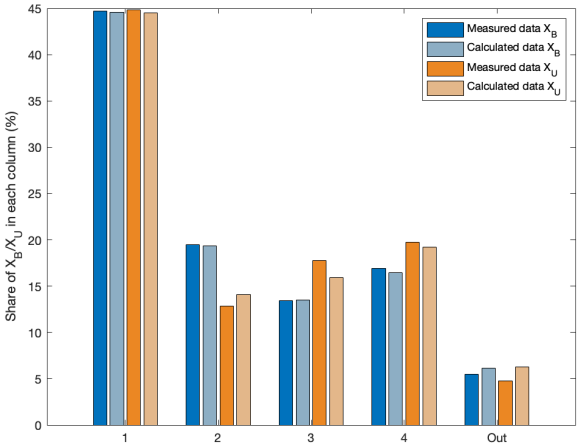


Figure 4.27: Estimated values using fitted CSVD-curve to experiment 3, $X_B$, $X_U$

## All distributions

To see how the different distributions compare with each other, all of them are shown in Figure 4.28 below. The distribution for the TSS and VSS are quite similar, and likewise so is the distribution for ISS and the $X_U$. The distribution of the $X_B$ again differ quite a lot from the others.

**Cumulative Settling Velocity Distribution Curves, Öresundsverket**

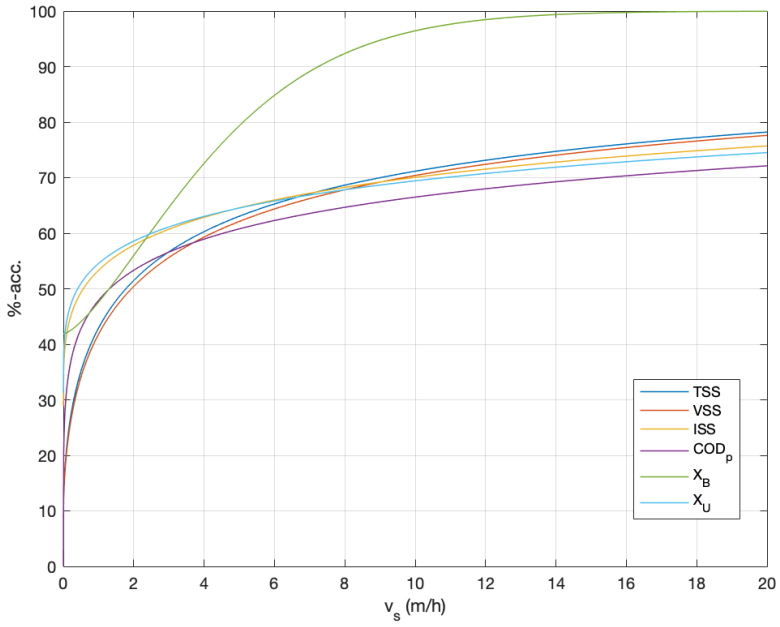


Figure 4.28: Combined CSVD-curves for the different substances at Öresundsverket

## 4.3 Comparing Källby WWTP and Öresundsverket

Comparing the CSVD curves at Källby WWTP and Öresundsverket in Figures 4.29a and b they are quite clearly grouped separately for the two WWTPs, albeit more so for the suspended solids. In general the CSVD curves at Källby WWTP start with higher non-settleable fractions than Öresundsverket and reach 100 % faster than the curves for Öresundsverket. This is also a common theme found with the CSVD curves adapted for individual data sets, although in the latter case mainly at Öresundsverket. The reason why it is found here as well may be due to the less accurate data at Källby however, it may just as easily be explained by different compositions of the influent wastewater at the two plants or by the different flow velocities used during the experiments as expanded upon below. The difference may also be due to where the samples are taken as the samples from Källby may include heavier particles as the sample is collected before the sand trap. How this would impact the CSVD-curve may depend on the range of upflow velocities measured.

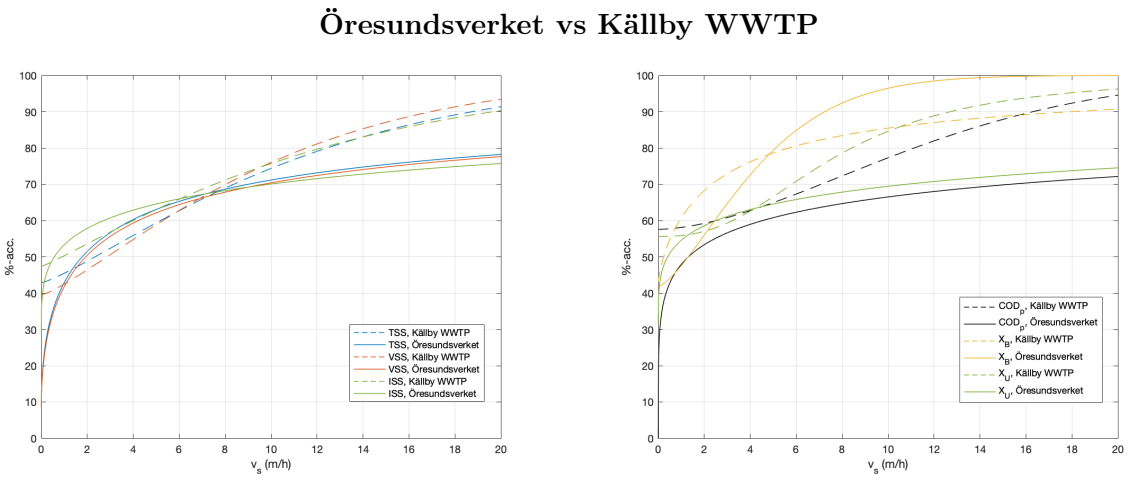


(a) TSS, VSS & ISS

(b) Particulate COD

Figure 4.29: Comparison of the Settling Velocity Distributions at Källby WWTP and Öresundsverket

Part of the reason for the very distinct groupings at Källby WWTP and Öresundsverket is likely the higher flows used during the experiments at Källby. This would give data points at higher velocities to fit the curve against, while for Öresundsverket the focus was mainly on the lower velocities at the beginning. Hence the CSVD curves are probably less accurate for lower velocities at Källby and likewise for the higher velocities at Öresundsverket. It seems quite unlikely that 20 % of the particles at Öresundsverket would have a higher settling velocity than 40 m/h (this is not shown in the figures though). In Bachis et al. (2015), the CSVD curves for the TSS reach 100 % at 20 m/h (i.e. half of that), which supports this premise. Regardless though whether these particles settle at 40 m/h or 4 m/h, their settling velocities are still substantially higher than the regular design overflow rate for the PST and should thus still be removed in the primary settlers.

In both plants the CSVD curves for the TSS and the VSS were very similar while the distribution of the ISS as well as the COD varied more. Especially the $X_B$-curves differed significantly from the rest. In Polorigni et al. (2021) (South Africa), different removal

rates in the PST have been observed in ranges of 60-70 %, 30-40 % and 70-90 % for the $X_U$, $X_B$ and ISS respectively. Based on the fractions read from the CSVD-curves at average overflow rates (0.8 m/h at Källby WWTP and between 0.5-2 m/h at Öresundsverket), the relative order between the $X_U$, $X_B$ and the ISS removals in the PST at Källby WWTP should theoretically be the same as that in Polorigni et al., while for Öresundsverket the $X_B$, rather than being the least removed should be the most removed. Even more so when considering the biological reactions occurring in the PST. These hypothetical calculations do however not take into consideration any contribution of particles of settling velocities higher than the average overflow rates in the effluent and assumes that none of the particles with a settling velocity less than that is removed. The numbers remain to be validated with actual plant data as only the particulate COD has been considered in the model validation here. However, as noted in the section on the model evaluation the initially estimated distribution for the $X_U$ and $X_B$ were modified quite heavily during the model calibration to achieve satisfactory results which might put into question the conclusions drawn above.

## 4.4 Determining the Settling Velocity Distribution

In this project a completely new calculation procedure for estimating the particle settling velocity distributions while taking into account misplacement of particles in the 5C-settleometer has been developed. In the following subsections different aspects of this procedure are discussed.

### 4.4.1 Comparison measured (settleometer) vs. estimated (CSVD) fractions

As is clear to see in Figure 4.30, there was a significant difference between the measured and calculated fractions due to the misplacement of the particles in the settleometer. The largest difference (in both absolute and relative terms) was the difference in the outgoing sample. This is due to the fact that particles belonging to this velocity group were spread out over all of the previous samples and no accumulation of particles outside of that velocity group occurred. The second and third largest difference were found in the samples from the second column and last column respectively for the three last runs, though for the first run at Öresundsverket at a higher velocity, more particles were misplaced in the samples from the first and last column, the order varying on the substance in question.

### 4.4.2 Choice of settleometer

One of the mainly considered advantages for the 5C-settleometer over the ViCAs-settleometer at the start of this project was the simplicity in its design. While one had less flexibility in where to place the 5 SVGs, one could just from running it, simply retrieve the corresponding data (in mass of fractions) for each SVG. However, throughout this project it has been made clear that it was perhaps not as simple as initially thought. Unlike noted

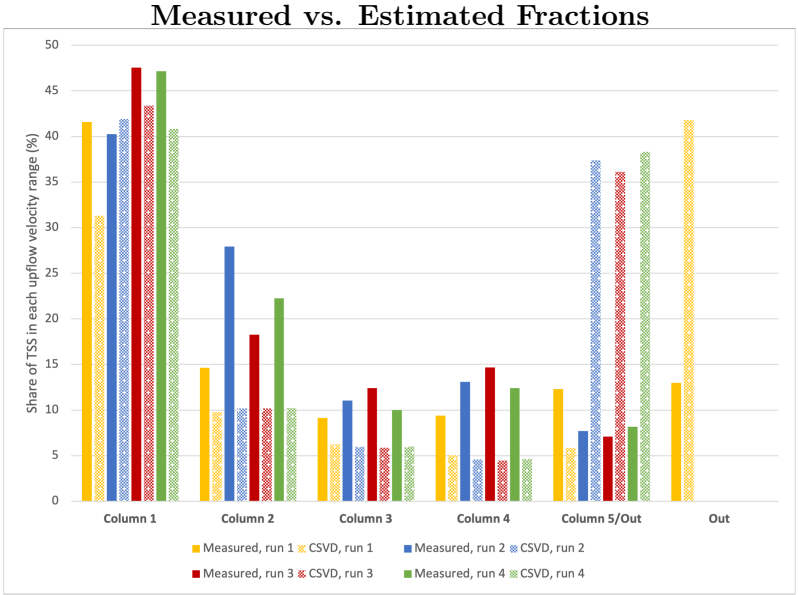


Figure 4.30: Comparison of the measured and calculated fractions of TSS at Öresundsverket

in Mazivila (2022) where the misplacement of particles in the settleometer was deemed negligible, its impact on the measured fractions became significant when lowering the flow velocity to match the overflow rates in the real PSTs. Hence, like with the ViCAs - settleometer an alternative form of using the retrieved data was developed by fitting and estimating the parameters for a cumulative settling velocity distribution curve.

Consequently the initial selling point for the settleometer may no longer be argued for. In terms of estimating a curve, the ViCAs protocol (second method) suggests a function with as many parameters as used here (see Functions 1 and 2), but no extra parameter was needed to account for the effect of the non-settleable fraction in the settleometer when estimating the parameters of the functions. Moreover, if the ViCAs experiment is run for as long as the 5C-settleometer generally has been run here (e.g. 4 h), 9+1 samples would be collected and used as a base for estimating the unknown parameters. Consequently one less parameter would be needed to estimate for the ViCAs protocol than for the method developed in this project and more data points are available to estimate them. Furthermore there is a smaller risk of flocculation interfering with the result compared to with the 5C-settleometer.

However, there are some downsides to the choice of the ViCAs settleometer as well. The total sample to be analysed takes up a volume of 4.5 litres in total. Hence, the total amount of particles to be analysed is much less than what is found in the 5C-settleometer where 5-10 times of the volume is used and they are spread out between more samples. In addition the samples collected from the ViCAs settleometer are very limited in size whereas over 1 litre can be collected from each column in the 5C-settleometer. This allows for more analyses of its contents and the possibility to e.g. also analyse the degradability of the particles, which according to results from South Africa differ a lot between the different organic fractions while here, not as much (although these results came with great uncertainties as mentioned due to the need to modify the distributions in the model). With the 5C-settleometer particles are also accumulated throughout the experiment increasing

the concentration of the particles over time in each column. Having said that it would be preferable to decrease the height of some of the columns in the 5C-settleometer in order to decrease the time required to fill them up. Moreover a slower increase in diameters would allow for a segregation of the particles in a more narrow range of interest.

### 4.4.3 Calculation procedure for estimating the CSVD curves

As mentioned earlier a completely new calculation procedure for estimating the CSVD-curves based on the measurements from the 5C-settleometer has been developed in this thesis taking into account the misplacement of particles in the settleometer. The calculation procedure is however still in need of further verification.

When estimating the parameters to the CSVD-curves 5-6 data points are available from a single run, depending on the number of columns in use during the experiment. From this, 4 different parameters are to be adjusted to achieve as good a fit as possible, i.e. almost as many parameters as data points! Combining several data sets yield more data points to fit the parameters against, however, it is possible that inclusion of certain data sets may have a large impact on the shape of the combined CSVD-curve as is seen with the combined and first data set at Öresundsverket. Furthermore, a small difference in measured data may change the shape of the CSVD-curve as seen for the particulate COD, run 3, and the $X_B$ at Öresundsverket which as seen in figure 4.9 have very similar distributions.

If some of the measured data is more reliable than others, their relative impact could be weighed when combining with other data. It is also possible that a different objective should be set than minimizing the sum of squared errors as this may yield an unproportionally large focus on the higher fraction measured in the first column compared to the rest. To change this, the errors could be calculated relative the measured values rather than as absolute values.

With a few exceptions the $d$-parameter, which does not describe the CSVD-function at all but the contribution of the non-settleable fraction in each column, has a value of, or close to, 1. To decrease the number of parameters to estimate, it could thus be possible to try and fix this parameter at a specific value such as 1 assuming the non-settleable particles to neither float nor sink in the columns relative the speed of the water. Finally it should also be investigated how much significance the starting set of parameters has when estimating the parameters for the CSVD-curves. Very little focus has been put on that in this project, but when testing a few different alternatives the same results were achieved, although at times a few warnings have been issued by MATLAB for the numerical calculations of the integrals during the search for the correct parameters. This may have impacted the direction in which the parameters were altered. No warnings were given however, when simply using the script with the parameter sets estimated.

### 4.4.4 Processes considered in the 5C-settleometer

As was clearly seen in Figure 4.30, there is a significant difference between the measured and calculated fractions due to the misplacement of the particles. Hence, this is important to consider when using the 5C-settleometer to fractionate the particles based on settling

velocity. However, there are more processes so far not considered that may affect the representativeness of the samples and the segregation of the particles such as degradation occurring during the experiment as well as potential flocculation occurring as the incoming particles have to travel through the sludge at the bottom of the column consisting of accumulated faster settling particles. Even if no flocculation is occurring, the density of the particles in the bottom increases the chance of inter-particle forces acting on the travelling particles, possibly reducing their movements (Mazivila, 2022). It is a challenge to create enough mixing in the incoming water for it to be proportional while not adding too much oxygen to the mix which may cause degradation of the particles. How much these processes will affect the result still remains to be seen.

It is also possible that not all particles from the incoming water are entering the settleometer due to getting stuck on the aquarium pumps stirring the incoming water or, this more in regards to the non-settleable particles, floating on the top of the water while the pump is sucking the water from further down in the bucket.

### 4.4.5 Choice of function for the CSVD curves

Two different functions were tested for the CSVD-curves in the calculation procedure, both yielding very similar results. When using the combined data sets at Öresundsverket the first function yielded a better fit for the TSS and VSS, the second function yielded the best fit for the particulate COD and $X_U$ (only one data set) and the ISS and $X_B$ (only one data set) achieved very similar results with both of the functions. For the separate data sets the opposite or mixed results were achieved, but much smaller difference than with the combined data sets, with the exception of ISS for which the second function once again yielded a slightly better fit. At Källby WWTP the second function yielded the best fit for all substances except the $X_B$ and $X_U$ when using the combined data sets, or in the case of ISS separate as it only had one data set in total. For the separate data sets mixed results were achieved for the different functions. However, it might be good to note that for the most part only the data retrieved from the third run at Källby was within the stated limits of the mass balance error.

When it comes to the CSVD-curves, two main characteristics can be discussed, the non-settleable fraction and the slope by which they reach 100 %. Generally the second function seems to result in a lower non-settleable fraction than the first function. The same trend is also observed when using several data sets to estimate the parameters rather than a single data set. In Bachis et al. (2015) the non-settleable fraction for the TSS seems to vary between 20-40 %. At Öresundsverket the non-settleable fractions for the individual data sets for the TSS and VSS ranges between 30-40 % while the non-settleable fractions for the combined data sets are much lower. For the particulate COD, the results is similar while for the ISS the non-settleable fractions are much higher. There is however a very steep incline around the y-axis for the functions with a very low non-settleable fraction, resulting in a more similar value for the non-settleable fraction "in practice". At Källby WWTP the estimated non-settleable fraction is generally higher than the one at Öresundsverket.

As mentioned in section 4.3, the combined CSVD-curves at Öresundsverket generally take a lesser slope and thus only reach 100 % at much higher settling velocities. It is not

clear whether this is due to the choice of function or if it comes from including certain types of data. When combining the data sets the combined CSVD-curve is usually found between the individual ones, the ISS at Öresundsverket being the exception. The first run at Öresundsverket has a much more flattened shape for all substances but the ISS, which might explain the more flattened shape of the combined curves. As the combined curve for the $COD_p$ run 3 & 4 at Öresundsverket does not share this characteristic the latter explanation may seem more likely. However, this does not explain why the same occurs for the ISS at Öresundsverket, despite none of the individual curves exhibiting this characteristic to that extent.

## 4.5 Model Evaluation

Based on the results in the previous chapter a model based on the PSVD-concept was set up. However, only the distributions for the $X_B$, $X_U$ and ISS were used which unfortunately also happen to be the ones with the least amount of data to back them up. Rather than modelling the TSS separately, the TSS was calculated based on the particulate COD and the ISS. The following conversion factors were used (Ahnert et al., 2021):

- $X_{OHO}$ & $X_P$: 1.42 g COD/g VSS
- $X_B$: 1.8 g COD/g VSS
- $X_U$: 1.3 g COD/g VSS

Why the TSS could not be modelled separately is due to the biological reactions included in the model. As there were some uncertainties in the data used, in particular for the subgroups of the particulate COD, these values may clash with another state variable partly describing the same particles, but with another distribution. The biological reactions are dependent on the concentrations of the biodegradable particulate COD and the biomass. Hence, more $X_B$ or $X_{OHO}$ can be removed (by hydrolysis or decay) in one settling velocity group than what is available when converting it to TSS, causing computing errors to occur.

### 4.5.1 Assigning settling velocities and fractions

In Table 4.5 the properties of the five settling velocity groups are presented. This is shown for both the originally estimated settling velocity distribution and the modified one. The modification is made by simply moving 25 %-units of SVG 1 for the two particulate COD subgroups to SVG 5.

Table 4.5: Boundaries and assigned fractions for the 5 SVGs

| | **SVG 1** | **SVG 2** | **SVG 3** | **SVG 4** | **SVG 5** |
|---|---|---|---|---|---|
| **Velocity interval (m/h)** | 0.01-0.5 | 0.5-0.85 | 0.85-1.2 | 1.2-2.1 | 2.1 - 40 |
| **Assigned velocity (m/h)** | 0.071 | 0.652 | 1.010 | 1.732 | 9.165 |
| **Original Distribution (%)**: | | | | | |
| ISS | 49.3212 | 3.0106 | 2.125 | 3.7238 | 41.8194 |
| $X_B$ & $X_{OHO}$ | 44.0593 | 2.3771 | 2.7208 | 7.7116 | 43.1312 |
| $X_U$ & $X_P$ | 50.9662 | 2.6983 | 1.8961 | 3.3116 | 41.1278 |
| **Modified distribution (%)**: | | | | | |
| ISS | 49.3212 | 3.0106 | 2.125 | 3.7238 | 41.8194 |
| $X_B$ & $X_{OHO}$ | 19.0593 | 2.3771 | 2.7208 | 7.7116 | 68.1312 |
| $X_U$ & $X_P$ | 25.9662 | 2.6983 | 1.8961 | 3.3116 | 66.1278 |

Which CSVD-curves were chosen for each substance when determining the SVG distributions are shown in Table 4.6.

Table 4.6: Functions/data sets chosen for each substance

| | **Function** | **Experiments/Runs** |
|---|---|---|
| ISS | 2 | 1 & 4 |
| $X_B$ & $X_{OHO}$ | 2 | 3 |
| $X_U$ & $X_P$ | 2 | 3 |

To illustrate how much the SVGs would differ by use of different functions and/or data sets Figure 4.31 was included. As is clearly seen most of the ISS (but very similar for the other substances) belonged to the first or last SVG and very little belonged to the middle groups. For the ISS this was the most pronounced as only 1-4.5 % in total was found among the three middle groups for the individual runs. For the other substances, the sum of the fractions for the three middle groups from the first run was between 6.5-8 %, while for the other three runs the sum was between 12-17 %. For the combined CSVD-curves the total share was, with the exception of ISS, found in the upper range of the individual values. For the ISS at Öresundsverket the value was twice that of the largest individual one, but then the combined CSVD-curve for the ISS at Öresundsverket also differed more from the individual ones than for the other substances.

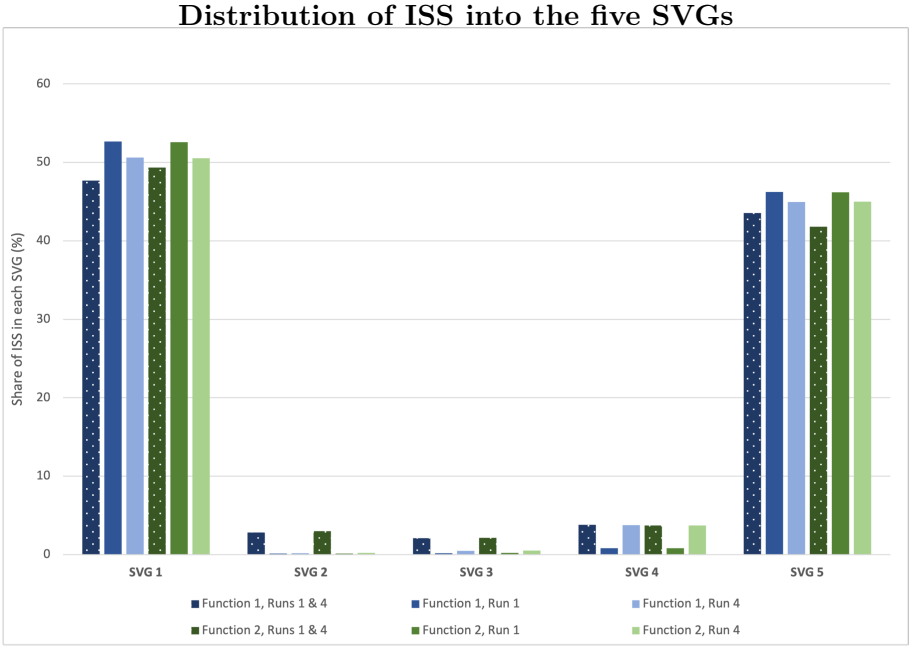


Figure 4.31: Distribution of ISS in the five SVGs for different functions and runs

### 4.5.2 Calibration - 10$^{th}$ of January

Calibration of the hydrolysis reaction parameters as well as the SVG distribution for the particulate biodegradable and inert COD was made on collected data from the 10$^{th}$ of January. The kinetic parameters used in the final version can be found in table 4.7 below. Note that the decay kinetic parameters are shown as well, despite not having altered those.

Table 4.7: Calibrated kinetic parameters

| Parameter | Description | Value |
|---|---|---|
| **Hydrolysis:** | | |
| $k_{h,20}$ | Hydrolysis rate constant at 20 °C | 3 |
| $\eta_{kh}$ | Correction factor for hydrolysis under anaerobic conditions | 0.14 |
| $\theta_{kh}$ | Temperature correction factor for $k_h$ | 1.2 |
| **Decay:** | | |
| $b_{OHO,20}$ | Heterotrophic decay rate constant at 20 °C | 0.4 |
| $\eta_{bOHO}$ | Correction factor for decay under anaerobic conditions | |
| $\theta_{bOHO}$ | Temperature correction factor for $b_{OHO}$ | 1.072 |

The hydrolysis and heterotrophic decay rate constants at 20 °C as well as the temperature correction factor for the decay rate constant were both taken as standard values from ASM (Henze et al., 2000). In ASM2d the correction factor for hydrolysis under anaerobic conditions is set as 0.4 (Henze et al., 2000), but in several commercial modelling softwares this can be found as much lower (Evans et al., n.d.). Finally the value for the anaerobic decay correction factor is taken from Sumo (Dynamita, 2022). What mainly differs from the literature values is the temperature correction factor for the hydrolysis rate constant.

This kinetic parameter was calibrated to the validation set in the next subsection where the temperature varied much more. In ASM (Henze et al., 2000) this kinetic parameter has a value of approximately 1.041 while here a value of 1.2 was used. It might not sound like a big difference, but as it is powered to the difference in temperature from 20 °C, it becomes a very large increase. A possible explanation however, is likely an inadequate description of the incoming data in the validation set where the same characterization of the incoming COD was used all-year round while in reality there is probably more soluble COD during the summer.

In Figures 4.32a-f the simulated effluent (Figures a-e) and underflow (Figure f) for the $10^{th}$ of January using the original distribution are shown. The measurements were done for the TSS, soluble COD, ammonium and ISS. The particulate COD in the influent and effluent was calculated from the TSS as their measurements were not deemed reliable.

For the influent particulate substances, there was a clear peak at the end of the measured data. This peak was based on one measurement of the TSS and ISS respectively. As one more sample was analyzed for the effluent than the influent the last incoming concentration was set identical to the previous, thus extending the peak. Due to the significant increase in the influent concentration, naturally the simulated effluent concentration was increased as well. This is however, not noticeable in the measured effluent indicating that perhaps the measured TSS and ISS in this last sample was not reliable. When initializing the states in the PST, these concentrations in the influent were set as identical to the first measurement. There was also a peak at the start for the measured particulate substances in the effluent, but this was not caught by the model, likely due to lack of knowledge of previous conditions causing the release of the sludge in the effluent.

As is seen in the figures the soluble components ($COD_s$ and $S_{NH}$) varied more throughout the day compared to the particulate components as they are more dependent on the incoming concentrations. The trend was also clearly seen in the simulated effluent, although slightly delayed. Likely, there was a measurement error in measured $COD_s$ in the fifth sample (t = 0.33 d) and the $S_{NH}$ in the eighth sample (t = 0.58 d) for the influent or the effluent as the measured effluents exhibit a significant drop in concentration not explained by the influent at these times. Apart from the influent, the soluble components were also affected by the biological reactions occurring in the PST, although the soluble COD was more significantly so than the ammonium as was clearly demonstrated by the need for modifying the hydrolysis kinetic parameters.

For the calibration data set on the $10^{th}$ of January 2023, it was also clearly seen how the modelled effluent with the original distribution of the particulate biodegradable and inert COD overestimated the particulate COD and thus also the TSS with around 100 mg/L. The overestimation of the particulate COD and the TSS in the effluent was directly related to the high incoming concentrations of these substances within the first settling velocity group. The ISS however, had a much better fit and was thus not altered in the modification of the distributions. As the overestimating of the particulate COD and the TSS in the effluent was directly related to the high incoming concentrations of these substances within SVG 1, it was investigated whether decreasing the fraction corresponding to this SVG would improve the simulation. Thus, 25 %-units were moved from SVG 1 to SVG 5. The much improved modelled results can be seen in Figures 4.33a-d for the modified distribution. Changing the distribution of the particulate biodegradable

**Results Calibration 10/1-2023, Original distribution**

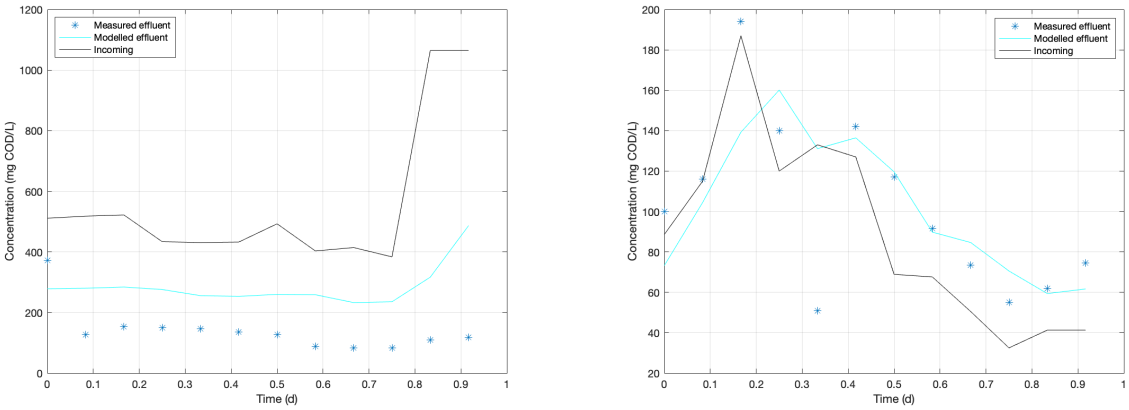


(a) $COD_p$




(b) $COD_s$

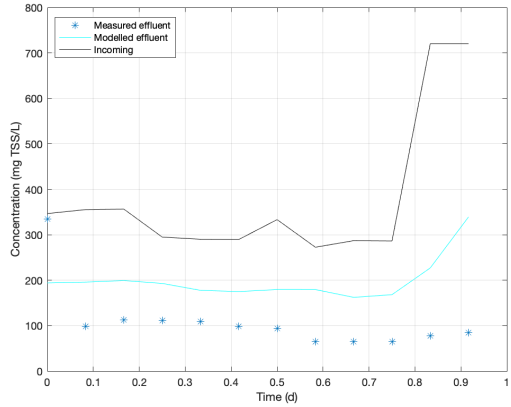


(c) TSS

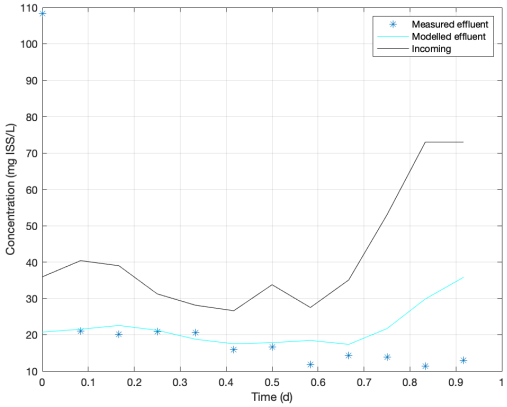


(d) ISS

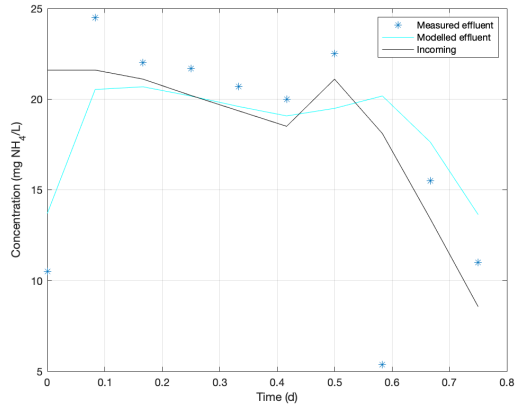


(e) $S_{NH}$

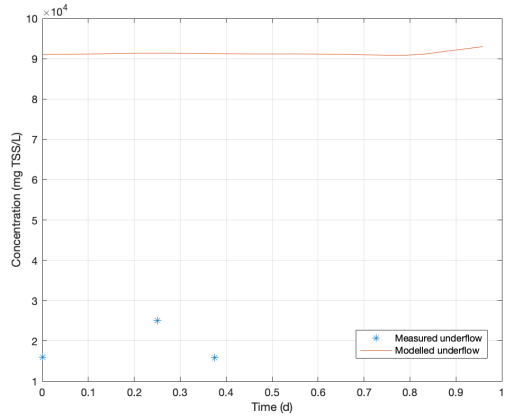


(f) TSS - underflow

Figure 4.32: Calibrated values on the $10^{th}$ of January 2023, using the original distribution. The measured values are shown with blue dots, the incoming in solid black lines and the simulated effluent and underflow in solid cyan and red lines respectively.

and inert COD only affected the COD (particulate and soluble) and the TSS (in effluent and underflow), hence only these are shown for the modified distribution.

Something that was not simulated very well with the data set however, was the TSS concentration in the underflow. The simulated values started with around 6 times the measured concentration with the original distribution and was increased up to 10 times the measured values when using the modified distribution. The increase in concentration in the underflow with the modified distribution is natural as what is taken from the effluent should end up in the underflow to preserve the mass balance. However, why it differs so much from the measured values is still cause for speculation. When calculating the mass balance of what enters and leaves the PST on the day before the displayed values, i.e. the day that was looped to initialize the states in the PST without the peak at the end for the incoming $COD_p$/TSS/ISS, this held true for the simulated values with a relative mass balance error for the total COD (compared to the incoming mass) of the size $10^{-5}$. As the volume of sludge removed each day (not taking into consideration the recirculation streams) was very small in comparison to the effluent, a small error in the effluent would give cause to a much larger change in the underflow concentration to preserve the mass balance. However as the $COD_p$ and the TSS in the effluent was generally overestimated, in particular for the original distribution, this should rather give cause to a much smaller concentration in the underflow to preserve the mass balance. Thus, the mass balance of the streams entering and leaving the PST for the measured values do not add up and the PST must thus in practice be accumulating sludge during this particular day. On the day in question the incoming flow was about 50 % higher than the average dry weather flow. The error in the measured and simulated underflow concentration may thus very well be from looping the measured values to initialize the states in the PST, when this in fact does not represent the previous flows to the PST. Moreover, a constant sludge flow rate was used in the model, when in fact this differed some (albeit for most of the values during the day only with a few %) which may have had some impact on the outcome.

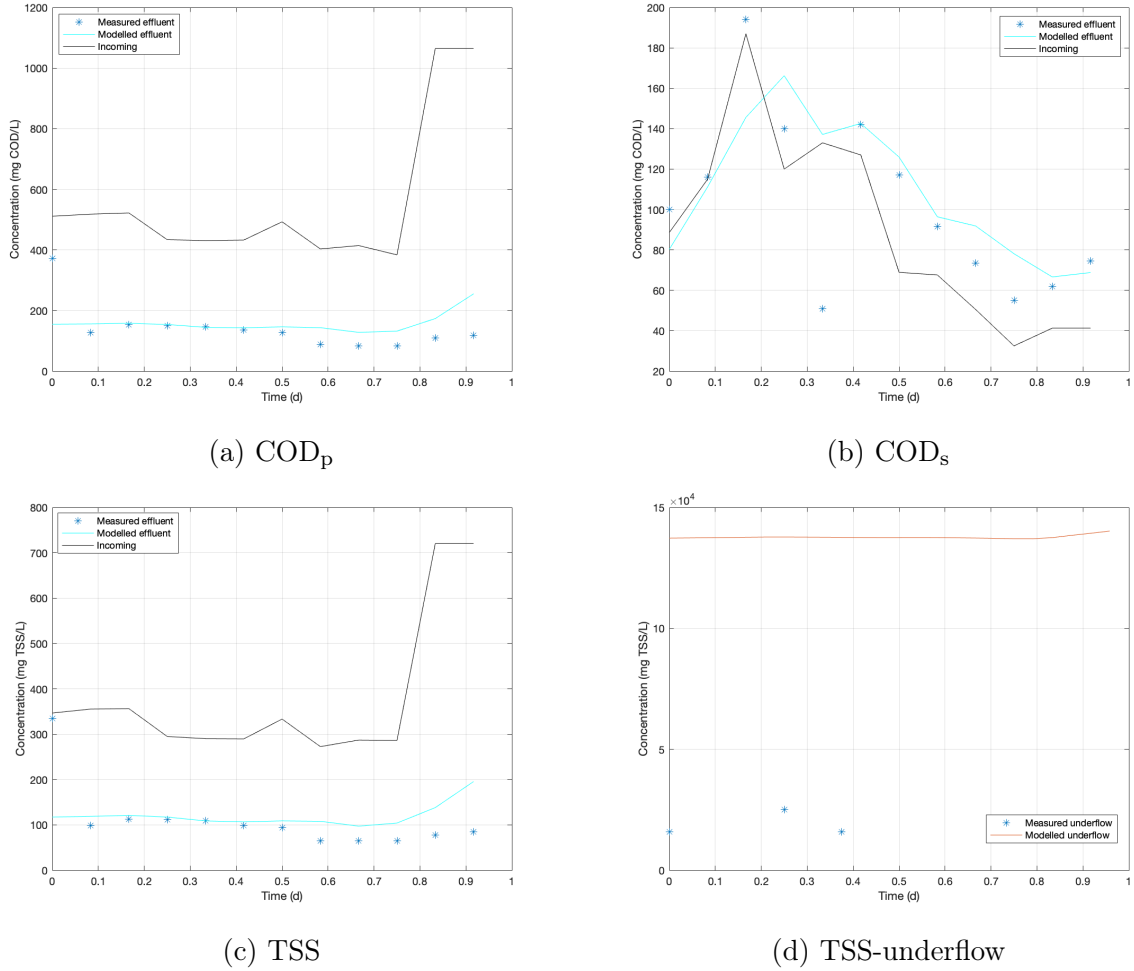


(a) $COD_p$

(b) $COD_s$

(c) TSS

(d) TSS-underflow

Figure 4.33: Calibrated values on the 10th of January 2023, using modified distribution

### 4.5.3 Validation - 2020

The model was also validated on a much longer data set for 2020. The influent flow and concentrations were given as hourly values and the measured effluent was given as flow-weighted daily measurements throughout the year. In Figures 4.34a and b the water temperature and flow throughout the year is shown with the temperature clearly peaking in the summer while the flow was decreasing with the exception of some rain events. Due to the large difference in temperature the temperature dependency of the hydrolysis rate constant was also calibrated to this data set, but not the rest of the parameters.

The results from the validation are shown in Figures 4.35a-c and 4.36a-c for the original and modified distribution respectively. When validating the model it could be seen that the measured outflows were predicted pretty well for the modified distribution of the particulate biodegradable and inert COD. For the original distribution however, the TSS and total COD were somewhat overestimated in the effluent and the soluble COD less prevalent in the effluent due to the lower concentrations of heterotrophs in the underflow and thus a slower hydrolysis rate. The latter could be dealt with by some additional tweaking of the reaction rates and temperature dependency of the hydrolysis reaction but

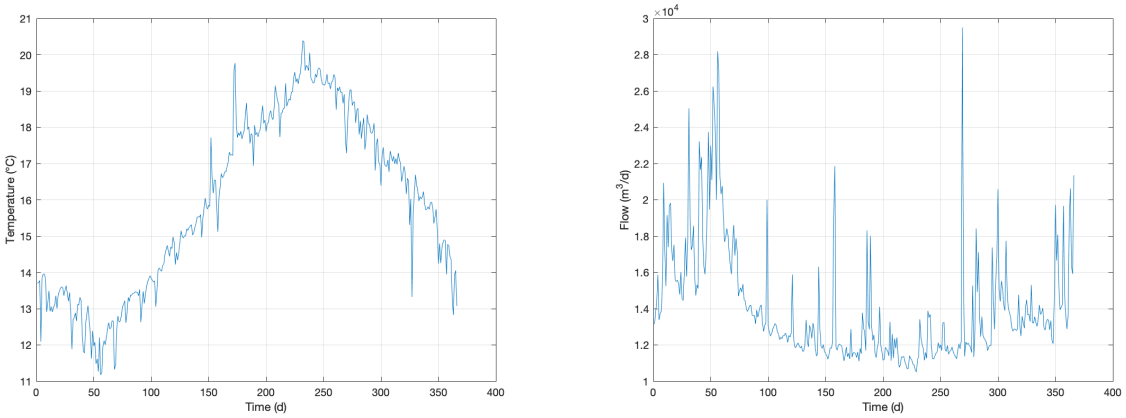


(a) Temperature (b) Flow

Figure 4.34: Temperature and Flow in to the PST during 2020

this would not solve the former issue.

As noted there was a discrepancy between the measured effluent and simulated one in the PST using the originally estimated distribution of the particulate COD (biodegradable and inert), where the former seemed to heavily overestimate the concentrations in the effluent. The solution in the calibration process was to move 25 %-units of the particulate biodegradable and inert COD from the first SVG to the last. Why this had to be done is not ascertained, but the source of the discrepancy is likely found in the data collected, the methodology used for estimating the distributions or the model used to describe the PST.

The first alternative for explaining the discrepancy could be unrepresentative data collected on which the estimation of the settling velocity distribution is based on. The settling velocity distributions of the particulate biodegradable and inert COD were both based solely on values from the third data set. One thing that stood out with the measurements during this run was the significantly lower concentrations of COD compared to the other runs at a similar velocity and end time. However, the calculated distribution during this run was still very similar to the others and this does not therefore explain the discrepancy between the original and modified distributions in the model.

So far the estimation of the CSVD curves does not consider any physical or biological processes such as flocculation or degradation/hydrolysis occurring in the settleometer. As flocculation in the settleometer would have the opposite effect as described here, i.e. it would increase the amount of heavier particulates, this can not have been the reason for the discrepancy. Degradation of COD requires a source of electron acceptors to occur, i.e. oxygen or nitrogen oxides. As the environment in the settleometer was mainly anaerobic, the primary source of electron acceptors for the degradation to occur would be found in the incoming water at the inlet of the first column. The fact that the soluble COD concentration in the samples from the columns and the outgoing sample was less than that of the incoming sample taken at the start of the experiment is an indication that some degradation was occurring, the question is how much. If say the incoming water had a dissolved oxygen concentration of about 8 mg/L (i.e. near the dissolved oxygen saturation level at this temperature), the total amount of oxygen could in worst case scenario (i.e.

**Results Validation 2020, Original distribution**

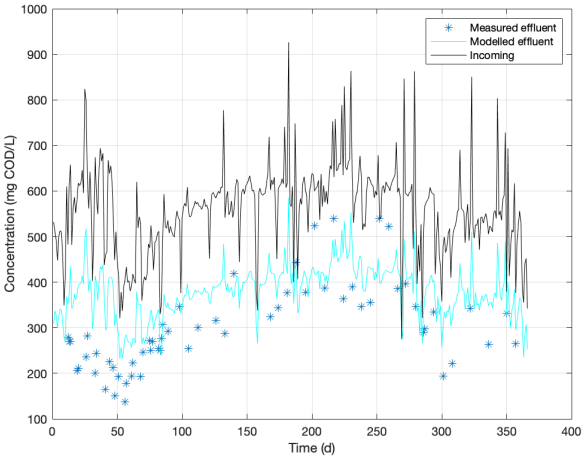


(a) $COD_{tot}$

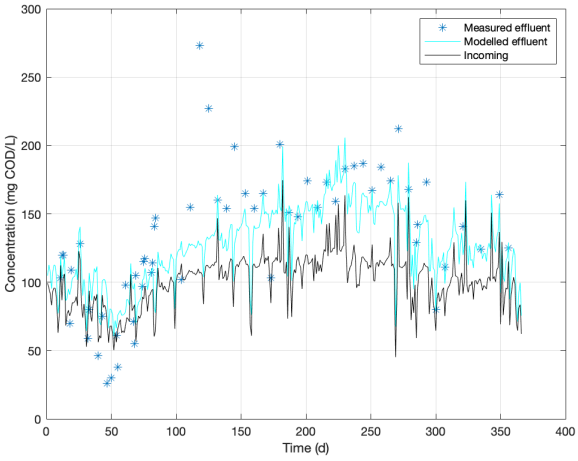


(b) $COD_s$

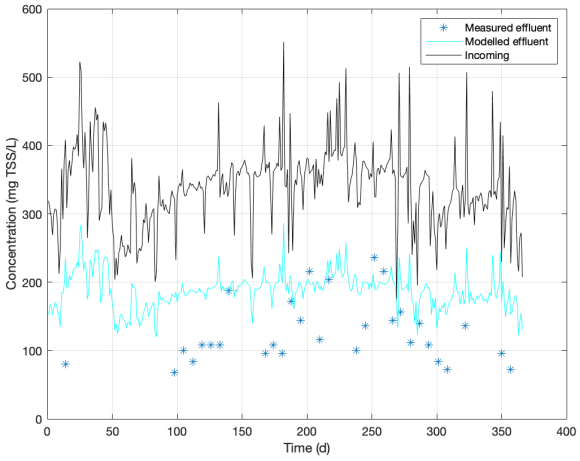


(c) TSS

Figure 4.35: Validation results 2020, using original distribution

**Results Validation 2020, Modified distribution**

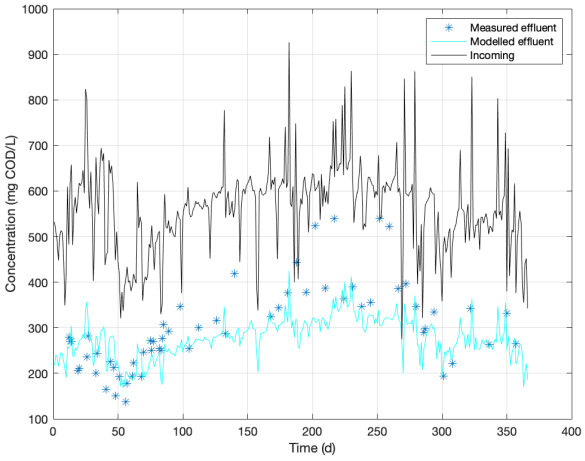


(a) $COD_{tot}$

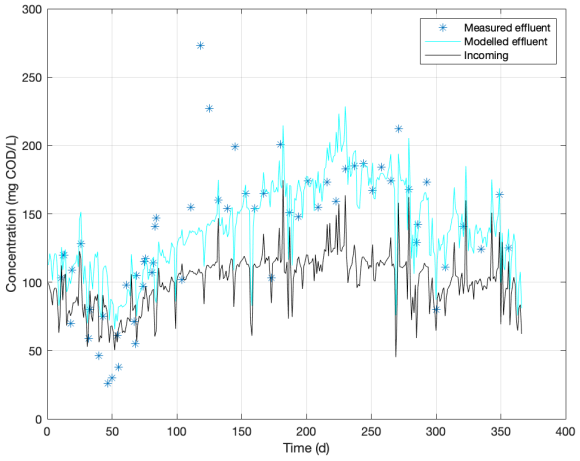


(b) $COD_s$

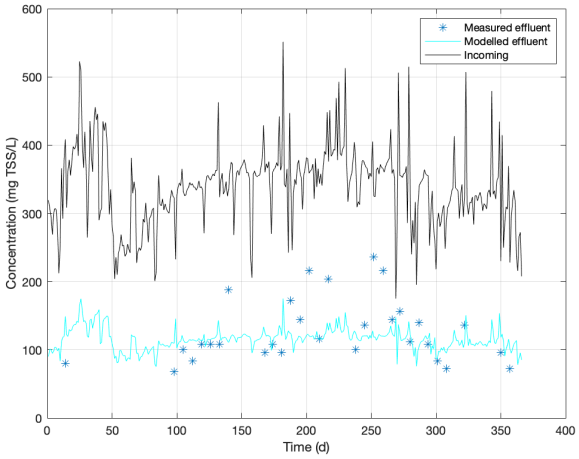


(c) TSS

Figure 4.36: Validation results 2020, using modified distribution

during the third run) amount up to just below 3 % of the total incoming particulate COD. The degradation of soluble COD would of course not impact the distribution of the particulate COD, but it would however, in these calculations, act as an upper boundary of how much hydrolysis may have occurred in the first column. Hence, at most 3 extra %-units may be added to the fraction found in the first column. However, this is a very rough estimation and not all of this would be reasonable to add on as some of the soluble COD degraded would be converted into biomass. The effect on the measured data in itself would thus not be very large, but the effect when closing the mass balance may be somewhat larger and it may or may not result in an even larger effect when estimating the parameters for the CSVD curve.

Potentially, some of the hydrolysis occurring in the settleometer might not have converted the particulate COD all the way to soluble COD, but simply to smaller particulates with a smaller settling velocity. This would then have had more of an effect on the heaviest particles explaining the discrepancy, as the highest concentrations and thus the fastest hydrolysis rates were found at the inlet of the first column. If this was occurring in the settleometer however, it should also likely have been occurring at the bottom of the PST where the concentrations of particulates were high. Yet, as this would have the opposite effect on the distribution as the modification applied to the original distribution (which was clearly improving the simulated effluent concentrations), this seems unlikely an explanation.

Secondly, the discrepancy could be caused by an inaccurate estimation of the settling velocity distribution from the given measurements. As seen previously when combining more data sets, the non-settleable fraction tends to be decreased compared to when only using a single data set. When estimating the SVG-fractions however, the difference between the combined and individual data sets was normally only up to 5 %-units for the first SVG which was then mainly distributed among the middle settling velocity groups. This change is not in the same size of that of the modification where 25 %-units each of SVG 1 for the particulate COD were moved to SVG 5. A more likely explanation would rather be that the methodology for estimating the CSVD curves was developed here for this very project and it has consequently not been previously tested and verified. This could thus very well be the cause for the discrepancy described above.

Finally a possible explanation of the discrepancy could be an inadequate description of the model. The PSTs at Öresundsverket are a bit more complicated than most others including resuspension of settled (hydrolyzed and fermented) primary sludge by a pump to the top of the settler. As the high concentrations of $COD_p$ and TSS in the effluent were directly related to the incoming concentrations of these substances belonging to the slowest settling velocity group, it is possible that the composition of this group was affected when including resuspension of the sludge. Potentially some flocculation occurred for these particles when including the resuspension of the primary sludge, moving them to a heavier settling velocity group. Validating this methodology on a WWTP without sludge resuspension might answer whether this might be the case. Another factor which may have had an impact is the location of the feed layer in the model. Here it was taken as in the Takács model. This should however be set based on the PST configuration.

### 4.5.4 Comparison with design guidelines

Finally the validated model was used to compare against the design guidelines in terms of surface area to inflow ratio. In Figure 4.37 the removal rates in the PST for different overflow rates were compared with the design guidelines. As is seen in the figure, the lines representing the removal rates were quite flat and did not change that much with the overflow rate, apart from the last value which was taken at an extreme scenario. In truth they seem a bit too flat as the difference in removal rate when doubling the overflow rates is simply by a few %-units and should probably be taken with a grain of salt. A likely explanation as for why they did not differ that much is the choice of settling velocity groups used. Here, the SVGs were chosen with two very large groups, one consisting of the particles that almost never settle, and one with the particle that almost always do. In model terms this means that the former group had a very low settling velocity while the latter group had a very high one. When decreasing the overflow rate a larger portion of each group was settling and vice versa, but as the first and last SVGs were very large with a very small or large settling velocity respectively a lot more change would be needed in the model to cause a significant change in the removal rates when approaching their boundaries. This, as the distribution within these groups were not taken into consideration. The upper and lower boundaries for the middle SVGs were here quite similar to those of the design guidelines.

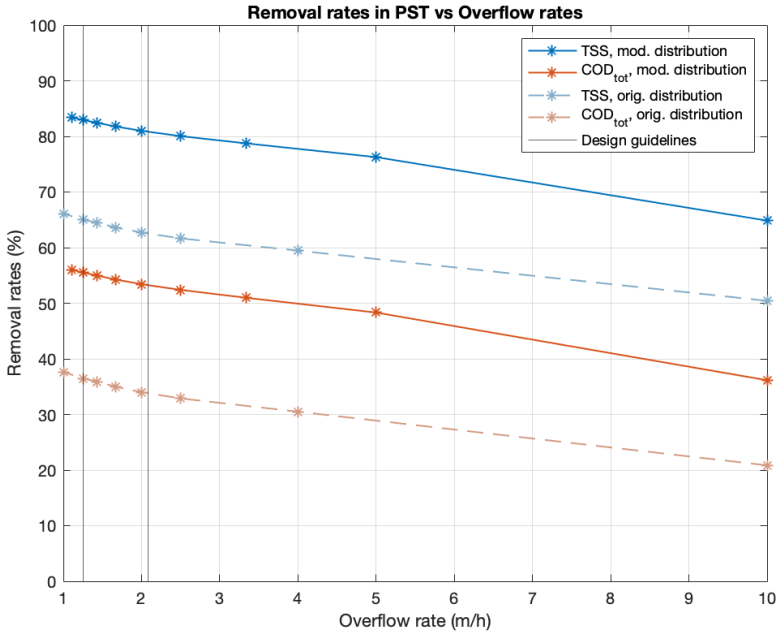


Figure 4.37: Removal rates vs overflow rates in the PST

In Figure 4.37 the removal rates using both the original and the modified settling velocity distribution are shown. This, as it was not known whether the modification of the settling velocity distribution was needed mainly due to the recirculation of the primary sludge in the validation, or due to other factors. Something worth noting however, is that the standard removal rates in the PST for the TSS and BOD with ranges of 50-70% and 25-40 % respectively (Metcalf & Eddy et al., 2014), fit better within the range of the

design guidelines with the original distribution than the modified one. Something that could suggest that the resuspension of the sludge may very well be the cause for the need to modify the settling velocity distributions.

As the choice of SVGs had a high importance for this purpose, one might ask how relevant the three middle SVGs are when calibrating and validating the model. For the three distributions used here, the sum of all particles in these three groups added up to less than 15 % of the total. Considering the individual runs for the ISS, this should perhaps even have been a third of that. 15 % is large enough that it probably should be considered, but perhaps it is a bit redundant dividing it into three separate groups when considering the sizes of the two boundary groups. Hence, for the purpose of simply predicting the performance of the PST at normal conditions, 3 SVGs might be sufficient. For another purpose such as the above, more settling velocity groups would be needed with a wider range for the distribution.

# Chapter 5

# Summary and Conclusions

In this thesis a completely new calculation procedure for estimating the settling velocity distributions based on measurements from the 5C-settleometer has been developed, taking into account the misplacement of particles in the settleometer. Over the course of eight weeks, the particles in the incoming water at two different WWTPs have then been characterized based on their settling velocity distributions for the TSS, VSS & ISS and the particulate COD. Moreover, an aerobic degradation experiment has been made on the samples during one run at each WWTP, determining the distributions for the biodegradable and inert parts of the particulate COD. Finally the results at Öresundsverket have been used to set up a model and the results evaluated. Some conclusions which may be drawn are as follows:

- The misplacement of particles in the 5-column settleometer was significant when applying surface loading rates typically used at the PSTs, suggesting that redesign of the settleometer is necessary.
- The settling velocity distributions of the TSS and VSS at the same WWTP were very similar, while the rest differed a bit more. Especially the distribution of the biodegradable particulate COD seemed to differ significantly from the others
- The settling velocity distributions differed significantly between the two WWTPs suggesting that the PST should be designed based on the composition of the incoming wastewater and not simply on the incoming flow. The accuracy of the results however, still needs to be verified.
- A model of the PST based on the particle settling velocity distribution concept achieved good results when simulating the effluent, but some modification of the calculated distributions had to be made when calibrating against real data. Simply using the settleometer and calculation procedure derived here was not sufficient in this case.
- A broader distribution of the settling velocity groups and potentially more groups are needed to fully estimate the performance of the PST outside its normal overflow range.

# Chapter 6

# Recommendations for Future Work

**5C-settleometer, design and operation:**

- Design of the settleometer:
  - Decrease the height of the subsequent columns to decrease the time at which it needs to run.
  - Depending on purpose for characterization, potentially alter the increase in diameters.
- Measure the volume at the end and add up to get the incoming volume rather than estimating them on flow velocity and time. Use this to estimate the average flow velocity when calculating the upflow velocities.
- Perform multiple measurements (TSS/COD etc.) as a base when closing the mass balances
- Try and fit the upflow velocity range with the desired overflow range to investigate
- To prevent biological reactions from occurring, cool the samples directly upon collecting them. Potentially cool the entire set-up while running it as well.

**Degradation test:**

- Repeat and verify the results
- Investigate whether aerobic biodegradability is the same as anaerobic biodegradability

**Calculation Procedure:**

- Investigate the effect of flocculation, interparticular forces and degradation/hydrolysis
- Fix parameter $d$ to decrease the number of parameters needed to be estimated

- Try changing the objective function to consider relative errors rather than absolute ones
- Investigate how many runs are needed for adequate estimations and whether they should be done individually or combined.

**Modelling the PST:**

- Verify the calculation procedure with a model based on a WWTP without sludge resuspension
- Verify the other settling velocity distributions and not just the $X_B$, $X_U$ and ISS
- Investigate how broad a distribution and how many SVGs are needed to estimate the performance of the PST outside of its normal overflow range
- Investigate how the model developed compares to a more simple one in terms of accurate model predictions. Is there a need for such a complex model?
- Investigate how the subsequent processes are affected by the use of a more complex model based on the PSVD-concept for the different subgroups

# References


Ahnert, M., Schalk, T., Brückner, H., Effenberger, J., Kuehn, V., & Krebs, P. (2021). Organic matter parameters in wwtp–a critical review and recommendations for application in activated sludge modelling. *Water Science and Technology*, *84*(9), 2093–2112.

Amerlinck, Y. (2015). *Model refinements in view of wastewater treatment plant optimization: Improving the balance in sub-model detail* (Doctoral dissertation). Ghent University, Ghent, Belgium.

Arnell, M. (2013). *Modellering av Linköpings avloppsreningsverk. Uppdragsnummer: 120043*. CIT Urban Water Management AB. Linköping, Sverige.

Bachis, G., Maruéjouls, T., Tik, S., Amerlinck, Y., Melcer, H., Nopens, I., Lessard, P., & Vanrolleghem, P. A. (2015). Modelling and characterization of primary settlers in view of whole plant and resource recovery modelling. *Water Science and Technology*, *72*(12), 2251–2261.

Bürger, R., Diehl, S., Farås, S., Nopens, I., & Torfs, E. (2013). A consistent modelling methodology for secondary settling tanks: A reliable numerical method. *Water Science and Technology*, *68*(1), 192–208.

Chebbo, G., & Gromaire, M.-C. (2009). ViCAs—An operating protocol to measure the distributions of suspended solid settling velocities within urban drainage samples. *Journal of Environmental Engineering*, *135*(9), 768–775.

Davis, M. L. (2010). *Water and wastewater engineering: Design principles and practice*. McGraw-Hill Education. New York, USA.

Dynamita. (2022). Sumo 2s, two-step whole-plant model.

Evans, Rosenthal, Downing, & Neethling. Biological phosphorus removal - use of simulations to assess performance and the function of key design parameters. In: 8th Water Resource Recovery Modelling Seminar (South Africa).

Forså, N. (2022). Process Engineer at Källby WWTP. Personal communication.

Gernaey, K., Vanrolleghem, P., & Lessard, P. (2001). Modeling of a reactive primary clarifier. *Water science and technology*, *43*(7), 73–81.

Gernaey, K. V., & Jeppsson, U. (2014). *Benchmarking of control strategies for wastewater treatment plants*. IWA publishing. London, UK.

Hach. (n.d.). *Cod cuvette test 150-1000 mg/l o, 25 tests*. https://uk.hach.com/cod-cuvette-test-150-1000-mg-l-o-25-tests/product?id=26370268939 (accessed: 2022-11-20)

Härtel, L., & Pöpel, H. (1992). A dynamic secondary clarifier model including processes of sludge thickening. *Water science and technology*, *25*(6), 267–284.

He, C., Marsalek, J., & Rochfort, Q. (2004). Numerical modelling of enhancing suspended solids removal in a cso facility. *Water Quality Research Journal*, *39*(4), 457–465.

Henze, M., Gujer, W., Mino, T., & van Loosdrecht, M. C. (2000). *Activated sludge models asm1, asm2, asm2d and asm3*. IWA publishing. London, UK.

Jiang, J., & Zhou, Y. (2020). A specious correlation between sludge rheology and dewaterability. *Environmental Science & Technology*, *54*(10), 5928–5930.

Larsen, I., & Vesilind, P. A. (1968). Discussion of "evaluation of activated sludge thickening theories". *Journal of the Sanitary Engineering Division*, *94*(1), 182–191.

Liu, X., & Garcıa, M. H. (2011). Computational fluid dynamics modeling for the design of large primary settling tanks. *Journal of Hydraulic Engineering*, *137*(3), 343–355.

Lundin, E. (2014). *Modelling chemically enhanced primary settlers treating wastewater using particle settling velocity distribution*. (Master thesis report). Uppsala University, Uppsala, Sweden.

Lyn, D., Stamou, A., & Rodi, W. (1992). Density currents and shear-induced flocculation in sedimentation tanks. *Journal of hydraulic Engineering*, *118*(6), 849–867.

Maruéjouls, T., Vanrolleghem, P., Pelletier, G., & Lessard, P. (2012). A phenomenological retention tank model using settling velocity distributions. *Water research*, *46*(20), 6857–6867.

Matesun, J., Mazivila, C., & Ikumi, D. (2021). The development of a calibration methodology for a realistic primary settling tank (PST) model. *Journal of Water Process Engineering*, *40*, 101936.

Mazivila, C. (2022). *Evaluation of a data-driven primary sedimentation tank model using settleometer data*. (Master thesis report). University of Cape Town, Cape Town, South Africa.

Metcalf & Eddy, Abu-Orf, M., Bowden, G., Burton, F. L., Pfrang, W., Stensel, H. D., Tchobanoglous, G., Tsuchihashi, R., & AECOM (Firm), (2014). *Wastewater engineering: Treatment and resource recovery*. McGraw Hill Education. Boston, USA.

NSVA. (n.d.-a). *Öresundsverket*. https://www.nsva.se/vatten-och-avlopp/spillvatten/reningsverk-inom-nsva/oresundsverket/ (accessed: 2022-10-15)

NSVA. (n.d.-b). *Processchema Öresundsverket*. https://www.nsva.se/wp-content/uploads/2019/11/processchema_oresundsverket.pdf (accessed: 2022-10-15)

Orhon, D., Artan, N., & Ateş, E. (1994). A description of three methods for the determination of the initial inert particulate chemical oxygen demand of wastewater. *Journal of Chemical Technology & Biotechnology: International Research in Process, Environmental AND Clean Technology*, *61*(1), 73–80.

Otterpohl, R., & Freund, M. (1992). Dynamic models for clarifiers of activated sludge plants with dry and wet weather flows. *Water Science and Technology*, *26*(5-6), 1391–1400.

Poinapen, J., Ekama, G., & Wentzel, M. (2009). Biological sulphate reduction with primary sewage sludge in an upflow anaerobic sludge bed (UASB) reactor–Part 4: Bed settling characteristics. *Water SA*, *35*(5).

Polorigni, C., Ikumi, D., & Ekama, G. (2021). Primary sedimentation modelling with characterized setting velocity groups. *Water Research*, *189*, 116621.

Ribes, J., Ferrer, J., Bouzas, A., & Seco, A. (2002). Modelling of an activated primary settling tank including the fermentation process and vfa elutriation. *Environmental technology*, *23*(10), 1147–1156.

Roeleveld, P., & Van Loosdrecht, M. (2002). Experience with guidelines for wastewater characterisation in the netherlands. *Water Science and Technology*, *45*(6), 77–87.

Takács, I., Patry, G. G., & Nolasco, D. (1991). A dynamic model of the clarification-thickening process. *Water research*, *25*(10), 1263–1271.

Tay, J.-H. (1982). Development of a settling model for primary settling tanks. *Water Research*, *16*(9), 1413–1417.

Tebini, S. (2020). *Karakterisering av kommunalt avloppsvatten-partikelstorleksfördelning och sammansättning av COD*. (Master thesis report). Lund University, Lund, Sweden.

Norsk Vann. (2009). *Veiledning for dimensjonering av avløpsrenseanlegg*. https://va-kompetanse.no/wp-content/uploads/rapport168_2009.pdf (accessed: 2023-02-20)

VA SYD. (2021). *Källby avloppsreningsverk lund, miljörapport 2021*. https://www.vasyd.se/-/media/Dokument_ny_webb/Miljorapporter/2021/MR-2021-K%C3%A4llby-arv-ver-1.pdf (accessed: 2022-05-11)

Tyack, J. N., Hedges, P. D., & Smisson, R. P. (1996). The relationship between settling velocity grading and the characteristics of the contributing catchment. *Water Science and Technology*, *33*(9), 135–142.

Wärff, C. (2022). Industrial Phd Student at RISE with focus on modelling of Öresundsverket. Personal communication.

# Appendix A

# More detailed methodology

## A.1 Closing the mass balances

Table A.1: Example of how to close the mass balances (single measurements)

| | **IN** | **1** | **2** | **3** | **4** | **5** | **OUT** | **MB error** | |
|---|---|---|---|---|---|---|---|---|---|
| SS (g/L) | 0.249 | 3.373 | 0.540 | 0.209 | 0.144 | 0.115 | 0.098 | | |
| Volume (L) | 51.65 | 1.60 | 3.59 | 5.86 | 8.76 | 14.2 | 17.65 | | |
| SS (g) | 12.85 | 5.41 | 1.94 | 1.23 | 1.26 | 1.64 | 1.73 | -0.34 g | -2.66 % |
| Modification (g) | 0.049 | -0.049 | -0.049 | -0.049 | -0.049 | -0.049 | -0.049 | | |
| Mod SS (g) | 12.90 | 5.36 | 1.89 | 1.18 | 1.21 | 1.59 | 1.67 | 0 g | 0 % |
| Mod SS (g/L) | 0.250 | 3.342 | 0.526 | 0.201 | 0.138 | 0.112 | 0.095 | | |

Table A.2: Example of how to close the mass balances (multiple measurements)

| | **IN** | **1** | **2** | **3** | **4** | **OUT** | | |
|---|---|---|---|---|---|---|---|---|
| Test 1 SS (g/L) | 0.279 | 1.981 | 0.452 | 0.128 | 0.106 | 0.081 | | |
| Test 2 SS (g/L) | 0.274 | 1.873 | 0.432 | 0.126 | 0.099 | 0.083 | | |
| Standard deviation (g/L) | 0.004 | 0.077 | 0.014 | 0.001 | 0.005 | 0.002 | Sum: | 0.102 |
| % of Sum (g/L) | 3.98 | 74.9 | 13.5 | 1.11 | 4.69 | 1.80 | | |
| Average SS (g/L) | 0.276 | 1.927 | 0.442 | 0.127 | 0.103 | 0.082 | **MB error** | |
| Volume (L) | 27.2 | 1.60 | 3.59 | 5.86 | 8.76 | 7.34 | | |
| SS (g) | 7.51 | 3.09 | 1.59 | 0.74 | 0.90 | 0.60 | 0.58 g | 7.74 % |
| Modification (g) | -0.023 | 0.44 | 0.08 | 0.01 | 0.03 | 0.01 | | |
| Mod SS (g) | 7.48 | 3.52 | 1.66 | 0.75 | 0.93 | 0.61 | 0 g | 0 % |
| Mod SS (g/L) | 0.276 | 2.198 | 0.464 | 0.128 | 0.106 | 0.083 | | |

## A.2 Estimating the CSVD curves - MATLAB code

### A.2.1 Function 1

```
function f = test_funktion4(t_end, Q,col, a)
    ff = zeros(1,col);
    for i = 1:col
        if i == 1
            S_i0 = t_end.*(ax_F(a, 10000)-ax_F(a, v_upi(i,Q)));
        else
            S_i0 = t_end.*(ax_F(a, v_upi(i-1,Q))-ax_F(a, v_upi(i,Q)));
        end
        h_i0 = zeros(1,length(Q));
        for j = 1:length(Q)
            h_i0(j) = integral(@(x) ax_f(a, x).*t_i(i,Q(j),x), 0, ...
                ↪ v_upitt(i,Q(j),t_end(j)));
        end
        V_i = [1.604599864 3.589081111 5.862965874 8.758257663 ...
            ↪ 14.18692977]/1000; %m3
        V_in = Q.*t_end;
        h_i0_neg = ax_F(a, 0)./V_in*V_i(i)*a(4); % %integral -Inf -> 0.
        h_iitt = t_end .* (-ax_F(a,v_upitt(i,Q, t_end)) + ax_F(a, ...
            ↪ v_upi(i, Q)));

        if i == 1
            S_ii = 0;
            h_ii = h_iitt;

        elseif i == 2
            S_i1 = S_iX(i, 1, Q, t_end, a);
            h_i1 = h_iX(i,1,Q,t_end,a);


            S_ii = S_i1 + ...
                ↪ t_end.*(-ax_F(a,v_upitt(i-1,Q,t_end))+ax_F(a, ...
                ↪ v_upi(i-1,Q)));
            h_ii = h_iitt - h_i1;

        elseif i == 3
            S_i2 = S_iX(i, 2, Q,t_end, a);
            S_i1 = S_iX(i, 1, Q,t_end, a);

            h_i2 = h_iX(i,2,Q,t_end,a);
            h_i1 = h_iX(i,1,Q,t_end,a);

            S_ii = S_i1 + S_i2 + ...
                ↪ t_end.*(-ax_F(a,v_upitt(i-1,Q,t_end))+ax_F(a, ...
                ↪ v_upi(i-1,Q)));
            h_ii = h_iitt - (h_i1 + h_i2);

        elseif i == 4
            S_i3 = S_iX(i, 3, Q,t_end, a);
            S_i2 = S_iX(i, 2, Q,t_end, a);
            S_i1 = S_iX(i, 1, Q,t_end, a);

```

```
45              h_i3 = h_iX(i,3,Q,t_end,a);
46              h_i2 = h_iX(i,2,Q,t_end,a);
47              h_i1 = h_iX(i,1,Q,t_end,a);
48
49              S_ii = S_i1 + S_i2 + S_i3 + ...
                    ↪ t_end.*(-ax_F(a,v_upitt(i-1,Q,t_end))+ax_F(a, ...
                    ↪ v_upi(i-1,Q)));
50              h_ii = h_iitt - (h_i1 + h_i2 + h_i3);
51
52          elseif i == 5
53              S_i4 = S_iX(i, 4, Q,t_end, a);
54              S_i3 = S_iX(i, 3, Q,t_end, a);
55              S_i2 = S_iX(i, 2, Q,t_end, a);
56              S_i1 = S_iX(i, 1, Q,t_end, a);
57
58              h_i4 = h_iX(i,4,Q,t_end,a);
59              h_i3 = h_iX(i,3,Q,t_end,a);
60              h_i2 = h_iX(i,2,Q,t_end,a);
61              h_i1 = h_iX(i,1,Q,t_end,a);
62
63              S_ii = S_i1 + S_i2 + S_i3 + S_i4 + t_end.*(-ax_F(a, ...
                    ↪ v_upitt(i-1,Q,t_end))+ax_F(a, v_upi(i-1,Q)));
64              h_ii = h_iitt - (h_i1 + h_i2 + h_i3 + h_i4);
65
66      %      elseif i == 6 %Ut
67      %          S_i5 = S_iX(i, 5, Q,t_end, a);
68      %          S_i4 = S_iX(i, 4, Q,t_end, a);
69      %          S_i3 = S_iX(i, 3, Q,t_end, a);
70      %          S_i2 = S_iX(i, 2, Q,t_end, a);
71      %          S_i1 = S_iX(i, 1, Q,t_end, a);
72      %
73      %          h_i5 = h_iX(i,5,Q,t_end,a);
74      %          h_i4 = h_iX(i,4,Q,t_end,a);
75      %          h_i3 = h_iX(i,3,Q,t_end,a);
76      %          h_i2 = h_iX(i,2,Q,t_end,a);
77      %          h_i1 = h_iX(i,1,Q,t_end,a);
78      %
79      %          S_ii = S_i1 + S_i2 + S_i3 + S_i4 + S_i5 + + ...
            ↪ t_end*(-ax_F(a(1),a(2),v_upitt(i-1,Q,t_end))+ax_F(a(1),a(2), ...
            ↪ v_upi(i-1,Q)));
80      %          h_ii = h_iitt - (h_i1 + h_i2 + h_i3 + h_i4 + h_i5);
81          end
82
83          S_i = S_i0 - S_ii;
84          h_i = h_i0 + h_ii; %+h_i0_neg;
85
86          V_in = Q.*t_end;
87          ff(i) = Q./V_in.*(S_i + h_i) + h_i0_neg;%/m_tot*100;
88      end
89      f_ut = 100-sum(ff);
90      f = [ff,f_ut];
91  end
92
93
94  %      S_i5 = @(a) integral(@(x) ax_f(a(1), a(2), x)*t_i(5,Q,x), ...
        ↪ v_upi(i, Q), v_upitt(i-1, Q, t_end));
95  %      S_i4 = @(a) integral(@(x) ax_f(a(1), a(2), x)*t_i(4,Q,x), ...
        ↪ v_upi(i, Q), v_upitt(i-1, Q, t_end));
```

```
96  %     S_i3 = @(a) integral(@(x) ax_f(a(1), a(2), x)*t_i(3,Q,x), ...
        ↪ v_upi(i, Q), v_upitt(i-1, Q, t_end));
97  %     S_i2 = @(a) integral(@(x) ax_f(a(1), a(2), x)*t_i(2,Q,x), ...
        ↪ v_upi(i, Q), v_upitt(i-1, Q, t_end));
98
99  %     h_i5 = @(a) integral(@(x) ax_f(a(1), a(2), x)*t_i(5, Q, x), ...
        ↪ v_upitt(i, Q, t_end), v_upi(i, Q));
100 %     h_i4 = @(a) integral(@(x) ax_f(a(1), a(2), x)*t_i(4, Q, x), ...
        ↪ v_upitt(i, Q, t_end), v_upi(i, Q));
101 %     h_i3 = @(a) integral(@(x) ax_f(a(1), a(2), x)*t_i(3, Q, x), ...
        ↪ v_upitt(i, Q, t_end), v_upi(i, Q));
102 %     h_i2 = @(a) integral(@(x) ax_f(a(1), a(2), x)*t_i(2, Q, x), ...
        ↪ v_upitt(i, Q, t_end), v_upi(i, Q));
103 %     h_i1 = @(a) integral(@(x) ax_f(a(1), a(2), x)*t_i(1, Q, x), ...
        ↪ v_upitt(i, Q, t_end), v_upi(i, Q));
104
105 %     E2 = @(a) sum((y-100*(1-a(1)./(a(1)+(x+0.2).^a(2)))).^2);
106 %     [d, fval] = fminsearch(E2,var);
107 %     R2 = 1-fval/SS_tot;
108 %     min = [d, R2];
109
110
111
112 function F1 = ax_F(a,x)
113     F1 = (100-a(3))*(1-a(1)./((a(1) + x.^a(2))))+a(3);
114
115     %F1 = (100-15)*(1-a(1)./((a(1) + x.^a(2))))+15;
116     %F1 = 100*(1-a(1)./((a(1) + (x+0.2).^a(2))));
117     %F1 = 100*(1-a(1)./((a(1) + (x+a(3)).^a(2))));
118 end
119
120 function f1 = ax_f(a,x)
121     f1 = (100-a(3))*a(1)*a(2)*x.^(a(2)-1)./((a(1)+x.^a(2)).^2);
122
123     %f1 = (100-15)*a(1)*a(2)*x.^(a(2)-1)./((a(1)+x.^a(2)).^2);
124     %f1 = 100*a(1)*a(2)*(x+0.2).^(a(2)-1)./((a(1)+(x+0.2).^a(2)).^2);
125     %f1 = 100*a(1)*a(2)*(x+a(3)).^(a(2)-1)./((a(1)+(x+a(3)).^a(2)).^2);
126     %100*(1-a./((a + (x+0.2).^b).^2));
127 end
128
129 function t = t_i(i,Q,vs) %Q: m3/h. vs: m/h
130     v_netto = v_upi(i,Q) - vs;
131     t = 1./v_netto;
132 end
133
134 function v_up = v_upi(i,Q)
135     A = [1.604599864 3.589081111 5.862965874 8.758257663 ...
            ↪ 14.18692977]/1000; %m3/m2
136     v_up = Q./A(i);
137 end
138
139 function v_upitt = v_upitt(i,Q,t_end)
140     syms vs
141 %     s = double(vpasolve(sum_t_i(i,Q,vs) == t_end, vs));
142 %     v_upitt = min(s); %?Vektor
143     s = zeros(1,length(Q));
144     for j = 1:length(Q)
145         s(j) = min(double(vpasolve(sum_t_i(i,Q(j),vs) == t_end(j), vs)));
```

```
146     end
147     v_upitt = s;
148 end
149 
150 function sum_t = sum_t_i(i,Q,vs) %Q: m3/h. vs: m/h
151     j = 1;
152     t_sum = 0; %%ej i+1?
153     while j < i+1
154         t_sum = t_sum + t_i(j,Q,vs);
155         j = j + 1;
156     end
157     sum_t = t_sum;
158 end
159 
160 function s_ix = S_iX(i, j, Q, t_end, a)
161     Ss_ix = zeros(1,length(Q));
162     for k = 1:length(Q)
163         Ss_ix(k) = integral(@(x) ax_f(a, x).*t_i(j,Q(k),x), v_upi(i, ...
            ↪ Q(k)), v_upitt(i-1, Q(k), t_end(k)));
164     end
165     s_ix = Ss_ix;
166 end
167 
168 function h_ix = h_iX(i, j, Q,t_end, a)
169     Hh_ix = zeros(1,length(Q));
170     for k = 1:length(Q)
171         Hh_ix(k) = integral(@(x) ax_f(a, x).*t_i(j, Q(k), x), ...
            ↪ v_upitt(i, Q(k), t_end(k)), v_upi(i, Q(k)));
172     end
173     h_ix = Hh_ix;
174 end
```

### A.2.2 Function 2

```
1  function f = ex_funk2(t_end, Q,col, a)
2      ff = zeros(1,col);
3      for i = 1:col
4          if i == 1
5              S_i0 = t_end.*(ax_F(a, 10000)-ax_F(a, v_upi(i,Q)));
6          else
7              S_i0 = t_end.*(ax_F(a, v_upi(i-1,Q))-ax_F(a, v_upi(i,Q)));
8          end
9          h_i0 = zeros(1,length(Q));
10         for j = 1:length(Q)
11             h_i0(j) = integral(@(x) ax_f(a, x).*t_i(i,Q(j),x), 0, ...
                   ↪ v_upitt(i,Q(j),t_end(j)));
12         end
13         V_i = [1.604599864 3.589081111 5.862965874 8.758257663 ...
               ↪ 14.18692977]/1000; %m3
14         V_in = Q.*t_end;
15         h_i0_neg = ax_F(a, 0)./V_in*V_i(i)*a(4);  %integral -Inf -> 0.
16         h_iitt = t_end .* (-ax_F(a,v_upitt(i,Q, t_end)) + ax_F(a, ...
               ↪ v_upi(i, Q)));
17 
```

```
18          if i == 1
19              S_ii = 0;
20              h_ii = h_iitt;
21
22          elseif i == 2
23              S_i1 = S_iX(i, 1, Q, t_end, a);
24              h_i1 = h_iX(i,1,Q,t_end, a);
25
26
27              S_ii = S_i1 + ...
                    ↪ t_end.*(-ax_F(a,v_upitt(i-1,Q,t_end))+ax_F(a, ...
                    ↪ v_upi(i-1,Q)));
28              h_ii = h_iitt - h_i1;
29
30          elseif i == 3
31              S_i2 = S_iX(i, 2, Q,t_end, a);
32              S_i1 = S_iX(i, 1, Q,t_end, a);
33
34              h_i2 = h_iX(i,2,Q,t_end, a);
35              h_i1 = h_iX(i,1,Q,t_end, a);
36
37              S_ii = S_i1 + S_i2 + ...
                    ↪ t_end.*(-ax_F(a,v_upitt(i-1,Q,t_end))+ax_F(a, ...
                    ↪ v_upi(i-1,Q)));
38              h_ii = h_iitt - (h_i1 + h_i2);
39
40          elseif i == 4
41              S_i3 = S_iX(i, 3, Q,t_end, a);
42              S_i2 = S_iX(i, 2, Q,t_end, a);
43              S_i1 = S_iX(i, 1, Q,t_end, a);
44
45              h_i3 = h_iX(i,3,Q,t_end, a);
46              h_i2 = h_iX(i,2,Q,t_end, a);
47              h_i1 = h_iX(i,1,Q,t_end, a);
48
49              S_ii = S_i1 + S_i2 + S_i3 + ...
                    ↪ t_end.*(-ax_F(a,v_upitt(i-1,Q,t_end))+ax_F(a, ...
                    ↪ v_upi(i-1,Q)));
50              h_ii = h_iitt - (h_i1 + h_i2 + h_i3);
51
52          elseif i == 5
53              S_i4 = S_iX(i, 4, Q,t_end, a);
54              S_i3 = S_iX(i, 3, Q,t_end, a);
55              S_i2 = S_iX(i, 2, Q,t_end, a);
56              S_i1 = S_iX(i, 1, Q,t_end, a);
57
58              h_i4 = h_iX(i,4,Q,t_end, a);
59              h_i3 = h_iX(i,3,Q,t_end, a);
60              h_i2 = h_iX(i,2,Q,t_end, a);
61              h_i1 = h_iX(i,1,Q,t_end, a);
62
63              S_ii = S_i1 + S_i2 + S_i3 + S_i4 + ...
                    ↪ t_end.*(-ax_F(a,v_upitt(i-1,Q,t_end))+ax_F(a, ...
                    ↪ v_upi(i-1,Q)));
64              h_ii = h_iitt - (h_i1 + h_i2 + h_i3 + h_i4);
65
66
67          end
```

```
68
69          S_i = S_i0 - S_ii;
70          h_i = h_i0 + h_ii; %+h_i0_neg;
71
72          V_in = Q.*t_end;
73          ff(i) = Q./V_in.*(S_i + h_i) + h_i0_neg;%/m_tot*100;
74      end
75      f_ut = 100-sum(ff);
76      f = [ff,f_ut];
77  end
78
79
80
81  function F1 = ax_F(a,x)
82      F1 = (100-a(2))*(1-exp(-a(1).*x.^a(3)))+a(2);
83
84      %F1 = 100*(1-exp(-a(1).*(x+0.2).^a(3)));
85      %F1 = 100*(1-exp(-a(1).*(x+a(2)).^a(3)));
86      %F1 = 100*(1-exp(-b.*(x+0.2)));
87  end
88
89  function f1 = ax_f(a,x)
90      f1 = (100-a(2))*a(1)*a(3)*x.^(a(3)-1).*exp(-a(1).*x.^a(3));
91
92      %f1 = 100*a(1)*a(3)*(x+0.2).^(a(3)-1).*exp(-a(1).*(x+0.2).^a(3));
93      %f1 = 100*a(1)*a(3)*(x+a(2)).^(a(3)-1).*exp(-a(1).*(x+a(2)).^a(3));
94      %100*b*exp(-b.*(x+0.2));
95  end
96
97  function t = t_i(i,Q,vs) %Q: m3/h. vs: m/h
98      v_netto = v_upi(i,Q) - vs;
99      t = 1./v_netto;
100 end
101
102 function v_up = v_upi(i,Q)
103     A = [1.604599864 3.589081111 5.862965874 8.758257663 ...
            ↪ 14.18692977]/1000; %m3/m2
104     v_up = Q./A(i);
105 end
106
107 function v_upitt = v_upitt(i,Q,t_end)
108     syms vs
109 %     s = double(vpasolve(sum_t_i(i,Q,vs) == t_end, vs));
110 %     v_upitt = min(s); %?Vektor
111     s = zeros(1,length(Q));
112     for j = 1:length(Q)
113         s(j) = min(double(vpasolve(sum_t_i(i,Q(j),vs) == t_end(j), vs)));
114     end
115     v_upitt = s;
116 end
117
118 function sum_t = sum_t_i(i,Q,vs) %Q: m3/h. vs: m/h
119     j = 1;
120     t_sum = 0; %%ej i+1?
121     while j < i+1
122         t_sum = t_sum + t_i(j,Q,vs);
123         j = j + 1;
124     end
```

```
125     sum_t = t_sum;
126 end
127
128 function s_ix = S_iX(i, j, Q, t_end, a)
129     Ss_ix = zeros(1,length(Q));
130     for k = 1:length(Q)
131         Ss_ix(k) = integral(@(x) ax_f(a, x).*t_i(j,Q(k),x), v_upi(i, ...
                ↪ Q(k)), v_upitt(i-1, Q(k), t_end(k)));
132     end
133     s_ix = Ss_ix;
134 end
135
136 function h_ix = h_iX(i, j, Q,t_end, a)
137     Hh_ix = zeros(1,length(Q));
138     for k = 1:length(Q)
139         Hh_ix(k) = integral(@(x) ax_f(a, x).*t_i(j, Q(k), x), ...
                ↪ v_upitt(i, Q(k), t_end(k)), v_upi(i, Q(k)));
140     end
141     h_ix = Hh_ix;
142 end
```

# Appendix B

# More detailed results

## B.1 Results Källby WWTP

### B.1.1 Measured values

Table B.1: Measured values the 10/10

| | In | 1 | 2 | 3 | 4 | 5 | Out |
|---|---|---|---|---|---|---|---|
| **TSS (mg/L)** | 315 | 2737 | 391 | 247 | 135 | 107 | 94.7 |
| **$COD_{tot}$ (mg/L)** | 482 | 3830 | 722 | 515 | 313 | 274 | 326 |

Table B.2: Measured values the 18/10

| | In | 1 | 2 | 3 | 4 | 5 | Out |
|---|---|---|---|---|---|---|---|
| **TSS (mg/L)** | 195 | 1082 | 344 | 169 | 97.3 | 72.8 | 61.8 |
| | 205 | 992 | 369 | 166 | 97.4 | 72.9 | 68.1 |
| **VSS (mg/L)** | 166 | 955 | 303 | 149 | 78.6 | 57.7 | 48.5 |
| | 183 | 890 | 338 | 147 | 83.3 | 63.9 | 59.9 |
| **ISS (mg/L)** | 29.3 | 127 | 40.9 | 20.8 | 18.8 | 15.1 | 13.3 |
| | 21.4 | 102 | 30.6 | 19.3 | 14.1 | 9.07 | 8.20 |
| **$COD_{tot}$ (mg/L)** | 415 | 1975 | 600 | 325 | 236 | 209 | 248 |
| **$COD_s$ (mg/L)** | - | - | - | - | - | - | 57 |

Table B.3: Measured values the 24/10

| | In | 1 | 2 | 3 | 4 | 5 | Out |
|---|---|---|---|---|---|---|---|
| **TSS (mg/L)** | 267 | 1355 | 1310 | 387 | 192 | 143 | 116 |
| **VSS (mg/L)** | 210 | 1084 | 1107 | 309 | 153 | 113 | 90.7 |
| **ISS (mg/L)** | 56.5 | 271 | 204 | 77.9 | 38.4 | 30.3 | 25.5 |
| **$COD_{tot}$ (mg/L)** | 370 | 2135 | 1955 | 547 | 315 | 258 | 224 |
| **$COD_s$ (mg/L)** | - | - | - | - | - | - | 43.4 |

### B.1.2 Data after closing mass balances

Table B.4: Values after closing mass balances, 10/10

| | **In** | **1** | **2** | **3** | **4** | **5** | **Out** |
|---|---|---|---|---|---|---|---|
| **TSS (mg/L)** | 302 | 3156 | 578 | 361 | 211 | 155 | 132 |
| **$COD_{tot}$ (mg/L)** | 480 | 3901 | 754 | 534 | 326 | 282 | 332 |
| **$COD_p$ (mg/L)** | 432 | 3849 | 711 | 491 | 282 | 235 | 281 |

Table B.5: Values after closing mass balances, 18/10

| | **In** | **1** | **2** | **3** | **4** | **5** | **Out** |
|---|---|---|---|---|---|---|---|
| **TSS (mg/L)** | 195 | 2466 | 531 | 181 | 97.5 | 73.1 | 73.9 |
| **VSS (mg/L)** | 167 | 1792.5 | 529 | 154 | 92.4 | 70.1 | 67.8 |
| **ISS mod. (mg/L)** | 24.4 | 212 | 54.0 | 21.6 | 19.8 | 14.7 | 12.5 |
| **ISS = TSS - VSS (mg/L)** | 27.9 | 674 | 2.48 | 27.5 | 5.04 | 3.07 | 6.11 |
| **$COD_{tot}$ (mg/L)** | 402 | 2406 | 793 | 443 | 315 | 258 | 287 |
| **$COD_p$ (mg/L)** | 348 | 2347 | 744 | 394 | 265 | 204 | 229 |

Table B.6: Values after closing mass balances, 24/10

| | **In** | **1** | **2** | **3** | **4** | **5** | **Out** |
|---|---|---|---|---|---|---|---|
| **TSS (mg/L)** | 264 | 1457 | 1356 | 415 | 211 | 155 | 121 |
| **VSS (mg/L)** | 209 | 1137 | 1131 | 324 | 163 | 119 | 93.3 |
| **ISS mod. (mg/L)** | 55.3 | 320 | 226 | 91.2 | 47.4 | 35.8 | 27.9 |
| **ISS = TSS - VSS (mg/L)** | 55.3 | 320 | 226 | 91.2 | 47.4 | 35.8 | 27.9 |
| **$COD_{tot}$ (mg/L)** | 376 | 1895 | 1848 | 481 | 271 | 231 | 212 |
| **$COD_p$ (mg/L)** | 335 | 1853 | 1812 | 445 | 233 | 190 | 169 |

### B.1.3 Distributions

VSS:

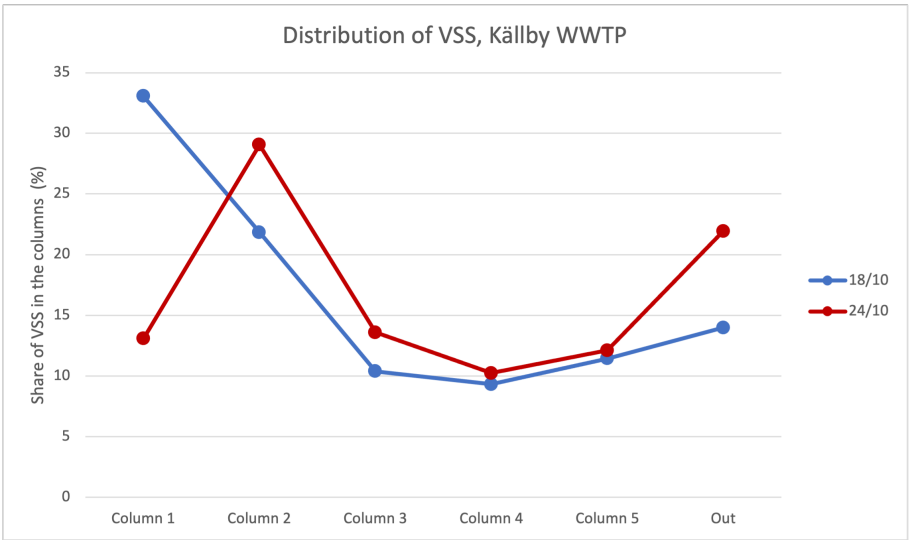


Figure B.1: Distribution of VSS in the columns

ISS:

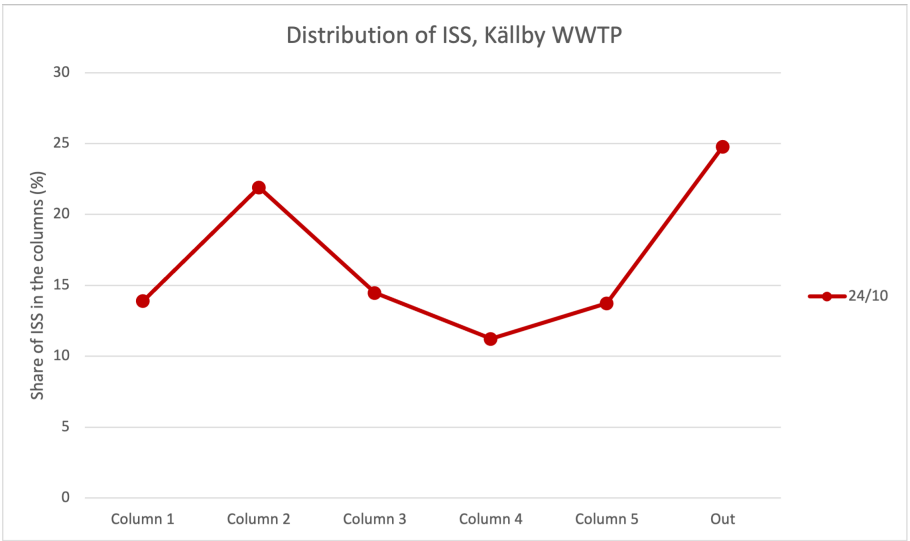


Figure B.2: Distribution of ISS in the columns

$COD_{tot}$:

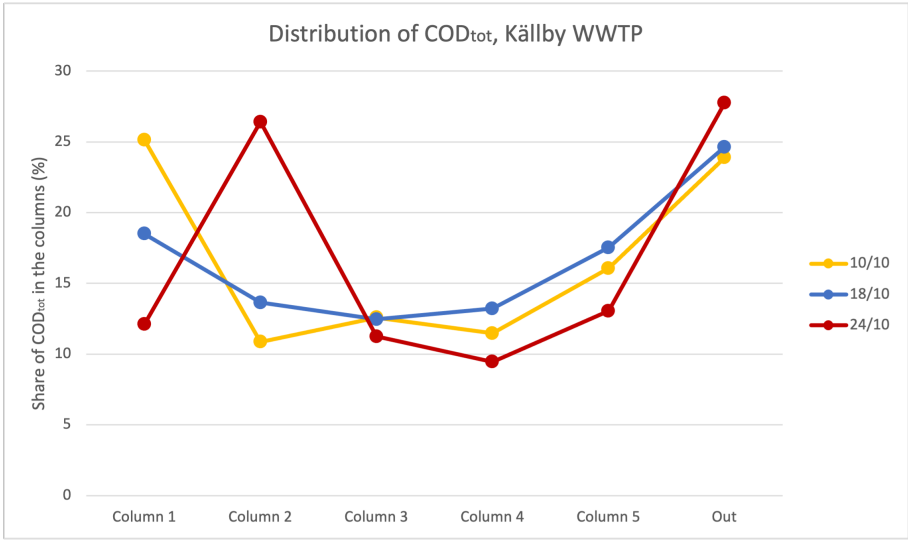


Figure B.3: Distribution of $COD_{tot}$ in the settleometer

### B.1.4 Aerobic degradation

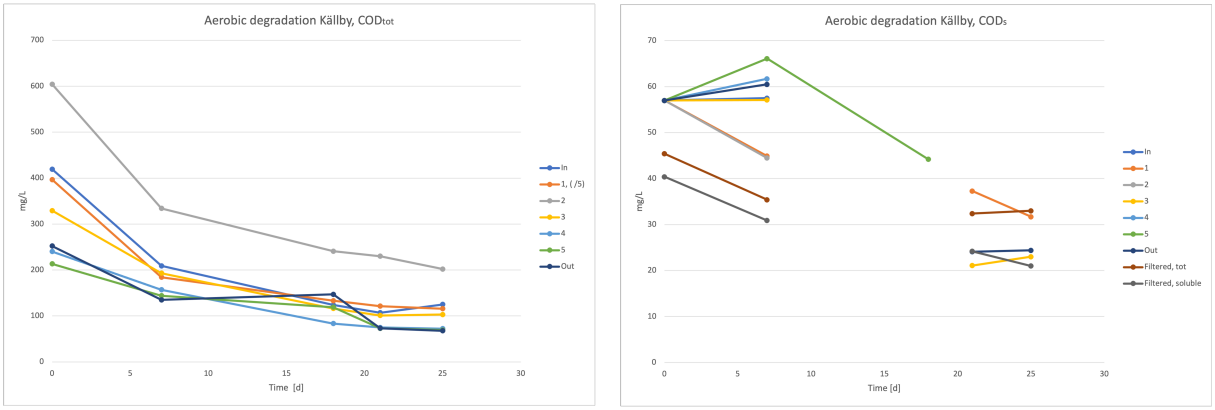


(a) $COD_{tot}$ (b) $COD_{soluble}$ + Filtered reactor

Figure B.4: Measured COD during the aerobic degradation experiment

Table B.7: Results for method by Orhon

| | **In** | **1** | **2** | **3** | **4** | **5** | **Out** | **Filtered Reactor** |
|---|---|---|---|---|---|---|---|---|
| $\mathbf{COD_{tot,\ 0}\ (mg/L)}$ | 415 | 1975 | 600 | 325 | 236 | 209 | 248 | 40.4 |
| $\mathbf{COD_{s,\ 0}\ (mg/L)}$ | 57 | 57 | 57 | 57 | 57 | 57 | 57 | 40.4 |
| $\mathbf{COD_{tot,\ end}\ (mg/L)}$ | 123 | 576 | 200 | 102 | 70.7 | 67.9 | 66.2 | 31.4 |
| $\mathbf{COD_{s,\ end}\ (mg/L)}$ | 23[a] | 31.7 | 25[a] | 23 | 24[a] | 24[a] | 24.4 | 21 |
| $\mathbf{\Delta C_T}$ | 292 | 1399 | 400 | 223 | 165 | 141 | 182 | 9.0 |
| $\mathbf{X_{P1}\ (mg/L)}$ | 340 | 1629 | 465 | 260 | 192 | 164 | 212 | 10.4 |
| $\mathbf{X_U\ (mg/L)}$ | -239 | -1085 | -290 | -181 | -146 | -120 | -170 | 0 |
| $\mathbf{X_{B,\ 0}\ (mg/L)}$ | 597 | 3003 | 833 | 449 | 325 | 272 | 361 | 0 |

[a] Interpolated

Table B.8: ASM calculations for the aerobic degradation

| | **In** | **1** | **2** | **3** | **4** | **5** | **Out** |
|---|---|---|---|---|---|---|---|
| **$COD_{p,\ 0}$ (mg/L)** | 348 | 2347 | 744 | 394 | 265 | 204 | 229 |
| **Assumed amount of $S_U$ (mg/L)** | 20.0 | 20.0 | 20.0 | 20.0 | 20.0 | 20.0 | 20.0 |
| **$S_{B,\ 0}$ (mg/L)** | 37.0 | 37.0 | 37.0 | 37.0 | 37.0 | 37.0 | 37.0 |
| **Fraction $X_B$** | 0.920 | 0.895 | 0.894 | 0.938 | 0.963 | 0.906 | 0.936 |
| **$X_{B,\ 0}$ (mg/L)** | 320 | 2101 | 665 | 369 | 255 | 185 | 214 |
| **$X_U$ (mg/L)** | 27.7 | 246.1 | 78.9 | 24.4 | 9.77 | 19.2 | 14.6 |
| **$X_{P,\ formed}$ (mg/L)** | 49.9 | 298.8 | 98.1 | 56.8 | 40.8 | 31.0 | 35.1 |
| **$COD_{p,\ end,\ calc.}$ (mg/L)** | 77.6 | 545 | 177.0 | 81.2 | 50.6 | 50.2 | 49.7 |
| **$COD_{p,\ end,\ meas.}$ (mg/L)** | 100.4 | 544.2 | 175 | 78.6 | 46.7 | 43.9 | 41.8 |
| **Error (mg/L)** | -22.80 | 0.70 | 1.58 | 2.57 | 3.85 | 6.23 | 7.88 |
| **Sum of squared errors** | | | | | | | **645.3** |

### B.1.5 Parameters for the CSVD-curves

Table B.9: Estimated parameters for the CSVD-curves, Källby WWTP

| | | $a$ | $b$ | $c$ | $d$ | $R^2$ |
|---|---|---|---|---|---|---|
| **TSS** | **Function 1** | | | | | |
| | Runs 1-3 | 70.9518 | 1.9088 | 45.8501 | 1.0000 | 0.8961 |
| | Run 1 | 1.2725 | 0.4903 | 5.0770 | 0.0000 | 0.9920 |
| | Run 2 | 14.5562 | 1.2619 | 33.3011 | 0.9415 | 0.9999 |
| | Run 3 | 249.3824 | 2.3567 | 47.2830 | 1.0000 | 0.9757 |
| | **Function 2** | | | | | |
| | Runs 1-3 | 0.0466 | 1.2355 | 42.8720 | 1.0000 | 0.9242 |
| | Run 1 | 0.6214 | 0.3196 | 4.8818 | 0.0000 | 0.9892 |
| | Run 2 | 0.0934 | 0.9688 | 31.3286 | 0.9179 | 0.9998 |
| | Run 3 | 0.0215 | 1.4893 | 45.0915 | 1.0000 | 0.9957 |
| **VSS** | **Function 1** | | | | | |
| | Runs 2-3 | 88.3158 | 2.0970 | 43.7330 | 1.0000 | 0.9285 |
| | Run 2 | 27.7942 | 1.6801 | 39.8822 | 0.9949 | 0.9995 |
| | Run 3 | 366.2566 | 2.5030 | 46.3970 | 1.0000 | 0.9752 |
| | **Function 2** | | | | | |
| | Runs 2-3 | 0.0505 | 1.2626 | 39.5096 | 0.9708 | 0.9471 |
| | Run 2 | 0.0538 | 1.3068 | 38.5664 | 0.9812 | 0.9998 |
| | Run 3 | 0.0167 | 1.5832 | 44.2900 | 1.0000 | 0.9947 |
| **ISS** | **Function 1** | | | | | |
| | Run 3 | 57.7828 | 1.8087 | 50.0729 | 1.0000 | 0.9880 |
| | **Function 2** | | | | | |
| | Run 3 | 0.0572 | 1.1308 | 47.3774 | 1.0000 | 0.9959 |
| **$COD_P$** | **Function 1** | | | | | |
| | Runs 1-3 | 209.9113 | 2.3745 | 61.5768 | 1.0000 | 0.6337 |
| | Run 1 & 3 | 577.9877 | 2.6949 | 59.2357 | 1.0000 | 0.7823 |
| | Run 1 | 1.0007 | 0.4356 | 10.6081 | 0.0002 | 0.9816 |
| | Run 2 | 3.7741 | 0.9487 | 50.8140 | 0.8780 | 0.9997 |
| | Run 3 | 1145.3 | 2.8508 | 51.5082 | 1.0000 | 0.9928 |
| | **Function 2** | | | | | |
| | Runs 1-3 | 0.0259 | 1.4846 | 59.2586 | 0.9922 | 0.6721 |
| | Runs 1 & 3 | 0.0120 | 1.7163 | 57.5867 | 1.0000 | 0.8059 |
| | Run 1 | 0.7409 | 0.2744 | 10.7808 | 0.0000 | 0.9799 |
| | Run 2 | 0.4039 | 0.5422 | 41.2992 | 0.8100 | 0.9988 |
| | Run 3 | 0.0057 | 1.9202 | 50.4155 | 1.0000 | 0.9982 |
| **$X_B$ and $X_U$** | **Function 1** | | | | | |
| | $X_B$ | 2.2146 | 0.8102 | 43.0584 | 0.7947 | 1.0000 |
| | $X_U$ | 176.4002 | 2.5207 | 55.6218 | 1.0000 | 0.8944 |
| | **Function 2** | | | | | |
| | $X_B$ | 0.7042 | 0.3891 | 19.7471 | 0.4249 | 0.9998 |
| | $X_U$ | 0.0076 | 2.2096 | 55.6197 | 1.0000 | 0.8928 |

## B.2 Results Öresundsverket

### B.2.1 Measured values

Table B.10: Measured values the 31/10

| | In | 1 | 2 | 3 | 4 | 5 | Out |
|---|---|---|---|---|---|---|---|
| **TSS (mg/L)** | 249 | 3373 | 540 | 209 | 144 | 115 | 97.6 |
| **VSS (mg/L)** | 229 | 3110 | 498 | 193 | 130 | 103 | 86.2 |
| **ISS (mg/L)** | 20.3 | 262 | 42.4 | 16.1 | 13.5 | 12.6 | 11.4 |
| **$COD_{tot}$ (mg/L)** | 507 | 6270 | 874 | 433 | 364 | 348 | 269 |

Table B.11: Measured values the 8/11

| | In | 1 | 2 | 3 | 4 | Out |
|---|---|---|---|---|---|---|
| **TSS (mg/L)** | 279 | 1584 | 469 | 117 | 99.5 | 74.2 |
| | - | 1619 | 505 | 125 | 97.5 | 87.6 |
| **VSS (mg/L)** | 229 | 3110 | 498 | 193 | 130 | 103 |
| **ISS (mg/L)** | 32.7 | 136 | 48.4 | 9.43 | 12.5 | 7.17 |
| **$COD_{tot}$ (mg/L)** | 657 | 2540 | 791 | 307 | 269 | 242 |
| **$COD_s$ (mg/L)** | - | - | - | - | - | 91.4 |

Table B.12: Measured values the 15/11

| | In | 1 | 2 | 3 | 4 | Out |
|---|---|---|---|---|---|---|
| **TSS (mg/L)** | 217 | 1407 | 233 | 92.2 | 79.3 | 68.7 |
| | 228 | 1398 | 226 | 96.9 | 75.4 | 58.9 |
| **VSS (mg/L)** | 193 | 1301 | 197 | 82.1 | 66.6 | 55.7 |
| | 194 | 1284 | 187 | 86.7 | 64.8 | 53.3 |
| **ISS (mg/L)** | 23.4 | 106 | 35.2 | 10.2 | 12.8 | 12.9 |
| | 34.2 | 114 | 39.2 | 10.2 | 10.6 | 5.62 |
| **$COD_{tot}$ (mg/L)** | 372 | 2080 | 400 | 204 | 208 | 192 |
| | 388 | 1910 | 409 | 244 | 203 | 192 |
| | 366 | 2250 | 408 | 272 | 210 | 191 |
| **$COD_s$ (mg/L)** | 92.7 | 76.9 | 70.7 | 71.5 | 73.9 | 83.1 |
| | 89.6 | 75.2 | 67.1 | 71.4 | 74.4 | 86.9 |
| | 90.3 | 79.8 | - | - | - | 100 |

Table B.13: Measured values the 28/11

| | In | 1 | 2 | 3 | 4 | Out |
|---|---|---|---|---|---|---|
| **TSS (mg/L)** | 279 | 1981 | 452 | 128 | 106 | 80.7 |
| | 274 | 1873 | 432 | 126 | 99.4 | 83.3 |
| **VSS (mg/L)** | 245 | 1791 | 406 | 112 | 86.9 | 69.2 |
| | 244 | 1689 | 384 | 112 | 88.4 | 69.8 |
| **ISS (mg/L)** | 34.2 | 191 | 45.7 | 16.0 | 19.3 | 11.5 |
| | 29.2 | 184 | 47.9 | 14.2 | 11.0 | 13.5 |
| **$COD_{tot}$ (mg/L)** | 508 | 2935 | 703 | 293 | 253 | 223 |
| | 497 | 2755 | 709 | 291 | 257 | 222 |
| **$COD_s$ (mg/L)** | 97.4 | - | 66.5 | - | - | - |
| | 95.1 | - | - | - | - | - |

### B.2.2 Data after closing mass balances

Table B.14: Values after closing mass balances, 31/10

| | In | 1 | 2 | 3 | 4 | 5 | Out |
|---|---|---|---|---|---|---|---|
| **TSS (mg/L)** | 250 | 3342 | 526 | 201 | 138 | 112 | 94.9 |
| **VSS (mg/L)** | 229 | 3091 | 489 | 188 | 127 | 100 | 84.4 |
| **ISS mod. (mg/L)** | 20.6 | 252 | 37.6 | 13.2 | 11.5 | 11.4 | 10.5 |
| **ISS = TSS - VSS (mg/L)** | 20.6 | 252 | 37.6 | 13.2 | 11.5 | 11.4 | 10.5 |
| **$COD_{tot}$ (mg/L)** | 514 | 6054 | 778 | 374 | 325 | 324 | 249 |
| **$COD_p$ (mg/L)** | 429 | 5962 | 701 | 297 | 246 | 239 | 159 |

Table B.15: Values after closing mass balances, 8/11

| | In | 1 | 2 | 3 | 4 | Out |
|---|---|---|---|---|---|---|
| **TSS (mg/L)** | 259 | 1665 | 517 | 125 | 99.1 | 87.7 |
| **VSS (mg/L)** | 242 | 1521 | 453 | 127 | 100 | 86.9 |
| **ISS mod. (mg/L)** | 31.1 | 161 | 59.6 | 16.2 | 17.1 | 14.0 |
| **ISS = TSS - VSS (mg/L)** | 17.2 | 144 | 63.8 | -2.27 | -1.05 | 0.79 |
| **$COD_{tot}$ (mg/L)** | 629 | 2994 | 994 | 431 | 352 | 367 |
| **$COD_p$ (mg/L)** | 543 | 2894 | 913 | 351 | 271 | 270 |

Table B.16: Values after closing mass balances, 15/11

| | In | 1 | 2 | 3 | 4 | Out |
|---|---|---|---|---|---|---|
| **TSS (mg/L)** | 215 | 1481 | 254 | 106 | 83.8 | 105 |
| **VSS (mg/L)** | 193 | 1429 | 229 | 94.5 | 68.3 | 63.5 |
| **ISS mod. (mg/L)** | 26.5 | 136 | 43.0 | 10.2 | 12.9 | 20.3 |
| **ISS = TSS - VSS (mg/L)** | 22.2 | 52.2 | 25.2 | 11.3 | 15.5 | 41.1 |
| **$COD_{tot}$ (mg/L)** | 375 | 2101 | 406 | 241 | 207 | 192 |
| **$COD_p$ (mg/L)** | 285 | 1844 | 334 | 161 | 132 | 105 |

Table B.17: Values after closing mass balances, 28/11

| | In | 1 | 2 | 3 | 4 | Out |
|---|---|---|---|---|---|---|
| **TSS (mg/L)** | 276 | 2198 | 464 | 128 | 106 | 83.5 |
| **VSS (mg/L)** | 245 | 1991 | 419 | 112 | 88.4 | 69.9 |
| **ISS mod. (mg/L)** | 31.1 | 201 | 48.6 | 16.0 | 17.9 | 13.3 |
| **ISS = TSS - VSS (mg/L)** | 30.9 | 207 | 44.5 | 16.0 | 17.6 | 13.6 |
| **$COD_{tot}$ (mg/L)** | 501 | 3377 | 714 | 294 | 257 | 223 |
| **$COD_p$ (mg/L)** | 405 | 3068 | 638 | 217 | 178 | 131 |

### B.2.3 Distributions

VSS:

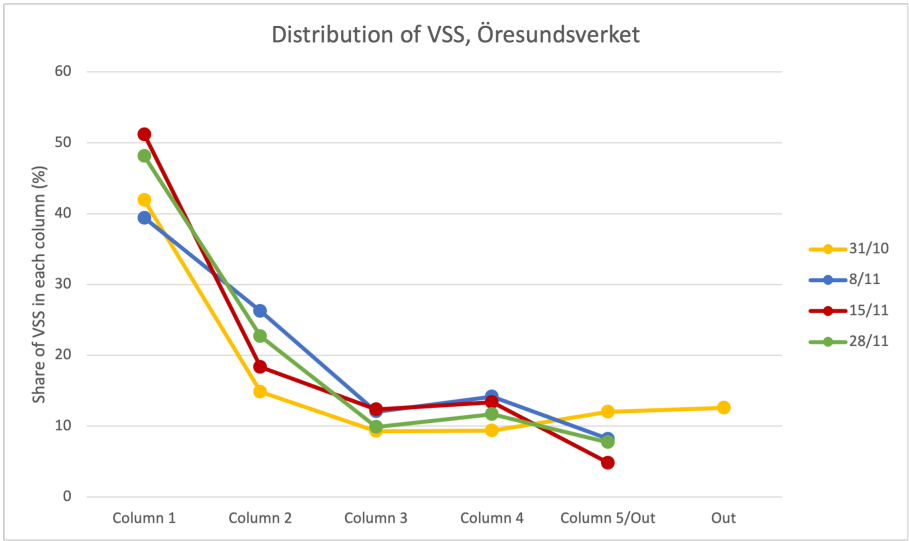


Figure B.5: Distribution of VSS in the settleometer

ISS:

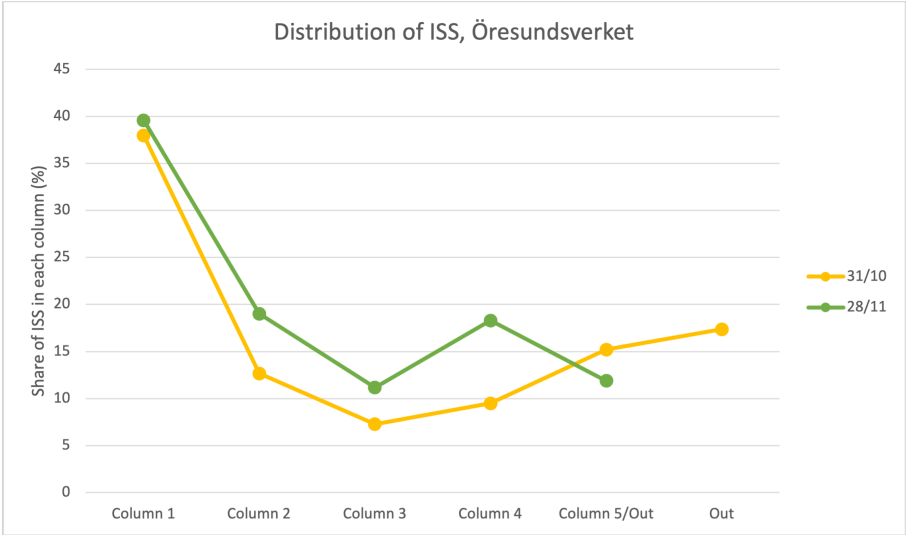


Figure B.6: Distribution of ISS in the settleometer

$COD_{tot}$:

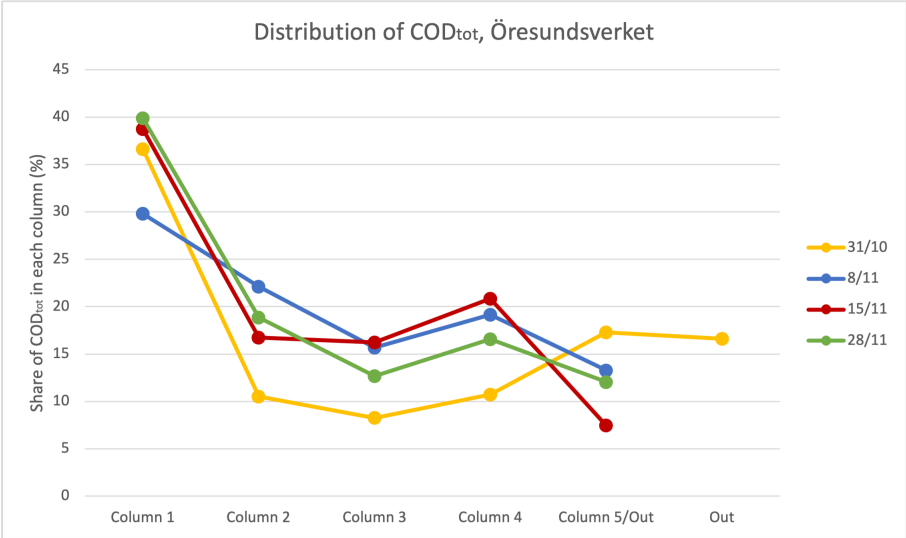


Figure B.7: Distribution of $COD_{tot}$ in the settleometer

### B.2.4 Aerobic degradation

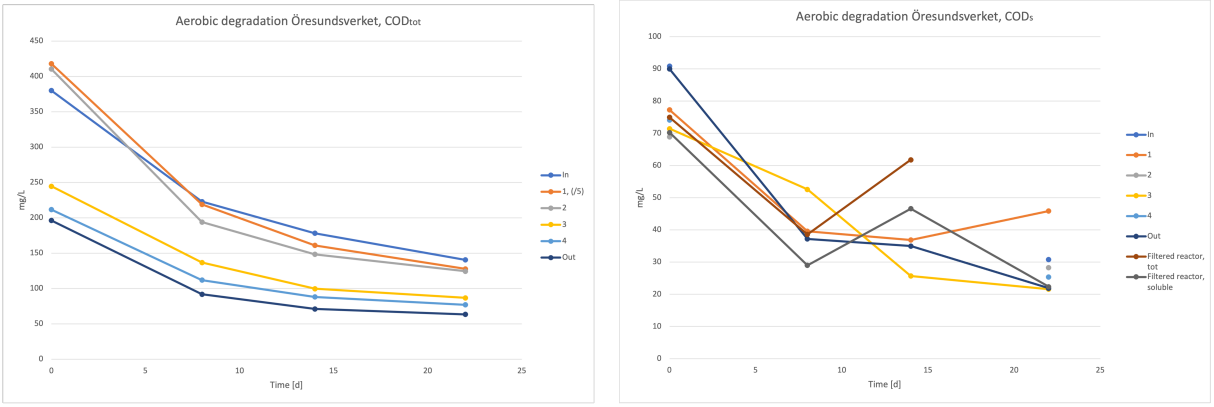


(a) $COD_{tot}$ (b) $COD_{soluble}$ + Filtered reactor

Figure B.8: Measured COD during the aerobic degradation experiment

Table B.18: Results for method by Orhon

| | **In** | **1** | **2** | **3** | **4** | **Out** | **Filtered Reactor** |
|---|---|---|---|---|---|---|---|
| **$COD_{tot,\ 0}$ (mg/L)** | 375 | 2080 | 406 | 240 | 207 | 192 | 70.3 |
| **$COD_{s,\ 0}$ (mg/L)** | 90.9 | 77.3 | 68.9 | 71.5 | 74.2 | 90 | 70.3 |
| **$COD_{tot,\ end}$ (mg/L)** | 138 | 634 | 122 | 84.4 | 74.6 | 61.1 | 33.6 |
| **$COD_{s,\ end}$ (mg/L)** | 30.8 | 45.9 | 28.3 | 21.6 | 25.4 | 21.9 | 22.4 |
| **$\Delta C_T$** | 237 | 1446 | 284 | 156 | 132 | 131 | 36.7 |
| **$X_{P1}$ (mg/L)** | 72.3 | 440.9 | 86.5 | 47.4 | 40.4 | 39.8 | 11.2 |
| **$X_U$ (mg/L)** | 34.9 | 147.4 | 7.24 | 15.4 | 8.86 | -0.66 | 0 |
| **$X_{B,\ 0}$ (mg/L)** | 250 | 1855 | 330 | 153 | 124 | 102 | 0 |

Table B.19: ASM calculations for the aerobic degradation

| | **In** | **1** | **2** | **3** | **4** | **Out** |
|---|---|---|---|---|---|---|
| **$COD_{p,\ 0}$ (mg/L)** | 285 | 1844 | 334 | 161 | 132 | 105 |
| **Assumed amount of $S_U$ (mg/L)** | 20.0 | 20.0 | 20.0 | 20.0 | 20.0 | 20.0 |
| **$S_{B,\ 0}$ (mg/L)** | 70.9 | 57.3 | 48.9 | 51.5 | 54.2 | 66.9 |
| **Fraction $X_B$** | 0.797 | 0.796 | 0.856 | 0.748 | 0.771 | 0.818 |
| **$X_{B,\ 0}$ (mg/L)** | 227 | 1469 | 286 | 121 | 102 | 86 |
| **$X_U$ (mg/L)** | 57.9 | 375.5 | 48.1 | 40.7 | 30.3 | 19.0 |
| **$X_{P,\ formed}$ (mg/L)** | 41.7 | 213.3 | 46.8 | 24.0 | 21.8 | 21.3 |
| **$COD_{p,\ end,\ calc.}$ (mg/L)** | 99.6 | 588.8 | 94.9 | 64.8 | 52.1 | 40.3 |
| **$COD_{p,\ end,\ meas.}$ (mg/L)** | 107.3 | 588.3 | 93.7 | 62.8 | 49.2 | 39.2 |
| **Error (mg/L)** | -7.68 | 0.53 | 1.19 | 1.94 | 2.90 | 1.12 |
| **Sum of squared errors** | | | | | | **74.05** |

### B.2.5 Parameters for the CSVD-curves

Table B.20: Estimated parameters for the CSVD-curves, Öresundsverket, TSS, VSS & ISS

| | | $a$ | $b$ | $c$ | $d$ | $R^2$ |
|---|---|---|---|---|---|---|
| **TSS** | **Function 1** | | | | | |
| | Runs 1-4 | 1.6779 | 0.5591 | 8.9032 | 0.6347 | 0.9151 |
| | Run 1 | 13.2998 | 1.0374 | 37.5170 | 1.0000 | 0.9996 |
| | Run 2 | 16.6636 | 2.5244 | 36.1206 | 1.0000 | 0.9994 |
| | Run 3 | 9.3012 | 1.5017 | 38.8155 | 0.9576 | 1.0000 |
| | Run 4 | 16.2093 | 1.9437 | 33.0819 | 1.0000 | 0.9974 |
| | **Function 2** | | | | | |
| | Runs 1-4 | 0.5444 | 0.3652 | 3.8165 | 0.0000 | 0.9119 |
| | Run 1 | 0.0859 | 0.8609 | 36.9128 | 1.0000 | 0.9998 |
| | Run 2 | 0.0628 | 2.1704 | 35.9072 | 1.0000 | 0.9994 |
| | Run 3 | 0.1063 | 1.3261 | 38.5417 | 0.9563 | 1.0000 |
| | Run 4 | 0.0665 | 1.6808 | 32.7137 | 1.0000 | 0.9976 |
| **VSS** | **Function 1** | | | | | |
| | Runs 1-4 | 1.7524 | 0.5631 | 8.6099 | 0.7014 | 0.9257 |
| | Run 1 | 12.0611 | 1.0082 | 36.0417 | 1.0000 | 0.9997 |
| | Run 2 | 12.6607 | 2.2282 | 38.5594 | 1.0000 | 0.9989 |
| | Run 3 | 6.8396 | 1.2402 | 32.1739 | 0.9981 | 1.0000 |
| | Run 4 | 15.0839 | 1.9028 | 30.9269 | 1.0000 | 0.9981 |
| | **Function 2** | | | | | |
| | Runs 1-4 | 0.5308 | 0.3686 | 3.2161 | 0.0000 | 0.9230 |
| | Run 1 | 0.0940 | 0.8316 | 35.3963 | 1.0000 | 0.9999 |
| | Run 2 | 0.0823 | 1.8918 | 38.2453 | 1.0000 | 0.9991 |
| | Run 3 | 0.1443 | 1.0654 | 31.6212 | 0.9958 | 1.0000 |
| | Run 4 | 0.0709 | 1.6424 | 30.5450 | 1.0000 | 0.9983 |
| **ISS** | **Function 1** | | | | | |
| | Runs 1 & 4 | 3.2489 | 0.5312 | 36.5622 | 1.0000 | 0.9292 |
| | Run 1 | 177.7567 | 2.0447 | 52.5991 | 1.0000 | 0.9986 |
| | Run 4 | 136.1670 | 3.5074 | 50.5912 | 1.0000 | 0.9824 |
| | **Function 2** | | | | | |
| | Runs 1 & 4 | 0.4218 | 0.3124 | 28.8220 | 0.9480 | 0.9292 |
| | Run 1 | 0.0069 | 1.8694 | 52.5109 | 1.0000 | 0.9987 |
| | Run 4 | 0.0092 | 3.1546 | 50.4939 | 1.0000 | 0.9825 |

Table B.21: Estimated parameters for the CSVD-curves, Öresundsverket, COD

| | | $a$ | $b$ | $c$ | $d$ | $R^2$ |
|---|---|---|---|---|---|---|
| $\mathbf{COD_p}$ | **Function 1** | | | | | |
| | Runs 1, 3 & 4 | 1.7898 | 0.4452 | 13.6119 | 1.0000 | 0.9475 |
| | Runs 3 & 4 | 6.5058 | 1.2413 | 37.8730 | 1.0000 | 0.9865 |
| | Run 1 | 8.7600 | 0.7429 | 37.8662 | 1.0000 | 0.9994 |
| | Run 2 | 8.0007 | 1.8499 | 48.1640 | 0.9908 | 1.000 |
| | Run 3 | 6.1230 | 1.1684 | 41.4043 | 1.0000 | 0.9988 |
| | Run 4 | 8.2937 | 1.4318 | 34.9123 | 1.0000 | 0.9950 |
| | **Function 2** | | | | | |
| | Runs 1, 3 & 4 | 0.6522 | 0.2245 | 0.0007 | 0.6445 | 0.9521 |
| | Runs 3 & 4 | 0.1636 | 0.9970 | 36.7055 | 1.0000 | 0.9866 |
| | Run 1 | 0.2649 | 0.3710 | 28.8219 | 1.0000 | 0.9924 |
| | Run 2 | 0.1298 | 1.5132 | 47.5832 | 0.9879 | 1.000 |
| | Run 3 | 0.1635 | 0.9799 | 40.6911 | 1.0000 | 0.9990 |
| | Run 4 | 0.1276 | 1.1837 | 34.0972 | 1.0000 | 0.9956 |
| $\mathbf{X_B}$ **and** $\mathbf{X_U}$ | **Function 1** | | | | | |
| | $X_B$ | 9.6895 | 1.6335 | 42.1686 | 1.0000 | 0.9992 |
| | $X_U$ | 5.8104 | 0.7309 | 46.2690 | 1.0000 | 0.9835 |
| | **Function 2** | | | | | |
| | $X_B$ | 0.1029 | 1.4338 | 41.8875 | 1.0000 | 0.9992 |
| | $X_U$ | 0.4130 | 0.2924 | 31.3005 | 1.0000 | 0.9916 |